

PLASMA FUNCTIONALIZATION OF MULTI-WALLED CARBON
NANOTUBES FOR PRODUCTION OF NANOFLUIDS AND THEIR
USE FOR CAPTURE APPLICATIONS

Larissa Jorge

Doctoral Thesis

Department of Chemical Engineering
McGill University
Montréal, Québec

August 2018

Thesis submitted in partial fulfillment
of the requirements for the degree
of Doctor of Philosophy

© Larissa Jorge, 2018
All rights reserved.

DEDICATION

*Pour Louise, mon enseignante de 3e année
qui m'a placée sur le chemin de la recherche scientifique*

ACKNOWLEDGEMENTS

I would like to thank my supervisors, professor Sylvain Coulombe and professor Pierre-Luc Girard-Lauriault for their time, their patience and their trust in me. Thanks to their guidance and instruction, I was able to gain many skills inside and outside the laboratory. By observing their work, I learned how to become a better researcher and a better teacher.

Felipe, thank you so much for providing me with wisdom and another perspective that so often guided me towards the solution to my problems. Your help with Matlab, LaTeX and reviewing the introduction and conclusion of this thesis was much appreciated.

Evelyne, you were the best morning (and sometimes afternoon) coffee buddy! Thank you for all your support inside and outside the laboratory and for teaching me how to be a kinder person.

Pierre, Mathew, Pablo, I've gained many wrinkles from all the hilarious moments we shared. Thank you for keeping me sane during this degree.

I am also very thankful to Carole, Nathan, Norma, Mark, Mitchell, Elmira, Daniel, Cristina, Kathryn, Adya, Florent, and all members of the Plasma Processing Laboratory for showing me so many different approaches to science and life. I owe you all a lot!

I would also like to thank the departmental staff for their support and their kindness. Frank, Gerald, Lou, Czaba, Jo-Ann, Lisa, Louise, Melanie, Andrew, Ranjan: your dedication to the department of chemical engineering is what makes this a great department to work in! Thank you Andrew and Ranjan for the training on the various analytical instruments of the department. Thank you Gerald and Lou for all the help with programming and wiring our instruments. Frank, thank you for teaching me how to build setups, from the design stage all the way to cleaning it up after installation to make it "bijou".

I would like to thank Dr. David Liu for taking great TEM images. Thank you to Petr Fiurasek in the department of chemistry for training and help using the TGA/DSC. Thank you to M. Andreas Lippitz, Dr. Paul Dietrich, and Dr. Wolfgang E.S. Unger for obtaining the NEXAFS spectra.

I'd also like to thank professor Anne-Marie Kietzig and professor Noémie Dorval Courchesne for being amazing role models and always being available to provide sound advice.

I'd like to thank my dear friends and family for all their support and encouragements. Bianca: thank you for grounding me. Ekaterina and Dan: thank you for the wavy arms of energy. Rosana: thank you for the frequent chats even though you live far away. Mom, Dad, Ivan: only a thank you the size of the observable universe is fitting for you.

I would also like to acknowledge the generous financial support received from the Natural Sciences and Engineering Research Council of Canada (NSERC), Fonds de recherche du Québec, nature et technologies (FRQNT), and McGill University.

ABSTRACT

In this thesis, an aqueous nanofluid containing plasma treated multi-walled carbon nanotubes (MWCNTs) was developed for capture of CO₂ and dyes. The surface chemistry of the MWCNTs was tailored for their stability in water and affinity for the molecules to be captured.

MWCNTs grown directly on a stainless steel mesh, by thermal chemical vapor deposition, formed an open forest amenable for plasma treatment. Plasma polymerization of ethylene with ammonia or carbon dioxide led to the deposition of a thin coating on the MWCNTs. The coating contained nitrogen functional groups, such as amine groups, when using ammonia, and oxygen functional groups, such as carboxylic acid groups, when using carbon dioxide. The chemical composition of these coatings remained stable even after exposure to water or low heat (150°C).

The stability of the plasma treated MWCNTs in water was affected by the nature of the functional groups on the coatings and the pH of the mixture. At pH values where these functional groups are neutral (basic pH for nitrogen-containing coating, and acidic pH for oxygen-containing coating), MWCNTs agglomerated. However, these agglomerates were redispersed by changing the pH of the mixture such that the functional groups on the plasma polymer coating were again charged. Other factors that destabilized MWCNTs such as high ionic strength caused by high concentrations of salt also formed reversible agglomerates.

Nanofluids with plasma treated MWCNTs were tested for capture of CO₂ using a gas bubble column. CO₂ was bubbled through a column of nanofluid until saturation of the mixture. CO₂ concentration at the outlet of the column was measured continuously using a mass spectrometer in order to calculate the amount of CO₂ absorbed. Nanofluids with MWCNTs coated with oxygen-containing functional groups exhibited enhanced CO₂ absorption capacity compared to pure water. However, the highest absorption capacity for CO₂ was obtained with MWCNTs with a nitrogen-rich plasma polymer coating. This was due to the presence of amine functional groups which interacted favorably with CO₂. This proved that both the MWCNT and its surface chemistry tailored for the molecule to be captured

were necessary for maximum absorption. It was also shown that by bubbling argon into the mixture, CO₂ was removed and the nanofluid was reused for another CO₂ absorption cycle.

The two types of plasma treated MWCNTs were also tested for adsorption of dyes in water. Nanofluids were mixed with a dye solution at different pH values and left in the dark for a 24 hr period. The mixtures were centrifuged and the concentration of dye in the supernatant was measured by visible light absorption spectroscopy. MWCNTs coated with nitrogen functional groups, which provide a positive charge to the surface of the MWCNTs at acidic pH, were efficient at adsorbing methyl orange which is an anionic dye. Whereas MWCNTs with oxygen-containing functional groups, and thus carrying a negative charge at basic pH, were better at adsorbing a cationic dye, methylene blue. The dye was released from the MWCNTs by switching the pH of the mixture such that the functional groups on the MWCNTs were neutral. By redispersing these MWCNTs in a fresh dye solution, they could be reused for dye adsorption.

RÉSUMÉ

Dans cette thèse, un nanofluide aqueux contenant des nanotubes de carbone multi-parois (MWCNT) traités par plasma ont été développés pour la capture de CO_2 et de pigments. La chimie de surface des MWCNTs a été adaptée pour leur conférer stabilité dans l'eau ainsi qu'une affinité pour les molécules à capturer.

MWCNTs synthétisés directement sur une grille d'acier inoxydable, par dépôt chimique en phase vapeur, forment une forêt propice pour le traitement par plasma. Par polymérisation plasma d'éthylène avec de l'ammoniac ou du dioxyde de carbone, une couche mince a été déposée sur les MWCNTs. Cette couche mince contient des groupes chimiques azotés, tels que les groupes aminés, lorsque l'ammoniac est utilisé. La couche contient des groupes chimiques oxygénés, tels que les groupes d'acides carboxyliques, lorsque le dioxyde de carbone est utilisé. La composition chimique de ces films est restée stable même après contact avec l'eau ou chauffage à basse température (150°C).

La stabilité dans l'eau des MWCNTs traités par plasma était affectée par la nature des groupes chimiques des couches minces et le pH du mélange. Lorsque le pH du mélange rendait ces groupes chimiques neutres (pH basique pour les films azotés et pH acide pour les films oxygénés), les MWCNTs s'aggloméraient. Cependant, ces agglomérats étaient redispersés en changeant le pH de la solution vers une valeur qui rendait les groupes chimiques chargés à nouveau. Une force ionique élevée, due à une forte concentration de sel, causait aussi la déstabilisation des MWCNTs mais ces agglomérats étaient aussi réversibles.

Les nanofluides ont été testés pour capturer le CO_2 dans une colonne à bulles de gaz. Le CO_2 était injecté dans une colonne de nanofluide jusqu'à ce que le mélange soit saturé. La concentration de CO_2 était mesurée par spectrométrie de masse à la sortie de la colonne de façon continue afin de déterminer la quantité de CO_2 absorbé. Les nanofluides contenant des MWCNTs couverts par un film oxygéné absorbaient plus de CO_2 que l'eau pure. Cependant, la capacité d'absorption de CO_2 la plus élevée a été obtenue avec des MWCNTs recouverts d'un film azoté. Cela est dû aux groupes aminés qui peuvent interagir avec le CO_2 . Cela a prouvé que les MWCNTs ainsi que leur chimie de surface adaptée à la molécule à capturer

étaient nécessaires pour une absorption maximale. Il a aussi été démontré qu'en injectant de l'argon dans le nanofluide, le CO₂ était retiré et le nanofluide pouvait être réutilisé pour un autre cycle d'absorption de CO₂.

Les deux types de MWCNTs traités par plasma ont aussi été testés pour l'adsorption de pigments dans l'eau. Les nanofluides ont été mélangés à une solution contenant un pigment et conservés dans l'obscurité pour 24 hr. Les mélanges étaient centrifugés et la concentration de pigment dans le surnageant était mesurée par spectroscopie d'absorption de la lumière visible. Les MWCNTs recouverts du film azoté, qui porte une charge positive, étaient plus efficaces pour l'adsorption d'un pigment anionique, le méthylorange. Les MWCNTs recouverts d'un film oxygéné, qui porte une charge négative, adsorbaient mieux un pigment cationique, le bleu de méthylène. Pour la désorption des pigments, le pH du mélange était modifié de sorte que les groupes chimiques à la surface des MWCNTs soient neutres. Les MWCNTs pouvaient ensuite être redispersés dans une solution fraîche de pigments afin d'être réutilisés pour un autre cycle d'adsorption.

TABLE OF CONTENTS

	Acknowledgements	i
	Abstract	iii
	Résumé	v
	List of figures	x
	List of tables	xiv
1	Introduction	1
	1.1 Objectives	2
	1.2 Thesis organization	2
2	Background	4
	2.1 CNT synthesis	5
	2.2 CNT functionalization	6
	2.3 Plasma functionalization	7
	2.3.1 Plasma grafting and polymerization	9
	2.4 CNT nanofluid	11
	2.5 Capture applications	14
	2.5.1 Capturing carbon dioxide	14
	2.5.2 Capturing dyes	17
	2.6 Issues with CNT nanofluids for capture applications	20
3	Experimental methodology	21
	3.1 Material preparation	21
	3.1.1 Synthesis of MWCNTs by t-CVD	21
	3.1.2 Functionalization of MWCNTs	21
	3.1.3 Production of nanofluid	24
	3.2 Characterization of PPE:X and MWCNT-PPE:X	25
	3.2.1 Thermal gravimetric analysis and pyrolysis	25
	3.2.2 Optical emission spectroscopy	25
	3.2.3 Scanning and transmission electron microscopy	26
	3.2.4 Light absorption spectroscopy	26
	3.2.5 X-ray spectroscopy	28
	3.3 Testing for applications using nanofluids	30

3.3.1	Destabilization and dispersion cycles	30
3.3.2	Gas sorption column	31
3.3.3	Interaction with dyes	32
4	Effect of water and pH on PPE:X and MWCNT-PPE:X	35
4.1	Preface	35
4.2	Introduction	36
4.3	Experimental method	38
4.3.1	Nanofluid synthesis	38
4.3.2	Characterization of MWCNT-PPE:X	41
4.4	Results and discussion	45
4.4.1	Morphology and composition of MWCNT-PPE:X	45
4.4.2	Effect of pH on the stability of nanofluids	51
4.4.3	Destabilisation and dispersion of MWCNT-PPE:X through pH cycling	54
4.5	Conclusion	60
5	Addition of APTS and TEPA on MWCNTs	62
5.1	Preface	62
5.2	Introduction	63
5.3	Experimental method	65
5.3.1	Synthesis of PPE:O and MWCNT-PPE:O	65
5.3.2	Characterization of PPE:O and MWCNTs	67
5.4	Results and discussion	68
5.4.1	Plasma polymer structure	68
5.4.2	Effect of heat on MWCNT-PPE:O	70
5.4.3	APTS on MWCNT and MWCNT-PPE:O	72
5.4.4	TEPA on MWCNT and MWCNT-PPE:O	76
5.5	Conclusion	80
5.6	Supplementary information	80
6	Carbon dioxide capture	87
6.1	Preface	87
6.2	Introduction	89
6.3	Experimental method	92
6.3.1	Nanofluid synthesis	92
6.3.2	Characterization of the MWCNTs	93
6.3.3	Gas bubble column	96
6.4	Results and discussion	97
6.4.1	MWCNTs morphology	97
6.4.2	Gas-phase species in the plasma	98
6.4.3	MWCNTs chemical composition	101

6.4.4	Stability of nitrogen functionalization after water immersion . . .	107
6.4.5	NFs CO ₂ absorption capacity	109
6.5	Conclusion	114
7	Dye capture	115
7.1	Preface	115
7.2	Introduction	116
7.3	Experimental method	117
7.3.1	Nanofluid synthesis	117
7.3.2	Interaction of MWCNT-PPE:X with dyes	118
7.4	Results and discussion	122
7.4.1	Effect of pH, concentration and time on MO and MB	122
7.4.2	Adsorption, reuse and release	127
7.4.3	Experimental limitations	131
7.5	Conclusion	135
8	Conclusion	136
8.1	Summary	136
8.2	Statement of contributions	139
8.3	Recommendations for future work	140
	References	142
	REFERENCES	142
A	Spatial homogeneity of PPE:X deposition on MWCNTs	155

List of figures

<u>Figure</u>		<u>page</u>
2.1	Potential energy with respect to interparticle distance [44].	13
3.1	PECVD chamber.	23
3.2	Sample placement on PECVD electrode.	23
4.1	Picture (top) and schematic (bottom, not to scale) of semi-batch t-CVD setup for MWCNTs synthesis. Insert shows the boat inside the loading chamber.	40
4.2	Setup for pH cycling experiments.	44
4.3	TEM images of (a) MWCNT-PPE:N and (b) MWCNT-PPE:O. Straight red lines highlight the plasma polymer around the MWCNT.	46
4.4	TEM images of (a) MWCNT-PPE:N and (b) MWCNT-PPE:O after sonicating in water. Straight red lines highlight the plasma polymer around the MWCNT.	48
4.5	Elemental composition of MWCNT-PPE:N and Si-PPE:N before and after sonication in water.	48
4.6	Elemental composition of MWCNT-PPE:O and Si-PPE:O before and after sonication in water.	49
4.7	Experimental and fitted C 1s peaks for (a) as-synthesized Si-PPE:X, (b) after sonication, PPE:N on the left, PPE:O on the right. The component areas are also given as percentages. Insets show the high resolution N 1s peak for PPE:N (left) and O 1s peak for PPE:O (right).	50
4.8	Stability of nanofluids prepared with MWCNT-PPE:N at different pH over a period of one week.	52
4.9	Stability of nanofluids prepared with MWCNT-PPE:O at different pH over a period of one week.	53
4.10	Stability of nanofluids prepared with either MWCNT-PPE:N or MWCNT-PPE:O at different pH after boiling for 3 min.	55

4.11	Cycles of destabilisation (decrease in extinction coefficient) and dispersion (increase) of a MWCNT-PPE:N nanofluid.	56
4.12	Cycles of destabilisation (decrease in extinction coefficient) and dispersion (increase) of a MWCNT-PPE:O nanofluid.	57
4.13	Loss of MWCNT-PPE:N in suspension at pH 12 over a time span of 40 min. Insert shows nanofluid at the end of the experiment.	59
5.1	TGA spectra of LDPE, PPE and PPE:O.	69
5.2	DSC spectra of LDPE, PPE and PPE:O.	71
5.3	TEM images of MWCNT-PPE:O before (a) and after (b) heating at 150 °C for one hour in argon.	71
5.4	Composition of (a) MWCNT-PPE:O and (b) MWCNT, freshly prepared, after heating at 150 °C, after vapor functionalization with TEPA at 150 °C or APTS at 80 °C.	72
5.5	APTS hydrolysis and reaction with hydroxyl terminated surface.	74
5.6	Aqueous (a) and ethanol (b,c) dispersions containing APTS functionalized MWCNTs after (a, b) 24 hr, (c) 2 weeks.	74
5.7	Nanofluids containing TEPA functionalized MWCNTs after 48 hr (top) and 2 weeks (bottom).	78
5.8	Selectivity of nucleophilic groups $[Nu]_S$ (circles), and total nucleophilic groups concentration $[Nu]_T$ (crosses).	79
5.9	Elemental composition of (a) Si-PPE:N and (b) Si-PPE:O.	81
5.10	Experimental and fitted C 1s peaks for (a) as-synthesized Si-PPE:X, (b) after heating at 150 °C, PPE:N on the left, PPE:O on the right. The component areas are also given as percentages.	82
5.11	Fitted components for C 1s peaks of (a) Si-PPE:N and (b) Si-PPE:O after heating at 600 °C. The component areas are also given as percentages.	84
5.12	Fitted components for N 1s peaks of Si-PPE:N (a) before and (b) after heating at 600 °C. The component areas are also given as percentages.	84
5.13	Fitted components for O 1s peaks of Si-PPE:O (a) before and (b) after heating at 600 °C. The component areas are also given as percentages.	85
5.14	XRD of PPE:N after heating at 600 °C.	86

6.1	Gas bubble column for absorption of CO ₂ by NFs. 1) column, 2) gas inlet (a) and outlet (b), 3) gas diffuser, 4) argon inlet, 5) connection to mass spectrometer.	97
6.2	SEM images of as-produced MWCNTs (a and b) and MWCNTs-10:10 (c and d).	99
6.3	TEM images of a) MWCNT-20:0, b) MWCNT-20:4, c) MWCNT-10:10. The plasma deposited organic macromolecule layer is found between the two red lines.	100
6.4	OES spectra of the plasma used to functionalize the MWCNTs.	102
6.5	Nitrogen content (o) and total concentration (x) of nucleophilic groups on the surface of functionalized MWCNTs.	102
6.6	Selectivity of nitrogen functional groups for nucleophilic groups.	103
6.7	Experimental and fitted C 1s peaks for a) as-synthesized MWCNTs, b) MWCNT-20:0, c) MWCNT-20:4, d) MWCNT-10:10-O ₂	104
6.8	NEXAFS spectra of the C K-edge for as-synthesized MWCNTs and all functionalized MWCNTs.	107
6.9	Experimental and fitted carbon peaks for a) as-synthesized MWCNTs, b) MWCNT-20:0, and c) MWCNT-20:4.	108
6.10	NEXAFS spectra of the N K-edge for all functionalized MWCNTs.	109
6.11	Nitrogen content (o), and oxygen content (x) before (solid line) and after (dashed line) immersion of the MWCNTs in water.	110
6.12	Total amount of CO ₂ absorbed by RO water and aqueous MWCNT NFs as a function of time.	111
6.13	Absorption rate of CO ₂ in RO water and aqueous MWCNT NFs.	111
6.14	Maximum CO ₂ absorbed by NF MWCNT-10:10 through multiple absorption/desorption cycles.	113
6.15	Total amount of CO ₂ absorbed by two NFs with MWCNTS treated with oxygen or ammonia.	113
7.1	Methylene blue (left) and methyl orange (right).	117
7.2	Schematic of the adsorption and reuse (top) and release experimental procedures (bottom). MWCNT here refers to both MWCNTs and MWCNT-PPE:X, unless specified otherwise.	119

7.3	Absorption coefficient (squares) and wavelength of maximum absorption (diamonds) of MO with respect to (a) pH (28 mg L ⁻¹) and (b) concentration (filled markers at pH 2, empty markers at pH 5.5).	124
7.4	Absorption coefficient (squares) and wavelength of maximum absorption (diamonds) of MB with respect to (a) pH (19 mg L ⁻¹) and (b) concentration (pH 5.5).	125
7.5	Absorption spectrum of MB at different pH values and time since preparation.	126
7.6	Absorption coefficients of MB with respect to absorbance units. The dashed line corresponds to the regression line with equation: $-0.118x^2-0.004x+0.229$	127
7.7	Adsorption capacity of MO on MWCNT-PPE:X and MWCNT after 24 hr. The asterisks correspond to the adsorption capacity after adsorbent reuse.	129
7.8	Adsorption capacity of MB on MWCNT-PPE:X and MWCNT after 24 hr. The asterisk corresponds to the adsorption capacity after adsorbent reuse.	130
7.9	Absorption spectra of last wash solution and recovered dye.	132
A.1	Sample position on electrode, MWCNT mesh in the middle (dark grey) and Si wafer on the side (light grey). For XPS measurements, the MWCNT mesh was cut along the dashed line and one half of the sample was flipped in order to analyze its backside. The circles show the approximate measurement positions (spot sizes are not to scale).	157
A.2	Nitrogen content of MWCNT-PPE:N with respect to deposition time. Asterisks show N At% for Si-PPE:N.	158
A.3	Evolution of C 1s peak for MWCNT-PPE:N a) front, b) back.	158
A.4	Oxygen content of MWCNT-PPE:O with respect to deposition time. Asterisks show O At% for Si-PPE:O.	160
A.5	Evolution of C 1s peak for MWCNT-PPE:O a) front, b) back.	160
A.6	Evolution of O 1s peak for MWCNT-PPE:O (back side).	161

List of tables

<u>Table</u>		<u>page</u>
2.1	Examples of aqueous nanoparticle dispersions for CO ₂ absorption.	16
2.2	Examples of aqueous nanoparticle dispersions for dye adsorption.	19
4.1	Gas flow rates during plasma polymer deposition.	41
4.2	Characteristics of XPS fitted components for C 1s [21, 38, 39, 112].	47
5.1	Possible breakdown products (ions, radicals or excited species) of gases in the plasma.	69
5.2	Characteristics of XPS fitted components for N 1s [32, 157].	85
6.1	Gas flow rates during plasma functionalization.	93
6.2	XPS fit component positions [21, 173].	105
7.1	Operating conditions for plasma polymer deposition.	118
7.2	Properties of MO and MB.	127

List of abbreviations

APTS	(3-aminopropyl)triethoxysilane
BE	binding energy
CD	chemical derivatization
CNT	carbon nanotube
DSC	differential scanning calorimetry
FTIR	Fourier transform infrared spectroscopy
FWHM	full width half maximum
LDPE	low density polyethylene
MB	methylene blue
MO	methyl orange
MS	mass spectrometer
MWCNT	multi-walled carbon nanotube
NEXAFS	near edge X-ray absorption fine structure spectroscopy
NF	nanofluid
NP	nanoparticle
OES	optical emission spectroscopy
PECVD	plasma enhanced chemical vapor deposition
PP	plasma polymer
RF	radio frequency
RO	reverse osmosis
SEM	scanning electron microscope
SS	stainless steel

SWCNT single-walled carbon nanotube
t-CVD thermal chemical vapor deposition
TEM transmission electron microscope
TEPA tetraethylenepentamine
TFBA 4-(trifluoromethyl)benzaldehyde
TGA thermogravimetric analysis
XPS X-ray photoelectron spectroscopy

CHAPTER 1

Introduction

Industrial processes generate large volumes of waste containing very small compounds. Metal complexes, carbon dioxide, dyes and polymers are a few examples of harmful compounds that find themselves mixed in water or air as by-products of these processes. These compounds are too small to be simply filtered and they do not agglomerate nor sediment. Due in part to a lack of efficient cleaning methods, these waste streams are often released back into the environment, leading to the various pollution problems we face nowadays: global warming, destruction of wildlife, contamination of crops, etc. One way of removing the compounds from air or water is to capture them. New materials with high capacity and chemical affinity for these compounds must be developed so that industries might consider them worthwhile to implement in their processes.

Nanofluids, which are stable dispersions of solid nanoparticles in a liquid host, are advantageous for waste treatment. With solid particles mixed throughout the liquid phase, these can act as great adsorbents for the dissolved compounds that need to be captured. Furthermore, enhanced mass transfer rates of gas molecules into a liquid absorbent have been observed when the liquid phase contains solid particles [1, 2] making nanofluids a good material for capture of toxic gases.

Carbon nanotubes (CNTs), which consist the basis of the material developed in this work, are an interesting candidate as adsorbents in nanofluids. With their high aspect ratio (a few μm in length but less than 100 nm in diameter), they offer large surface areas for adsorption of a variety of compounds. Furthermore, it is possible to modify their surface

chemistry such that they interact more strongly with the compounds to be captured. However, as will be discussed in Chapter 2, their surface chemistry is not always tailored to ensure their stability in the liquid. Poor stability means that, over time, CNTs agglomerate which leads to loss of surface area and ultimately complete loss of material through sedimentation of the larger agglomerates. The efficiency of these CNTs as adsorbents in a nanofluid is therefore hindered. It is therefore interesting to investigate if surface modification of the CNTs that allows for stability and interaction with other compounds makes for a better material for capture applications.

1.1 Objectives

This Ph.D. thesis focuses on the production of stable multi-walled CNT (MWCNT) nanofluids for capture applications. Plasma polymerization is the chosen technique to modify their surface chemistry for two purposes: stabilization of the MWCNTs in water and increased affinity for capture of carbon dioxide and dyes. The following specific objectives are addressed in this thesis:

- Investigation of the plasma polymer (PP) chemical composition and structure, before and after exposure to water.
- Evaluation of the stability of PP-coated MWCNTs in pure water, and at different pH and ionic strength values.
- Quantification of the CO₂ absorption capacity and dye adsorption capacity by PP-coated MWCNTs in water.

1.2 Thesis organization

This manuscript-based thesis is comprised of 8 chapters. Chapter 2 reviews the different plasma treatments available to modify the surface chemistry of CNTs to make them stable

and well dispersed in water. A brief overview of how CNT nanofluids have been used to capture CO₂ and dyes is also presented. Chapter 3 describes the experimental methods and equipment used to synthesize and characterize the novel materials produced. Chapters 4, 5 and 6 are composed of articles published (or submitted for publication) in peer-reviewed journals. Chapter 4 presents the chemical composition of the PPs investigated, as well as their stability in water. The impact of pH on the agglomeration and dispersion of PP-coated MWCNTs is discussed. Chapter 5 investigates the structure of the PPs and their stability with respect to heat. Another method to modify the surface chemistry of CNTs using volatile molecules is shown. Chapter 6 presents a study on the use of PP-treated MWCNT nanofluids for CO₂ capture in a gas bubble column. Chapter 7 focuses on the use of the MWCNT nanofluids for dye capture. A summary of the work presented as well as recommendations for future work can be found in Chapter 8. The appendix includes observations and a discussion on the spatial homogeneity of the PP coating on MWCNTs.

CHAPTER 2

Background

Carbon, with its four valence electrons, can bond with itself in different ways giving rise to a vast family of allotropes, from crystalline structures such as diamond to the disorganized amorphous carbon. CNTs are a member of this family and share many properties with other carbon allotropes. In fact, the most common description of CNTs is based on its closest cousin: graphene. Graphene is a flat sheet of carbon atoms arranged in a honeycomb pattern. By rolling up a graphene sheet into a cylinder, a CNT is formed. A single tube is called a single-walled carbon nanotube (SWCNT) and many concentric tubes form a multi-walled CNT (MWCNT). SWCNTs are typically 1 nm in diameter, whereas MWCNTs can go up to 100 nm in diameter [3]. The spacing between each concentric tube in a MWCNT is typically 0.34 nm [4]. CNTs are usually hundreds of nanometers long, many reaching one or more μm in length.

Given their very large surface, CNTs are interesting structures for enhanced interaction with a variety of compounds (gas, liquid or solid) in applications involving detection, capture or delivery of products. Furthermore, the chemistry of carbon is extensive and there are numerous recipes to modify the CNTs' surface chemistry so that they can selectively interact with the desired compounds [5].

In this chapter, the synthesis and common modification methods of CNTs are presented, with a particular focus on plasma based treatments. The dispersion of these CNTs in liquids and the factors influencing their stability are discussed. And finally, a review of technologies employing dispersions of nanoparticles to capture CO_2 or dyes is presented. It is important to

note that for a more complete literature review, examples from both SWCNT and MWCNT are presented. Although slight differences in electrical properties and size make these two forms of CNTs suitable for different applications, when it comes to applications relying on their capacity to bind with other compounds, they are interchangeable. However, the results of this thesis only deal with MWCNTs given that it was the material synthesized in our laboratory.

2.1 CNT synthesis

The main methods for CNT synthesis are arc discharge, laser ablation and thermal chemical vapor deposition (t-CVD) [6]. The method chosen is usually based on the amount of CNTs required and the desired properties of the CNTs (length, density, straightness, defect density, etc.).

For large scale production, t-CVD is the most popular method [7]. It requires a metal catalyst, typically nanoparticles of iron, nickel or cobalt, which are supported on an appropriate substrate [8]. After the catalyst is brought to a temperature between 600 and 1000 °C [7], a carbon source, such as acetylene, C_2H_2 , methane, CH_4 , or ethylene, C_2H_4 , is injected into the system. The hydrocarbon adsorbs onto the surface of the catalyst, breaks down and the carbon dissolves into the metal. It then precipitates out of the nanoparticle into a carbon nanostructure depending on the size and properties of the metal catalyst used [6]. Changing the conditions of the reaction (temperature, flow rate and concentration of gases, heat treatment time of the substrate, etc.) affects the growth of the tubes.

The method used in this thesis is based on the works by Baddour [9] and Hordy [10]. They developed a t-CVD synthesis method where MWCNTs grow directly on metal substrates without the need for additional surface pretreatments or deposition of metal nanoparticles. In this process, a stainless steel (SS) mesh is first heated to create favorable iron-rich

sites for the growth of the nanotubes [11]. These sites are between 10 and 50 nm in diameter [12] which is in the correct range for the formation of MWCNTs. Acetylene, the carbon source, is injected in the tube and decomposes at 700 °C. MWCNTs usually between 3 and 5 μm long and 30 nm in diameter are produced all around the mesh wires [12]. Figure 6.2 shows the MWCNTs on the grid. Note that the tubes form an open forest where their surface is available for chemical or physical treatments.

2.2 CNT functionalization

Modifying the surface chemistry of CNTs can be as simple or as complicated as one requires it to be. The techniques used can be separated into two main categories: wet and dry chemistry.

Wet chemistry includes all techniques that occur when CNTs are in contact with a liquid phase. Most of the tools from organic and polymer chemistry are therefore available to modify the CNTs. As shown by the extensive review by Tasis et al. [5], the options are almost endless and allow the user to sequentially add more and more building blocks starting from the CNTs as scaffolds. In a liquid, it is also possible to work with very complex compounds which is necessary for applications such as drug delivery. However, given that CNTs cannot be dispersed in most solvents [5], when attempts are made to functionalize CNTs in a liquid, especially in water, many CNTs remain agglomerated. Therefore, regardless of the method chosen to treat the CNTs, many are left untreated leading to poor stability of the CNTs in a liquid medium.

Dry chemistry includes all techniques where CNTs are in contact with a gaseous phase. Dry chemistry on its own does not ensure that the surface of all CNTs in a sample are treated, as this depends on how the CNTs are delivered to the functionalization chamber (compact or loose powder, presence of physical obstacles between treatment source and sample, etc.).

However, it avoids further agglomeration of the starting material since it does not require interaction with a liquid solvent. Another advantage of dry chemistry is avoiding the use of large quantities of toxic solvents which cannot be reused. Eliminating liquid solvents also means there can be no solvent residue on the final product and no swelling of the material being treated [13]. The major disadvantage of dry chemistry techniques is that they require molecules with high vapor pressure at low temperatures (low enough that the substrate won't melt or react with its environment). Therefore, only simpler and smaller molecules can be used (i.e. no polymers), greatly limiting the scope of properties that can be imparted onto the CNTs by functionalization.

In order to take advantage of the open forest of CNTs produced in our laboratory, a dry technique was used to treat them: plasma functionalization. This method is often recognized as being capable of providing uniform coatings and treating only the sample surface without affecting the bulk material [13]. As will be described below, plasma functionalization can create different surface chemistries on the desired substrate based on the nature of the gases chosen.

2.3 Plasma functionalization

Plasma, the fourth state of matter, is a gaseous mixture of electrons, ions and neutral species. Equilibrium, thermal plasmas, where the electron and ion temperatures (T_e and T_i respectively) are of the same magnitude ($T_i \approx T_e \sim 10^4$ K), are used in welding and arc furnaces, for example. Non-equilibrium, cold plasmas, where $T_e \gg T_i$ ($T_i \sim 300$ K, $T_e \sim 10^4$ K), can be used for lighting, analytical chemistry, and various surface treatments. The low ion energy ensures that substrates do not reach high temperatures meaning that temperature sensitive substrates such as polymers and carbon nanotubes can be treated. Furthermore, at low pressures, relatively uniform treatments can be obtained over large

surface areas ($\sim 10^3 \text{ cm}^2$ [14]). The ability to tune the amount of energy delivered to the gaseous molecules also allows to control their fragmentation and thus the chemistry of the treatment.

A cold, non-equilibrium, plasma can be produced in a vessel equipped with electrodes and containing one or more gases at a reduced pressure. When a sufficient voltage difference is applied between the electrodes, the gas breaks down electrically and a plasma is ignited. The sample to be treated may be positioned anywhere inside the chamber, but typically is placed inside the plasma. With non-polymerizing gases such as argon, the plasma generates species at different excitation levels. These may then release their energy when colliding with the chamber walls, with other excited species or with the sample surface. Some of these collisions may break bonds on the sample surface leading to reorganization of the surface chemistry or even surface etching. With polymerizing gases such as hydrocarbons, possible reactions in the plasma are described by Yasuda's model called "rapid step-growth polymerization mechanism". This model resembles the classical polymerization reaction with an initiation step, a propagation step and a termination step [15]. The plasma breaks down the gas molecules and generates species with one or two reactive sites. These species can combine with other neutral or activated species to form longer chains. When they reach the sample, they may react with a dangling bond, adsorb onto an unreactive site and diffuse on the surface, not react and return to the gas phase or even etch away the coating already formed. Ion bombardment and UV light also affect the final structure of the coating by generating radicals, breaking bonds or crosslinking chains in the coating [16, 17, 18]. Operating conditions of the treatment (power, pressure, gas flow rates and nature of the gases) are chosen such that deposition reactions win over ablation reactions, therefore slowly building a coating on the sample.

For this thesis, the surface of MWCNTs needed to be modified in order to make them hydrophilic. The treated MWCNTs could then be used for capture of various compounds in aqueous mixtures. Plasmas using nitrogen or oxygen-containing gases are usually chosen for this purpose. A review of plasma treatment involving nitrogen or oxygen compounds follows.

2.3.1 Plasma grafting and polymerization

For a "soft" substrate such as CNTs, (where bonds in the substrate can be broken by the plasma), plasmas that produce non-polymerizable species [19] such as nitrogen, N_2 [17, 20], ammonia, NH_3 [21, 22], oxygen, O_2 [21] and carbon dioxide, CO_2 [23] may induce what is called plasma grafting. This treatment causes the replacement of carbon atoms on the CNTs by heteroatoms (nitrogen or oxygen) or the addition of functional groups on the CNT surface. It most frequently occurs at the open tips of CNTs, where weaker bonds can be found, or at defect sites. The latter are present due to the CNT synthesis or by voluntary defect generation through acid treatment [17] or plasma treatment with an inert gas [24]. In this project, MWCNTs synthesized in-house already contain the necessary defects for plasma grafting [6].

A plasma can also be used to coat the CNTs with an organic film. Igniting a plasma in a hydrocarbon gas generates the deposition of carbonaceous films on all surfaces that are accessible by the activated compounds. Common hydrocarbons used are ethane, C_2H_6 , ethylene, C_2H_4 , and acetylene, C_2H_2 , in increasing order of polymerizability. By adding a gas typically used for plasma grafting (NH_3 , CO_2 , O_2), it is possible to deposit a carbonaceous film with useful functional groups. This film is commonly called a plasma polymer (PP). However it is not a polymer and does not share the properties that polymers have such as

melting point and a repeating chain structure [25]. The choice of the word polymer rather refers to the process of gaseous molecules forming networks and attaching on a surface [26].

The choice of gases depends mostly on the desired chemistry of the final product. For most applications, a single chemical functional group is required. Obtaining surfaces with a single type of functional group can easily be achieved through wet chemistry. In order to mimic that in a plasma treatment, a gas carrying the desired functional group is selected. By keeping the energy input per molecule as low as possible, less fragmentation occurs and functional groups present on the initial gas molecules may be preserved on the sample surface. If using a plasma that delivers very high energy per molecule, the nature of the gas chosen has little impact on the final surface chemistry. All gaseous molecules are broken down into their smallest constituents before they can react with the sample surface.

As mentioned above, for this thesis, nitrogen and oxygen-containing functional groups are to be added onto CNTs. For addition of nitrogen, plasma treatments are often performed using N_2 and NH_3 . Ammonia is used more often given its lower ionization energy and therefore ease in activation for reaction with the desired substrate [27, 28]. To obtain nitrogen-rich PPs, NH_3 and C_2H_4 [29, 30, 31] or butadiene, C_4H_6 [29], are often used. Larger quantities of nitrogen are incorporated in the film when larger ammonia to hydrocarbon ratios are used. The functional groups often reported for nitrogen grafting or nitrogen-rich PPs are imines, $C=N$, amides, $N-C=O$, and amines, $-NH_2$ [32]. However, the most wanted functional group are amines due to the numerous reactions they can be used for, such as capture of CO_2 or attachment of biological compounds through reaction with an acyl chloride [5, 33]. Higher selectivity for amine groups is obtained when power is kept low. This avoids excessive dehydrogenation of the initial ammonia molecule or dehydrogenation of amines already attached on the surface [34]. Injection of hydrogen gas also has been shown to counteract the dehydrogenation processes and yields coatings with more amine functional groups [17].

Oxygen-containing plasma treatments can be generated with CO_2 [35, 36] or O_2 [21]. The main functional groups obtained are esters and carboxyls, COOR , hydroxyls and ethers, COR or carbonyls, C=O [37]. For oxygen-containing PPs, an increase in oxygen to hydrocarbon ratio also leads to an increase in oxygen content of the final coating [38, 39, 40, 41]. However, oxygen-containing gases produce non-polymerizable molecules that can etch the coating or scavenge a portion of the radicals formed in the plasma [19, 41], thus greatly reducing the deposition rates of the coatings in comparison to nitrogen-containing coatings.

The polar functional groups generated by nitrogen or oxygen-containing plasma treatments help make the CNT surface hydrophilic. A recent review by Saka [42] identified more than 70 papers on plasma treated CNTs, the majority involving either nitrogen or oxygen plasmas. However, are these treatments sufficient to produce stable CNT aqueous nanofluids? The next section reviews the factors influencing the stability of CNTs in water.

2.4 CNT nanofluid

Stability of CNTs (and other nanoparticles) in liquids is achieved through a balance of van der Waals forces, Lewis acid-base forces and electrostatic forces [43]. Figure 2.1 shows a schematic plot of the potential energy with respect to interparticle distance. Figure 2.1 curve a shows the case of an unstable dispersion, where no forces hinder the approach between two particles and as they get closer, they ‘fall’ into a deep potential minimum from which they cannot be removed. This is called coagulation and it is an irreversible process. Figure 2.1 curve b has an additional smaller secondary minimum. If this minimum is comparable to $k_b T$, where k_b is the Boltzmann constant and T is temperature, particles that enter this minimum form weakly bound agglomerates called flocs. Formation of flocs is reversible. Curve c shows the case of a stable dispersion where the potential barrier to

reach the coagulation minimum is too large and thus particles remain separated and well suspended in the liquid medium.

Debate exists on the models describing the interaction forces between water and nanoparticles, and how to quantify each force [43, 45, 46]. However it is accepted that for successful stabilization of particles in water, attractive forces between the particles must be low, and attractive forces between the particles and water must be high to overcome the very strong attractive force among water molecules (hydrogen bonding). Pristine CNT surfaces are hydrophobic and strong van der Waals forces keep the nanotubes together when they are dispersed in water. Researchers have therefore added on CNTs molecules with functional groups that carry charges to enhance electrostatic repulsion, or molecules with high electron donicity or accepticity to enhance hydration (and therefore stabilization) of the particles [43].

These functional groups that lead to stable dispersions of particles have been added onto CNTs by plasma treatment using a variety of gases. Hordy added oxygen functional groups on the surface of MWCNTs using mixtures of Ar, C₂H₆ and O₂. These treated CNTs, when dispersed in water, showed remarkable stability for long periods of time (years) and could also be heated to 85 °C without MWCNT agglomeration [47]. Hernández-Hernández et al. showed stability in water for carbon nanofibers treated in a NH₃/H₂O plasma [48]. Kim et al. presented stable (for more than 120 hr) dispersions of CNTs after plasma treating the CNTs with a mixture of CH₄ and O₂ [49]. Avila-Orta et al. plasma polymerized ethylene glycol onto CNTs and demonstrated good stability of these nanoparticles in water, methanol and ethylene glycol for at least 24 hr [50]. Nair et al. treated CNTs with either O₂ or NH₃ and reported good stability of the nanoparticles in water for ten days [51].

Evaluating the stability of functionalized nanoparticles in pure water is the first step in understanding the types of interaction forces present. The next step is to test their stability

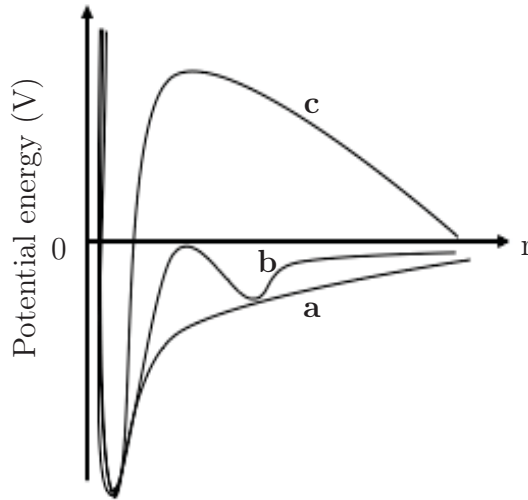


Figure 2.1: Potential energy with respect to interparticle distance [44].

while changing other conditions of the nanofluid. Changing pH of the suspension has an impact on charged functional groups. For acidic groups (usually from oxygen-containing functional groups), an increase in pH deprotonates them which then increases the repulsion force between nanoparticles [52, 53]. For basic groups (from nitrogen-containing functional groups), a decrease in pH protonates them and also increases nanoparticle repulsion. Increasing the ionic strength of the fluid, through the addition of salts for example, may lead to destabilization by thinning the double electrostatic layer around nanoparticles [43]. Other sources of ions, such as positive metallic ions which may leach from containers, are also detrimental to the stability of negatively charged oxygen-functionalized MWCNTs in water as shown by Karthikeyan et al. [54].

Not only does the composition of the fluid affect the nanoparticles' stability, but the coating itself may react over time with its environment. This is an important issue especially with PP coatings as they can be unstable in water. Embedded radicals in the coating and the density of the crosslinks determine the stability of the coating in water. Unstable films

are often oxidized and may even dissolve in water, leaving nothing or a base layer on the substrate [55].

Although numerous methods have been reported to make CNTs “stable”, and many techniques are widely used to quantify this stability (zeta potential, light scattering, particle counting) seldom is a definition of stability given. There is no standard to determine what is stability and with respect to which variable should this stability be checked: time, temperature, sedimentation rate? The conditions of the desired applications also play an important role in determining how stability is defined and measured. In particular, pH, temperature, ionic strength and other solutes all have an effect on the stability of the dispersion but are not necessarily relevant in all applications. Therefore, the stability of the MWCNTs suspensions must be investigated in the context of the two chosen applications for this thesis which are CO₂ and dye capture. Following is a short review of these two fields.

2.5 Capture applications

2.5.1 Capturing carbon dioxide

Industrial methods to capture CO₂ have been around for more than 80 years [56]. The Intergovernmental Panel on Climate Change stated in a special report published in 2005 [56] that current technologies used for CO₂ capture are mature and have a 85 to 95% efficiency. This technology relies mainly on liquid absorbents which are put into contact with the gaseous waste stream (also called flue gases). When CO₂ enters in contact with water it can react as shown in the following equation (Equation 2.1) to form carbonic acid. This acid can then dissociate partially into H⁺ and HCO₃⁻.



One of the common practices to increase the solubility and rate of absorption of CO_2 is to mix water with substances with high affinity for CO_2 . Given that CO_2 is an acidic gas, alkaline materials can enhance the solubility of CO_2 in water. For example, ammonia [57] forms a mixture of NH_3 and NH_4^+ in water and can improve the capture of CO_2 by making the solution more alkaline. In so doing, Equation 2.1 can proceed easily in the forward direction. Mixtures of water and other amine-containing molecules are also common CO_2 absorbers [58, 59]. Such molecules are monoethanolamine (MEA), diethanolamine (DEA), N-methyldiethanolamine (MDEA), diglycolamine (DGA), etc. [58, 60]. All these molecules contain a nitrogen atom with a free pair of electrons capable of reacting with CO_2 or its acid. However, amines are corrosive materials that can damage equipment [61]. They are also volatile at low temperature. New materials are being developed that attempt to address these issues while still maintaining the high efficiency in capturing CO_2 of aminated compounds.

Current research in the field of CO_2 capture focuses on the use of suspensions containing fine particles [62] which have shown enhanced gas mass transfer rates. Three main mechanisms are thought to contribute to this enhancement. The grazing or shuttle effect involves solid particles entering the boundary layer at the liquid-gas interface and adsorbing dissolved gas molecules [1]. These ‘loaded’ particles are then transported into the bulk liquid where the molecule can desorb and the solid particle is regenerated for another adsorption cycle. For solid particles with high adsorption capacity of the desired gas molecule, this causes a decrease in the concentration of dissolved gas molecules in this boundary layer, thus leading to increased transfer through the gas-liquid interface [2]. The next effect, usually referred to as the hydrodynamic effect, is linked to the Brownian motion of the particles. It is believed that the small particles affect the fluid flow and close to the gas-liquid interface, the particles may cause better mixing of the liquid thereby shrinking the diffusion layer [1]. The

last mechanism involves an increase in the gas-liquid interface area due to particles causing a decrease in gas bubble coalescence [63].

Studies on CO₂ absorption using nanofluids have shown enhancements in the mass transfer rates [60, 64, 65, 66, 67]. Table 2.1 presents a few examples of enhancement factors in absorption capacity observed in nanofluids with respect to the base solvent used. It is important to note that these nanofluids were prepared without a particular attention to the surface chemistry of the nanoparticles nor to their long term stability in the liquid. Careful tailoring of the surface chemistry of the nanoparticles can potentially lead to enhanced compatibility with the desired solute. Amine or nitrogen-functionalized carbon materials, such as CNTs and activated carbon have been investigated as solid adsorbents for CO₂ capture [59, 68, 69, 70, 71, 72, 73, 74].

Carbon nanotubes in particular are very interesting for CO₂ capture in a nanofluid on both a physical and chemical point of view. Their nanometric size makes them good candidates for enhanced shuttle and hydrodynamic effect [2]. It is also easy to add amine-containing molecules to their surface to enhance interaction with CO₂. This chemical modification may even enhance stability of the particles in the suspension, keeping them separate

Table 2.1: Examples of aqueous nanoparticle dispersions for CO₂ absorption.

Nanoparticle	Solvent	Surface treatment	Stability period	Enhancement (%)
SiO ₂ [60]	water	None	N/A	24
SiO ₂ [65]	methanol	None	24 hr	5.6
SiO ₂ [66]	water	None	N/A	20
Al ₂ O ₃ [67]	NaCl aqueous solution	Arabic gum	24 hr	12.5
Al ₂ O ₃ [65]	methanol	None	24 hr	4.5
CNT [66]	water	Acidification	N/A	40
CNT [75]	water	N/A	N/A	70

and avoiding formation of agglomerates which have less surface area available for interaction with the gas. By fixing the amines on a solid particle, it also avoids having volatile amine-containing molecules dissolved in the liquid [59].

2.5.2 Capturing dyes

To this day, the textile industry struggles with the treatment of huge volumes of toxic aqueous waste produced through processes such as fabric dyeing, bleaching and washing. In particular, dyes become an environmental problem [76] when released into water streams as they can be aesthetically unpleasing, toxic and detrimental to the plant and animal life by reflecting sunlight and depriving them from this energy source. Many techniques have been developed to treat these dye effluents based on chemical, physical or biological processes. Given the large volumes of effluent produced and the necessity to treat wastewater in a continuous flow manner, adsorption on solid particles is a popular method for wastewater treatment [77]. Although it is not the end of a full process of wastewater treatment, it is the simplest way of first concentrating the dye and then having a solid material that can be further processed in another location while allowing the bulk of the wastewater to be returned to the environment in a less harmful state.

Much research has been done on CNTs and other carbonaceous materials as dye adsorbents. Their carbon sp^2 bonds (more or less organized in hexagons depending on the crystallinity of the amorphous carbon or the defect quantity in CNTs) help form π - π bonds with the conjugated structure of most dyes [78]. Many chemical modifications are also made on the base material in order to enhance its interaction with the desired dye. More specifically, addition of functional groups that may carry a charge such as amines or carboxylic acids are used given that many dyes are cations or anions. Table 2.2 gives some examples of carbonaceous materials and their adsorption capacity for a variety of dyes. However, none of

these chemical modifications were made with the intent of making more stable nanoparticle dispersions. Stability of the particles would ensure that they are well separated offering the largest area possible for dye adsorption. It also avoids sedimentation of the adsorbent which becomes material unavailable for the adsorption process.

In particular, PP films could be an interesting part in the development of new materials for dye adsorption, contributing to both helping stabilize the nanoparticles and interacting with soluble dyes. The adsorption of dyes on PP films has been known for many years, as it is one of the techniques used for characterization of functional groups on PP films. Furthermore, PP films have also been used for enhancement of fabrics. Hegemann et al. showed that amine functional groups (positively charged) allowed for dye molecules (anions, negatively charged) to penetrate and bind to the PP film [90]. Furthermore, a single example of a plasma polymerized nanoparticle for dye adsorption was found. Jarvis et al. used quartz particles coated with plasma polymerized allylamine to adsorb acid orange 7 dye [91]. They showed a maximum adsorption capacity of about 0.6 mg g^{-1} at pH 3.

Table 2.2: Examples of aqueous nanoparticle dispersions for dye adsorption.

Nanoparticle	Surface treatment	Dye adsorbed	Adsorption capacity (mg g ⁻¹) (approx.)
CNT [79]	oxidation by nitric acid	malachite green	200
CNT [80]	N/A	acid red and reactive blue	45-60
CNT [81]	oxidation by nitric acid	malachite green	160
Graphene oxide (GO) CNT composite [82]	N/A	methylene blue	82
CNT [83]	None	direct blue	116
Activated carbon [78]	N/A	methyl orange and methylene blue	900 for MO and 600 for MB
Carbon nanocables on CNTs [84]	oxygen-containing functional groups	methylene blue	150
CNT [85]	oxidation	crystal violet	600
Metal organic framework with GO or CNT [86]	unclear	malachite green	1500
CNT [87]	APTS and TiO ₂	methyl orange	42
GO-CNT [88]	iron oxide nanoparticles + oxidation of CNTs	methylene blue	40
GO or CNT [89]	oxidation	basic red 46	140

2.6 Issues with CNT nanofluids for capture applications

As can be seen from this review, many materials are being investigated as contenders for the capture of CO₂ or dyes. Stability of the nanoparticles in the desired liquid and affinity for the molecules to be captured are the main concerns when developing new materials. CNTs modified by plasma treatment have been shown to be stable in pure water. CNTs modified by methods other than plasma have been used for capture of CO₂ and dyes. However, a modification of the CNT surface chemistry using plasma (and more specifically PPs) that allows for both stability in complex liquid mixtures and affinity for other molecules is still lacking.

CHAPTER 3 Experimental methodology

3.1 Material preparation

3.1.1 Synthesis of MWCNTs by t-CVD

MWCNTs were synthesized by t-CVD following a method developed by Baddour [9] and Hordy [10]. The method uses a 316-grade SS mesh (400 series, McMaster-Carr or TWP inc.) as a substrate. After cleaning the mesh in acetone with a sonication bath, the mesh is placed in a quartz boat, which goes inside a quartz tube furnace (120 V/30 A, Lindberg-Blue HTF 5500). Two setups were used over the course of this project, a batch (Chapter 6) and a semi-batch process (Chapters 4, 5 and 7, see Figure 4.1 in Chapter 4). In both cases, the following general sequence was followed: heat treatment at 700 °C, injection of acetylene, C₂H₂ (99%, dissolved in acetone), for 2 min at 68 sccm, 2 min growth period under Ar flow at 600 sccm, cool down. More details can be found in Chapters 4 and 6. Samples could be stored indefinitely at room temperature and in air.

3.1.2 Functionalization of MWCNTs

A plasma enhanced chemical vapor deposition system (PECVD) was used to functionalize MWCNTs (see Figure 3.1, a schematic of the system can be found in [92]). The system consisted of a ~10 L chamber equipped with a 8.7 cm diameter electrode. Gases are injected 4 cm above the electrode through a shower head, which also acts as the counter electrode. Two meshes covered with MWCNTs were held on the electrode with carbon tape as shown in Figure 3.2. The chamber base pressure was below 20 mTorr and functionalization was

conducted at 600 mTorr (80 Pa). Gases used were ammonia, NH_3 (99.99%), carbon dioxide, CO_2 (99.99%), and ethylene, C_2H_4 (99.70%). Gas flow rates were controlled using mass flow controllers (Brooks SLA5850). Two types of ethylene-based PP were prepared, one using NH_3 , which is labelled PPE:N, and another with CO_2 , labelled PPE:O. Before starting the plasma treatments, the chamber was cleaned with an Ar and O_2 plasma to minimize contamination from previous treatments. A low pressure capacitively-coupled radio frequency (RF, 13.56 MHz) glow discharge was generated using a power supply (Cesar generator, Advanced Energy) and a matching network (VM 1000 VarioMatch, Advanced Energy). Gas flow rates, power used and treatment times are presented in the respective chapters. MWCNTs after plasma treatment are named MWCNT-PPE:N or MWCNT-PPE:O. PPE:X is used to refer to both PPE:O and PPE:N.

Radicals formed on the sample's surface during the plasma treatment are still active after removal from the vacuum chamber. PP coatings undergo ageing after exposure to ambient air. The most noticeable change is the increase in oxygen in their chemical composition [17, 22]. Kasperek et al. (unpublished report) [93] showed that nitrogen-rich coatings prepared in our system had their oxygen content increase from the original 1 O at% (0 min air exposure) to almost 2 O at% after 30 min of air exposure, and reaching 10 O at% after 3 days. Storing samples in inert gases and at -18°C has been shown to decrease the ageing rate [94]. Whenever possible, such precautions were therefore taken for all samples studied. Whenever air exposure was inevitable, the amount of time that samples were exposed to air was kept constant for all samples studied. Samples used in Chapter 6 were exposed to ambient air after functionalization for less than 5 min. These samples were stored in nitrogen-filled bags (oxygen transfer rate $2.2 \text{ cc m}^{-2} \text{ day}^{-1}$, Duropac) in the freezer (-17°C). They were then used to prepare nanofluids or were analyzed less than a day after synthesis. For samples used in Chapters 4, 5 and 7, the PECVD chamber was kept in a nitrogen-filled glovebox

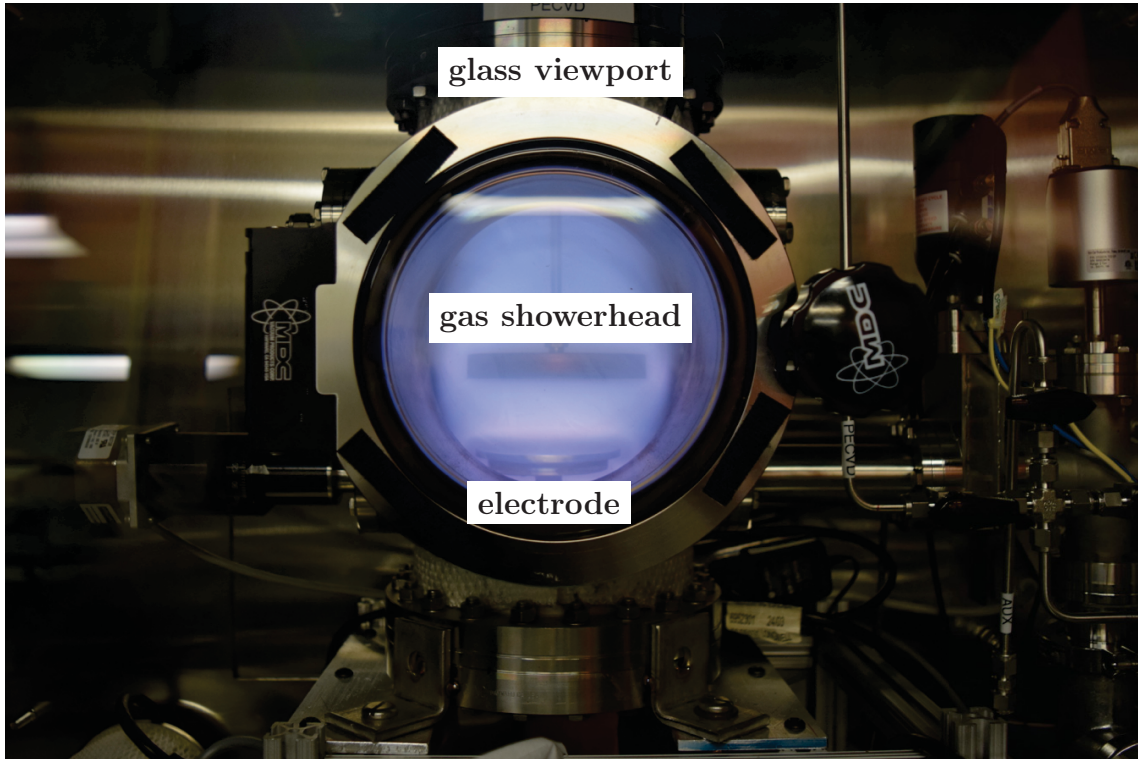


Figure 3.1: PECVD chamber.

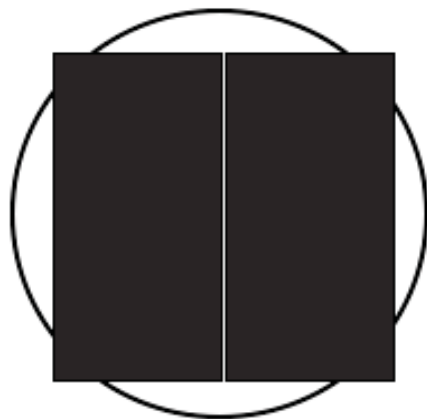


Figure 3.2: Sample placement on PECVD electrode.

(O₂ concentration < 0.1 ppm, model MB200B, MBraun). Therefore, after functionalization, meshes were not exposed to air. They were stored in the same bags as previously and in a freezer (−40 °C) located inside the glovebox. Given these conditions, samples could be stored for longer periods of time, but were typically used in less than a week.

MWCNT-PPE:O and MWCNT were also further treated with either tetraethylenepentamine (TEPA) or (3-aminopropyl)triethoxysilane (APTS) (both from Sigma-Aldrich) by vapor functionalization. SS meshes covered with MWCNT-PPE:O or MWCNTs were taped to the inside wall of glass jars. The bottom of the jars were lined with glass beads. Either 150 μL of TEPA or 50 μL of APTS was then added to the jar. The closed jars were put in an oven at 150 °C for 60 min for TEPA treatment, and 80 °C for 60 min for APTS treatment. After the samples had cooled down, they were stored in the glovebox and were used in less than a week.

3.1.3 Production of nanofluid

Water at the desired pH (2 to 12) and salinity (0.001 to 4.3 mol L^{−1}) was prepared using hydrochloric acid, HCl (Fisher), sodium hydroxide, NaOH (Aldrich) or sodium chloride, NaCl (Fisher) and reverse osmosis (RO) water. A pH meter (pHBasic+ series, Sartorius) equipped with a combination electrode (model 13-620-287A, single junction, Ag/AgCl reference, Accumet) was used to measure and record the pH. MWCNT-covered meshes were put in glass vials with water. The vials were sonicated for 10 min (100 W, Branson 2510). Nanofluids were transferred to clean new vials to avoid metal ions leaching from the mesh. Concentration of MWCNTs in nanofluids was between 40 and 150 mg L^{−1}.

3.2 Characterization of PPE:X and MWCNT-PPE:X

3.2.1 Thermal gravimetric analysis and pyrolysis

Thermogravimetric analyses (TGA) and differential scanning calorimetric (DSC) studies of the PPs were conducted to investigate their thermal properties. Measurements obtained from this instrument are only useful when compared to other similar polymers or PPs given that there was no detector attached to the TGA/DSC to analyze the exhaust's composition. Therefore, PPs and low density polyethylene (LDPE) were analyzed with this instrument.

To prepare samples for the TGA/DSC instrument, PPs were deposited for one hour on glass Petri dishes. They were scraped from the dish and loaded into alumina cups in the instrument (TGA/DSC 1 Star System, Mettler Toledo). Analysis was conducted under a flow of 60 mL min^{-1} of N_2 at a heating rate of $10 \text{ }^\circ\text{C min}^{-1}$ from 40 to $550 \text{ }^\circ\text{C}$.

In order to obtain compositional and structural information about the PP films after pyrolysis, PP films on silicon wafers or PP powder scraped from a Petri dish were pyrolyzed under argon atmosphere in the CVD tube furnace. The samples were heated to $600 \text{ }^\circ\text{C}$, held at this temperature for 30 s and then cooled down. They were then stored in nitrogen-filled bags until further use.

3.2.2 Optical emission spectroscopy

Optical emission spectroscopy (OES) was used for identification of the main excited species present in the plasma. Given the very complex and still unknown reaction mechanisms involved in plasmas containing NH_3 , CO_2 or C_2H_4 , as well as insufficient resolution of the detector, it was not possible to obtain more quantifiable information about the plasma (such as temperature, electron density and species concentration).

The emission spectrum was collected by a fiber optic cable (M22L01, Thorlabs) and recorded with a portable spectrometer (OceanOptics USB2000). The acquisition range was limited from 300 to 850 nm and the spectral resolution was 1 nm. The fiber optic was positioned outside the vacuum chamber, close to the large glass viewport, the distance between the fiber optic and the plasma being around 15 cm. The spectrum recorded was an average of 3 spectra obtained each with an integration time of 1000 s.

3.2.3 Scanning and transmission electron microscopy

A high resolution scanning electron microscope (SEM, Hitachi SU-3500) and a transmission electron microscope (TEM, Tecnai G2 F20 200 kV Cryo-STEM) were used to investigate the morphology of MWCNTs at different stages of preparation. MWCNT-covered meshes were loaded directly into the SEM for observation and did not require any special coating. As for TEM imaging, a 3 mm diameter circle was punched out of the MWCNT-covered mesh. These samples could be loaded directly in the TEM. In order to observe the effect of sonication on MWCNT-PPE:X, a droplet of nanofluid was deposited onto a TEM grid (lacey formvar stabilized with carbon on copper mesh, Ted Pella) and left to dry completely in air before imaging.

3.2.4 Light absorption spectroscopy

Tadros [95] identified the main studies required to fully characterize a suspension of particles in a liquid medium. First, it is necessary to investigate the solid/liquid interface at the molecular level. This involves identifying the structure of water molecules, ions, other particles and solutes (surfactants, polymers, etc.) around a given particle. The best tool for such studies are computer simulations. However, knowledge of all forces at play is incomplete and models available do not accurately describe atoms and the molecules they form. Furthermore, computer power is a limitation when it comes to analyzing systems

with hundreds of water molecules (such as a system with one CNT surrounded by liquid water). Zeta potential measurements, one of the most popular instruments to assess particle stability, provide information on the electrostatic double layer around the particles, but can only give a qualitative assessment of the suspension's stability. This tool also only probes particles in suspension and cannot quantify the material that has sedimented. Second, to properly characterize a suspension of particles, it is necessary to acquire information about its behavior upon standing. In such studies, researchers must characterize the size of the particles and their flocculation and sedimentation rates. For large particles and dilute solutions where individual particles can be distinguished, photographs of the solution over time can be used [96]. For suspensions of smaller particles, light scattering [96] and absorption are the most popular tools and when measured over time, can provide information about the amount of material settled and still in suspension.

Visible light absorption was the method chosen here to investigate the stability of the nanofluids produced. At pre-determined intervals from the time of production of the fluid, measurements were taken with a UV-Vis spectrometer (Evolution 300, Thermo). The liquid mixtures were put in disposable polystyrene cuvettes (Fisher) with a 1 cm pathlength. The cuvettes were transparent from 400 to 800 nm. The baseline was a cuvette filled with RO water. Hordy [6] had explained that the absorbance of MWCNT nanofluids is proportional to the concentration of MWCNTs suspended in the liquid. The changes in concentration of MWCNTs in the nanofluids over time are reported as a percentage change with respect to a reference initial absorbance of the nanofluid.

3.2.5 X-ray spectroscopy

X-ray photoelectron spectroscopy (XPS) was used for analysis of the surface elemental composition of MWCNTs and PPE:X at different stages of preparation. Through deconvolution of the peaks obtained and comparison with other materials with known functional groups, it was possible to suggest potential functional groups present. However, XPS probes the first ~ 10 nm of the sample and the composition reported assumes that the volume probed is homogeneous. For MWCNTs treated by plasma grafting or with PP coatings thinner than 10 nm, the reported elemental composition represents a mixture of PP coating and intact MWCNT. Therefore, these results can only be used to track trends and compare similarly prepared samples. For these reasons, whenever the composition of the PPE:X alone was needed, a sufficient thickness of PPE:X was deposited on silicon wafers such that only the PP was probed and not the substrate.

Samples for XPS analysis were removed from their storage bags, mounted onto the sample stage and inserted into the instrument. During this process, they were exposed to ambient air for a maximum of 20 min before entering the instrument. The analysis was conducted on a Thermo ScientificTM K-AlphaTM XPS. Monochromatic Al $K\alpha$ excitation with a 400 μm X-ray spot size was used. Survey spectra and high resolution spectra of C 1s, N 1s and O 1s were recorded. A flood gun was necessary when analyzing PPE:X deposited on silicon wafers.

CasaXPS software (version 2.3.16) was used for data treatment in Chapter 6. Avantage software (version 5.956) was used for data treatment in Chapters 4, 5 and 7. They have slightly different sensitivity factors for each element, but the same procedure was used on both to deconvolute the high resolution peaks, as described in more detail in Chapter 6.

Chemical derivatization (CD) using 4-(trifluoromethyl)benzaldehyde (TFBA, 98%, Sigma-Aldrich) in conjunction with XPS was used to quantify the nucleophilic groups (such as primary amines) present on the surface of the nanotubes. Originally meant for exclusive detection of primary amines, recent investigation of the reactivity of TFBA indicates that it may react with secondary amines, imines and even other nucleophilic groups [97]. Knowing that nitrogen-rich PP coatings contain all these functional groups, all results using CD-XPS are reported as concentrations of nucleophilic groups, and not amines exclusively.

In Chapter 6, samples were treated with TFBA in a vacuum chamber at room temperature for 4 hr. In Chapter 5, samples were treated with TFBA at atmospheric pressure at 45 °C for 3 hr. Equations 3.1 and 3.2 show how the total nucleophilic group concentration, $[Nu]_T$, and their selectivity, $[Nu]_S$, (both reported as percentages) are linked to the total nitrogen concentration, where $[X]$ is the atomic percentage of a given atom, and subscripts “nd” and “d” are for the non-derivatized and derivatized samples, respectively [98].

$$[Nu]_T = \frac{[F]_d}{3[N]_d} \cdot [N]_{nd} \quad (3.1)$$

$$[Nu]_S = \frac{[F]_d}{3[N]_d} \quad (3.2)$$

For a more in-depth study of unsaturated functional groups, near edge X-ray absorption fine structure spectroscopy (NEXAFS) was performed on a HE-SGM monochromator dipole magnet beam line at the BESSY II synchrotron radiation source (Berlin, Germany). The spectra of the C, N and O K-edges were recorded. More details on data acquisition procedure and deconvolution of peaks can be found in Chapter 6.

XRD spectra of the pyrolyzed PP were taken on a Bruker D8 Discovery X-Ray Diffractometer (VANTEC Detector, Cu-Source).

3.3 Testing for applications using nanofluids

3.3.1 Destabilization and dispersion cycles

The ability to destabilize and subsequently redisperse MWCNTs by changing the pH and salinity of the nanofluid was investigated.

A 10 mL sample of nanofluid was placed in a glass cuvette (Type 93 Colorimeter Cell, FireflySci Cuvette Shop) with a 2 cm pathlength. A small magnetic stir rod and a pH electrode attached to a meter were also added. One side of the cuvette was illuminated with a compact fluorescent lamp and light transmitted through the cuvette was collected with a fiber optic connected to a portable spectrometer. The lamp was turned on for one hour before beginning experiments in order to obtain a constant output from the lamp. Each experimental run consisted of alternatively adding 300 μL of 1 M NaOH or 1 M HCl until the nanoparticles could no longer be redispersed in the liquid. Throughout each run, the pH of the mixture was recorded every second. Stirring of the mixture was kept constant to avoid changing the shearing forces affecting the size of the agglomerates formed. Figure 4.2 presents a picture of the setup.

Using Beer-Lambert's law (Equation 3.3), the transmitted light was converted to the extinction coefficient α (cm^{-1}), which is a function of concentration, c (mg L^{-1}), and the absorption coefficient, ϵ ($\text{cm}^{-1} \text{mg}^{-1} \text{L}$) of the particles.

$$-\log(I/I_o) = A = \alpha l \quad (3.3)$$

where A is the absorbance, I is the measured intensity of the transmitted light, I_o is the measured intensity of the transmitted light through the cuvette with water, and l (cm) is the path length. The results are reported in terms of the extinction coefficient $\alpha = \epsilon c$ and not with respect to c given that ϵ is unknown and could be changing with the size of the particles in the nanofluid.

To test for regeneration of samples after pH cycles or addition of NaCl, destabilized nanofluids were filtered onto nitrocellulose membrane filters (porosity 0.22 μm , 47 mm diameter, Merck Millipore). They were washed with copious amounts of RO water and the MWCNTs were scraped off the filter, transferred to a vial with water at the desired pH and sonicated for 10 min.

3.3.2 Gas sorption column

A gas sorption column was chosen to test the CO_2 absorption capacity of the MWCNT-PPE:X nanofluids. In this setup, a gas was injected at the bottom of a column filled with the absorbent material. The choice of the column dimensions were determined by the necessity of having the longest column possible to increase contact between the gas and liquid phases (thus increasing gas absorption), while still taking into account our laboratory and equipment constraints (available space, range of mass flow controllers, time required to run one experimental run, quantity of nanofluid available, etc.). The flow rates and the pore size of the filter were also chosen to ensure a homogeneous bubble flow regime with the smallest bubbles possible [99]. Bubbles formed at the gas inlet port were uniform and rose through the column at about the same velocity in a non-coalescing manner. A turbulent or churn flow had to be avoided as these flows do not provide reproducible amounts of surface area between liquid and gas phases. Furthermore, larger volumes of gas can push the liquid and the MWCNTs out of the column.

A mass spectrometer (MS) (OmniStar GSD-301 O2, Pfeiffer Vacuum) was chosen for detection of the outlet gases as it is sufficiently sensitive for these experiments and it can detect more than just CO₂ (therefore capable of detecting impurities if present).

The setup for testing CO₂ capture by MWCNT nanofluids is presented in Figure 6.1. It consists of a glass column (16 mm inner diameter, 23 cm height), a porous metallic filter (4 μm pores) at the bottom end for bubble formation and a MS at the top end for measurement of the gas composition at the outlet. In a typical experiment, the column was filled with 25 mL of the desired nanofluid. It was then purged with Ar. CO₂ was injected into the system at 10 sccm from the bottom of the column. During the absorption process, Ar was injected at the top of the liquid column at a flow rate of 80 sccm to keep a low CO₂ concentration at the top of the liquid.

Equation 3.4 was used to calculate the amount of CO₂ absorbed by the nanofluid, where $V_{CO_2}^{max}$ is the total volume of CO₂ absorbed in mL, Q_{CO_2} is the flow rate of CO₂ going into the column in mL min⁻¹, C_t is the concentration of CO₂ in the outgoing gas stream at time t , C_{max} is the maximum concentration of CO₂ in the outgoing gas stream, and t_{eq} is the time in min required to reach a pseudo equilibrium in the system. It was assumed that the CO₂ absorption process reached equilibrium when the CO₂ concentration recorded with the MS remained constant for at least ten minutes.

$$V_{CO_2}^{max} = \int_0^{t_{eq}} \frac{Q_{CO_2}(C_{max} - C_t)dt}{C_{max}} \quad (3.4)$$

3.3.3 Interaction with dyes

In order to study the interaction of MWCNT-PPE:X with dyes, methyl orange (MO) and methylene blue (MB), two sets of experiments were conducted (see Figure 7.2 for schematic).

In the first set, 5 mL of dye solution, at 25 mg L⁻¹, were mixed with 5 mL of MWCNT nanofluid. After 24 hr, the samples were centrifuged and the quantity of dye left in the supernatant was measured by visible absorption spectroscopy. Some samples were then washed to release the adsorbed dye and mixed with a fresh batch of dye solution for a second adsorption step. The adsorption capacity for the reused adsorbent was measured on the following day. The second set of experiments also started with an adsorption step but samples were then filtered and washed in order to determine the amount of dye adsorbed that could be released. More details can be found in Chapter 7.

The design of these experiments was based on similar studies found in the literature. Given the very small yield of MWCNTs from our in-house t-CVD method, it was necessary to work with smaller volumes of solution to match adsorbent concentrations reported by others which typically range from 100 to 1000 mg L⁻¹. With a volume of 10 mL, MWCNT concentration obtained for the experiments described here would typically be between 50 and 150 mg L⁻¹. During adsorption, most researchers put their samples on automated shakers to ensure the adsorbent stays in contact with the dye solution and does not sediment. Using our MWCNT-PPE:X which are stable and well dispersed in water, it was not necessary to shake the samples. After the adsorption period, in order to separate the solid adsorbent from the dye solution, one of two methods is usually reported in the literature: filtration or centrifugation. In this work, it was necessary to centrifuge samples, given that the filters adsorbed too much of the dyes (especially MB) leading to errors in the measured adsorbed dye. Furthermore, although MWCNTs agglomerated on a filter can be redispersed in a liquid, a portion of the solid material is usually lost. Given the small initial quantity of MWCNTs used in each sample, if samples had been filtered, there wouldn't have been sufficient material to reuse them for another adsorption cycle. For this reason, adsorption and reuse experiments were done using centrifugation and release experiments were done separately on filters.

The dye concentration, c (mg L^{-1}), in the supernatant was measured by visible absorption spectroscopy (Evolution 300, Thermo) using Beer-Lambert's law (see Equation 3.5). Table 7.2 presents the wavelength and the absorption coefficient, ϵ ($\text{cm}^{-1} \text{mg}^{-1} \text{L}$), used for the two dyes. The path length of the cuvette, l , was 1 cm and A was the absorbance measured.

$$A = c\epsilon l \quad (3.5)$$

The adsorption capacity, q_t (mg g^{-1}), was then calculated according to Equation 3.6

$$q_t = \frac{(c_0 - c_a)V}{m} \quad (3.6)$$

where c_0 and c_a are, respectively, the initial and final dye concentration after adsorption, V is the volume of solution in L and m is the mass of MWCNTs in g.

The percentage of dye released, d , is calculated as shown in Equation 3.7

$$d = \frac{c_r V_r}{(c_0 - c_a)V} = \frac{m_r}{m_a} \quad (3.7)$$

where c_r is the concentration of dye released and V_r is the known volume of water used to release the dye. In other words, d is the fraction of mass of dye released, m_r , with respect to the mass of adsorbed dye m_a .

CHAPTER 4

Effect of water and pH on PPE:X and MWCNT-PPE:X

4.1 Preface

This chapter presents an article that was published in *Plasma Processes and Polymers*. The complete citation of the published article is:

Jorge, L., Girard-Lauriault, P. L. & Coulombe, S. (2017). pH-Reversible Destabilisation-Dispersion of MWCNTs Coated with Functional Plasma Polymer Films in Water, *Plasma Process. Polym.*, 14 (11), 1700026.

The work was planned, executed, analyzed and written by L. Jorge (Ph.D. candidate). TEM images were taken by Dr. David Liu. Dr. P.-L. Girard-Lauriault and Dr. S. Coulombe were responsible for supervision of the work and reviewing of the manuscript.

One of the main goals of this thesis was to develop stable aqueous dispersions of plasma treated MWCNTs. This chapter establishes this first step by presenting the two PP coatings chosen, how they interact with water and how treated MWCNTs are stabilized in different aqueous conditions. It is shown that the pH of the mixture determines if MWCNTs agglomerate or remain dispersed, confirming that the PP coatings carry a charge which will be useful for future applications.

pH-Reversible Destabilisation-Dispersion of MWCNTs Coated with Functional Plasma Polymer Films in Water

Larissa Jorge, Pierre-Luc Girard-Lauriault, Sylvain Coulombe

Plasma Processing Laboratory, Department of Chemical Engineering, McGill University,
Montreal, QC, Canada H3A 0C5

Abstract

The stability in water of multi-walled carbon nanotubes (MWCNTs) coated with N- or O-rich plasma polymers (PPs) is investigated at different pH values. MWCNTs are coated with PPs by plasma enhanced chemical vapor deposition of ethylene and ammonia or ethylene and carbon dioxide. MWCNTs coated with N-rich PP in water at pH 12 exist as agglomerates that readily sediment, whereas the agglomerate size decreases and suspension stability increases as the pH changes from 10 to 2. The reverse effect is observed for MWCNTs coated with O-rich PP which form agglomerates at pH 2, but are stable from pH 4 to 12. By switching the pH of suspensions containing either one of these coated MWCNTs, it is possible to cycle through destabilisation and dispersion steps.

4.2 Introduction

Molecules or nanoparticles with reversible properties when exposed to light or pH changes are of great interest for a number of applications such as gas detection [100], control of chemical reactions [101] or filtration of pollutants [102]. For example, agglomeration of solid material is a common technique for pollutant removal in wastewater. Typically, particles that have adsorption sites for the targeted pollutant are added to the liquid mixture.

Agglomeration of the formed composite facilitates its removal through settling or centrifugation. It is therefore desirable to design particles that can agglomerate at the desired conditions for pollutant removal and then be redispersed for reuse by switching the properties of the mixture. Given their large surface area, multi-walled carbon nanotubes (MWCNTs) with tailored surface modifications have been shown to be efficient adsorbers of a variety of molecules [103, 104] and could make good candidates for this application. Production of aqueous MWCNT nanofluids, which are engineered stable dispersions of MWCNTs in water, usually requires surface modifications of the MWCNTs using acid treatments [105] or surfactant wrapping [106].

Wet chemical methods to treat CNTs usually involve many steps and reagents. Simplifying the functionalization procedure while still having control over the nature of functional groups added to the CNT's surface is possible through plasma treatment methods. In particular, plasma enhanced chemical vapor deposition (PECVD) of gaseous precursors has been shown to add functional organic coatings on CNTs. Monomers such as heptylamine [107], acrylonitrile [108], and ethylene glycol [50] have been plasma polymerised over CNTs for enhanced adhesion with other polymers and stability in aqueous nanofluids. Similar coatings can also be obtained through the reaction of a hydrocarbon with a heteroatom-containing gas that provides the desired functional groups. In our previous work [109] (Chapter 6), multi-walled CNTs (MWCNTs) were plasma treated with ethylene and ammonia. The organic coating produced had nitrogen functional groups, such as amines, capable of capturing CO_2 but also stabilising the MWCNTs in the nanofluid.

MWCNTs' stability and agglomeration state in a host fluid are determined by their surface electrostatic potential as well as their capacity to undergo Lewis acid-base reactions with the surrounding molecules as described in the extended DLVO theory of van Oss [43].

Changing the pH of the solution interferes with the charged double layer around the MWCNTs and their electron donicity or accepticity character. Both processes have an impact on the MWCNTs' interactions between themselves and with the host fluid. By changing the pH of their nanofluid, Han et al. [110] could control the agglomeration and dispersion of negatively charged DNA-wrapped CNTs with ethylenediamine (EN). Xie et al. [105] observed that acid-treated CNTs, which had carbonyl and carboxylic acid groups at the surface, were less stable at pH 2 than at pH 6 and higher. Wang and Chen [111] also showed that by wrapping pH-responsive polymers around CNTs, they could control their agglomeration. In a similar fashion, the choice of functional groups on plasma polymers (PPs) deposited on MWCNTs has an impact on their stability. The overall charge of the PP in water can be tuned from positive to negative [38] through the amount of electron donating and electron accepting groups present, typically N and O groups respectively. Thus MWCNT-PP with different PPs are expected to be stable and well dispersed at different pH values.

In this contribution, we present MWCNT-PP aqueous nanofluids with controllable stability and agglomeration through pH adjustments. The composition of a nitrogen-containing and an oxygen-containing PP is studied after exposure to water. Each PP studied causes the MWCNTs to agglomerate and destabilise at a different extreme of the pH range, providing a simple method to tune the nanofluid's stability for the conditions of the desired application. Furthermore, it is possible to use this property to cycle multiple times through destabilisation and dispersion steps of the MWCNTs by changing the pH of the nanofluid.

4.3 Experimental method

4.3.1 Nanofluid synthesis

MWCNTs were produced by thermal chemical vapor deposition (t-CVD) in a semi-batch process at atmospheric pressure following a procedure similar to the one described by

Hordy et al. [10]. Figure 4.1 shows a picture and a schematic of the reactor which consists of a tubular furnace, a quartz tube, a gas injection port and a loading chamber for sample transfers. The loading chamber allows for quick insertion and removal of samples without the need to cool down the furnace. Pieces ($3.5 \times 7 \text{ cm}^2$) of 316 grade stainless steel (SS316) mesh (400 mesh, TWP Inc.) were loaded onto a quartz boat. The boat was slid in the quartz tube to the hot section of the furnace which was kept at 700°C . After allowing for oxidation of the sample for 2 min in ambient air, the quartz tube and loading dock were purged with argon, Ar (99.999%, all gases were purchased from MEGS Specialty Gases) until the oxygen concentration dropped to less than 0.5%. A mixture of acetylene, C_2H_2 (99%, dissolved in acetone), at 68 sccm and Ar at 600 sccm was then injected in the quartz tube for 2 min. Samples were left for two more minutes at high temperature to allow for MWCNT growth under Ar atmosphere. The boat with the samples was then slid back into the loading chamber and removed after a 5 min cool down period. Before adding the next batch of mesh pieces for MWCNT synthesis, the load chamber was left open for 3 min for ambient air to refill the quartz tube. MWCNTs produced in this manner have a mean diameter of $\sim 30 \text{ nm}$ and are 3 to $5 \mu\text{m}$ in length [12].

PPs were deposited onto MWCNT-covered stainless steel meshes using a low-pressure capacitively-coupled RF (13.56 MHz, continuous) glow discharge described in detail elsewhere [92]. Samples were positioned directly on the live electrode (8.7 cm in diameter), and gases were injected through a showerhead positioned 4 cm above this electrode. A mixture of either ammonia, NH_3 (99.99%), and ethylene, C_2H_4 (99.70%), (PPE:N) or carbon dioxide, CO_2 , and C_2H_4 (PPE:O) was injected into the chamber with the flow rate values reported in Table 7.1. Sample treatment was conducted at a pressure of 80 Pa (600 mTorr) and a power of 35 W for 4 min for PPE:N and 20 min for PPE:O. The PECVD system as well as the freezer (kept at -40°C) for sample storage are located inside a N_2 -filled glovebox

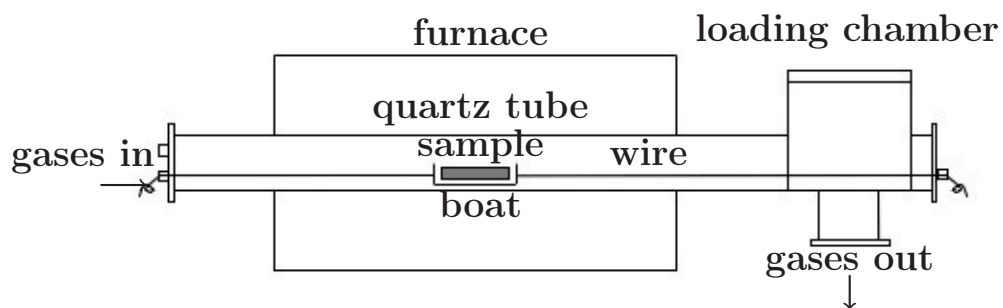
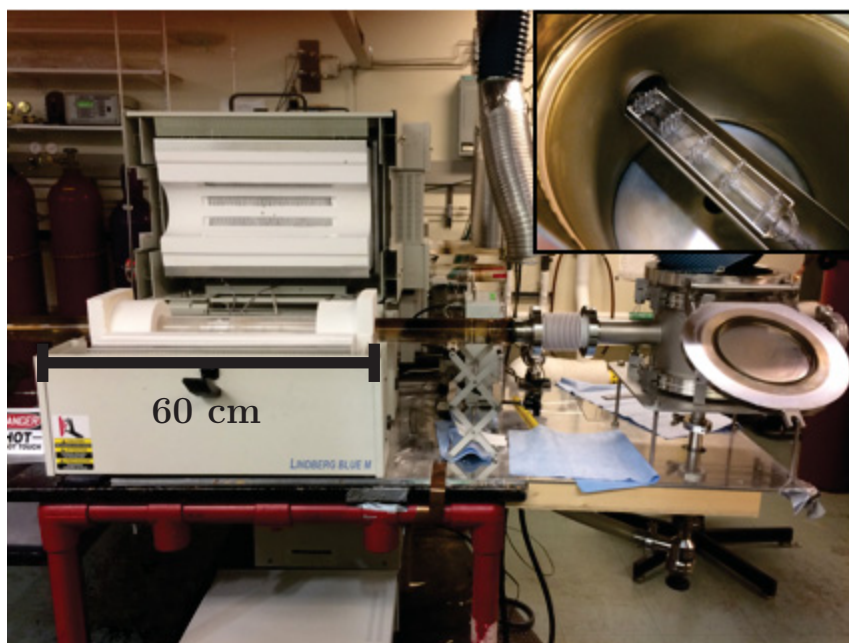


Figure 4.1: Picture (top) and schematic (bottom, not to scale) of semi-batch t-CVD setup for MWCNTs synthesis. Insert shows the boat inside the loading chamber.

(O₂ concentration < 0.1ppm, model MB200B, MBraun). Therefore, after plasma treatment, samples were not exposed to air until they were removed from the glovebox to be used in a nanofluid or analysed. This minimizes the ageing process of the PPs [112].

Reverse-osmosis (RO) water was used as the host liquid for the nanofluid. Solutions of 1 M HCl (Fisher), 1 M NaOH (Aldrich) or NaCl (Fisher) were prepared and used to adjust the pH and ionic strength of the fluid when necessary. Vials each containing one PP-coated MWCNT-covered SS316 mesh and 10 mL of pure RO water or water at different pH values were put in an ultrasonic bath for 10 min. This process breaks off the MWCNTs from the growth substrate. The meshes were then removed from the vials and disposed of. The nanofluids were stored at room temperature. The concentration of MWCNTs in the nanofluids was between 50 and 100 mg L⁻¹. When required, the NaCl concentration of the nanofluid was adjusted between 0.001 and 0.5 M.

4.3.2 Characterization of MWCNT-PPE:X

TEM

To investigate the morphology of MWCNT-PPE:X samples, a transmission electron microscope was used (TEM, Tecnai G2 F20 200 kV Cryo-STEM). The effect of sonication in water on the PP coating was also observed by drying a small droplet of nanofluid onto a carbon coated TEM grid.

Table 4.1: Gas flow rates during plasma polymer deposition.

Sample name	$Q_{\text{NH}_3 \text{ or } \text{CO}_2}$ (sccm)	$Q_{\text{C}_2\text{H}_4}$ (sccm)
MWCNT-PPE:N	10	10
MWCNT-PPE:O	30	4

XPS

The chemical composition of the PP coatings as-synthesized and after exposure to water was analysed by X-ray photoelectron spectroscopy (XPS). For these experiments, the PPs were deposited on MWCNTs and Si wafers. The comparison between the PPs on these two substrates is necessary due to the different thickness of the PP before and after water treatment. Given that only the photoelectrons generated in the first 10 nm of the sample can reach the detector, if the PP coating is thinner, then the signal detected by the XPS comes from the PP as well as the substrate under it. MWCNTs being made of carbon and oxygen, it is not possible to distinguish them from the PP coating. However, on Si wafers, if silicon is not present in the survey spectrum, then it is a good indication that only the PP coating is being detected. For the analysis of coated MWCNT samples after exposure to water and sonication, 10 mL of nanofluid were allowed to dry in air. The powder was then collected and fixed on copper tape for analysis. Si wafers coated with PPs were sonicated in water for 10 min, removed from water and left to dry in air. The Si wafers with the remaining PP coating were then analysed under the XPS.

The analysis was conducted on a Thermo ScientificTM K-AlphaTM+ XPS and monochromatic Al K α excitation with a 400 μ m X-ray spot size was used. Survey spectra were recorded at a pass energy of 200 eV and 1 eV resolution and a 90° take-off angle. High resolution spectra of C 1s, N 1s and O 1s were recorded at a pass energy of 50 eV and 0.1 eV resolution. The Avantage software (version 5.956) and the following relative sensitivity factors for C, N and O, 1, 1.676 and 2.881, were used to analyse the spectra. Error bars presented on the atomic composition represent one standard deviation between three samples prepared on different days. Peaks were fitted with a Tougaard background and components with a mixed Gaussian/Lorentzian peak shape, following a procedure described by Girard-Lauriault et al. [112].

UV-Vis spectrometry

To study the stability of nanofluids, UV-Vis absorbance spectra (Evolution 300, Thermo) of the nanofluids were taken (from 400 to 700 nm) in disposable polystyrene cuvettes (Fisher). The baseline was a cuvette filled with RO water. As explained by Hordy [6], the absorbance of the nanofluids has been shown to have a linear dependency on the amount of dispersed MWCNTs. Agglomeration and sedimentation, which are indicators of MWCNTs' stability, cause a reduction in the effective concentration of particles in suspension and thus a decrease in absorbance. The stability change of the nanofluid after different treatments is reported as a percentage change in absorbance of the fluid.

pH cycling

The capacity to adjust the extent of destabilisation of the MWCNTs by changing the nanofluid's pH was studied. A stirring bar and a pH electrode (model 13-620-287A, Accumet) connected to a meter (pHBasic+ series, Sartorius) were placed in a cuvette (Type 93 Colorimeter Cell, FireflySci Cuvette Shop) with dimensions 24x55x56 mm³ and a path-length of 20 mm, as seen in Figure 4.2. A compact fluorescent lamp was positioned behind the cuvette. A fiber optic cable (M22L01, Thorlabs) connected to a portable spectrometer (OceanOptics USB2000) was positioned in front of the cuvette, aiming 0.5 cm above the bottom of the cuvette. The light transmitted through the cuvette was recorded at a wavelength of 546 nm, a mercury line, which was the lamp's wavelength with strongest intensity.



Figure 4.2: Setup for pH cycling experiments.

Using Beer-Lambert's law (Equation 7.1), the transmitted light was converted to the extinction coefficient α (cm^{-1}), which is a function of concentration, c (mg L^{-1}), and the absorption coefficient, ϵ ($\text{cm}^{-1} \text{mg}^{-1} \text{L}$) of the particles.

$$-\log(I/I_o) = A = \alpha l \quad (4.1)$$

where A is the absorbance, I is the measured intensity of the transmitted light, I_o is the measured intensity of the transmitted light through the cuvette with water, and l (cm) is the path length. The results are reported in terms of the extinction coefficient $\alpha = \epsilon c$ and not with respect to c given that ϵ is unknown and could be changing with the size of the particles in the nanofluid.

Before beginning experiments, the lamp was turned on for an hour in order to attain a steady output intensity. The rotating speed of the stirring bar was kept constant for all experiments, as shearing forces affect the size of the agglomerates formed and thus the amount of light transmitted. Stirring was maintained throughout the duration of the experiment. The pH of the mixture was recorded every second. For each experiment, a 10 mL sample of

nanofluid was loaded into the cuvette. Then, 300 μL of NaOH and HCl 1 M solution were alternatively injected into the nanofluid.

4.4 Results and discussion

4.4.1 Morphology and composition of MWCNT-PPE:X

Figure 4.3 shows MWCNTs after plasma polymerization. PPE:N forms a uniform coating of about 8 nm in thickness on most MWCNTs, with the maximum thickness being 14 nm and minimum, 4 nm. Whereas for PPE:O on MWCNTs, the coating thickness can be as low as 3 nm and as high as 60 nm. Furthermore, the PPE:O coating thickness varies over the length of each MWCNT. It decreases along the length of the MWCNT from the tip towards the SS mesh (as shown in the red ellipse). It also varies along the MWCNT circumference (as shown in the right-hand part of Figure 4.3b). The difference in morphology of the two PPs must be due to different surface reactions during synthesis. The probability of a species produced in the plasma to be added to a growing coating depends on its ability to adsorb and migrate on the surface to a suitable reaction site, the density of available reaction sites and the competing reactions of etching and desorption [113]. It seems clear that for PPE:N, species reaching the surface can easily move on the MWCNT to form a coating with uniform thickness. Good conformality in plasma processes using ammonia was also observed for the deposition of silicon nitride [114]. On the other hand, the species formed in the C_2H_4 and CO_2 plasma must have low mobility on the PP coating causing them to accumulate on certain parts of the MWCNTs and yielding uneven coatings. It is also known that C_2H_4 and CO_2 mixtures produce oxygen fragments which can etch away some of the PP coating or scavenge a portion of the radicals formed in the plasma. Yasuda calls it the “poisoning effect” of oxygen-containing molecules which reduces the deposition rate of the PP as well as affect the nature of the species that get deposited [19].

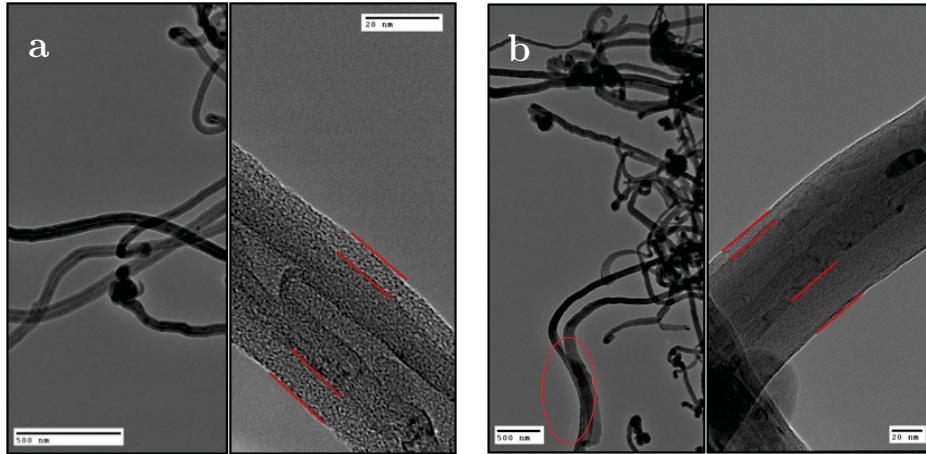


Figure 4.3: TEM images of (a) MWCNT-PPE:N and (b) MWCNT-PPE:O. Straight red lines highlight the plasma polymer around the MWCNT.

The coated MWCNTs used in this work are to be dispersed in water. It is known that PPs can be soluble in water [115, 116, 117]. To confirm the presence of the PPs on MWCNTs after sonication in water, TEM images and XPS spectra of the nanofluid's solid content after complete drying in air were collected. As can be seen in Figure 4.4, most of the PPE:X coating has been removed leaving behind an uneven coating of PP of thickness less than 1 nm. The XPS analysis of MWCNT-PPE:N confirms that there is still nitrogen present albeit the quantity is much lower than with the original sample (Figure 4.5). This can be explained by the fact that only the photoelectrons generated in the first 10 nm of the sample can reach the detector. The as-synthesized PP coating thickness being around 10 nm as mentioned previously, only information about the PP is obtained for those samples. However, when analysing the MWCNT-PPE:X samples after exposure to water, the XPS spectrum obtained contains information about the PP coating and MWCNT under it. The chemistry of PPE:X before and after water exposure was investigated on Si wafers. Although the substrate might influence the PP chemistry in the first few nanometers of the coating [118, 119, 120], especially when comparing "hard" substrates (such as silicon wafers) and "soft" substrates (such as MWCNTs), these differences are typically small. Therefore, the impact of water on

the chemistry of Si-PPE:X should be similar on MWCNT-PPE:X. As shown in Figure 4.5, Si-PPE:N changes slightly after water exposure. For PPE:N, the presence of dangling bonds and nitrogen functional groups capable of undergoing oxidation can be responsible for oxygen incorporation. As for Si-PPE:O, its composition did not change significantly after water exposure (Figure 4.6).

Comparison of the PPs' C 1s peak shape also reveals information on the changes in structure of the material. Figure 4.7 shows the C 1s peaks with fitted components and their respective area percentages for both PPs deposited on Si. The peaks were fitted with four components, C1 to C4, and their properties are presented in Table 4.2. Given the complexity of the PP, it is not possible to assign a single functional group to each component. Table 4.2 suggests possible groups for each one, knowing that C1 is usually attributed to C-C, C=C and C-H bonds and then components from C2 to C4 correspond to increasingly electronegative functional groups. We can observe a decrease in C2 and an increase in C3 after exposure of PPE:N to water, which could be due to the oxidation of nitrogen functional groups on the PP. As for PPE:O, water led to a slight decrease in the C2 component and an increase in C1 with respect to the original PPE:O.

Insets in Figure 4.7 show the N 1s peak for as-synthesized PPE:N and O 1s peak for as-synthesized PPE:O. In PPE:N, the N 1s peak at 399 eV is usually assigned to imines,

Table 4.2: Characteristics of XPS fitted components for C 1s [21, 38, 39, 112].

Component name	BE (eV)	FWHM (eV)	Chemical assignment	
			PPE:N	PPE:O
C1	285	~1.5	C-C, C=C, C-H	same as PPE:N
C2	286	~1.5	C-N, C=N, C*-C≡N, C-O	C*-COOR (R = C or H)
C3	287	~1.5	C≡N, C*-O-C=O	COR, C=O
C4	288.5	~2.5	N-C-O, N-C=O, C=O	COOR

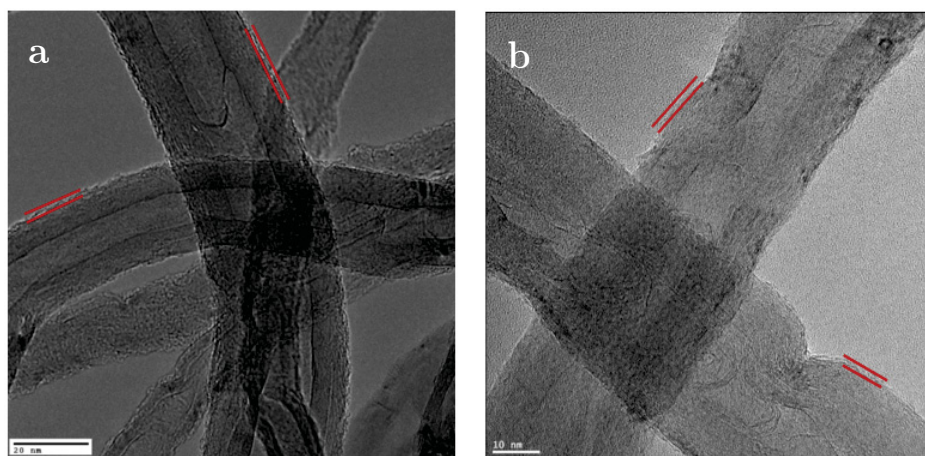


Figure 4.4: TEM images of (a) MWCNT-PPE:N and (b) MWCNT-PPE:O after sonicating in water. Straight red lines highlight the plasma polymer around the MWCNT.

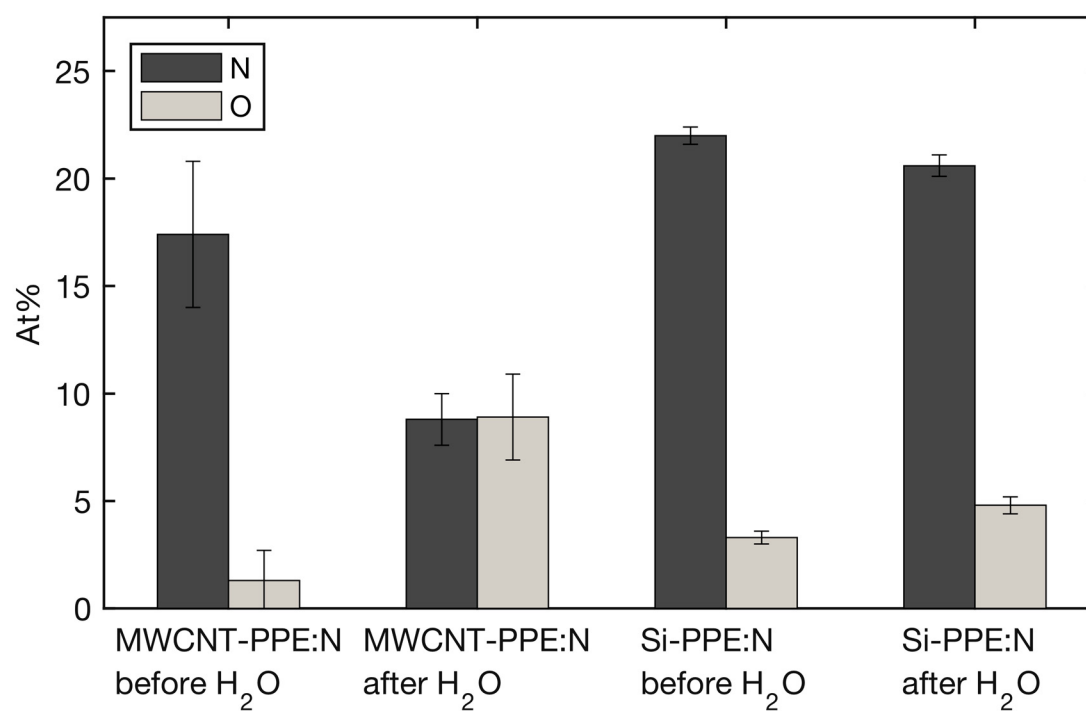


Figure 4.5: Elemental composition of MWCNT-PPE:N and Si-PPE:N before and after sonication in water.

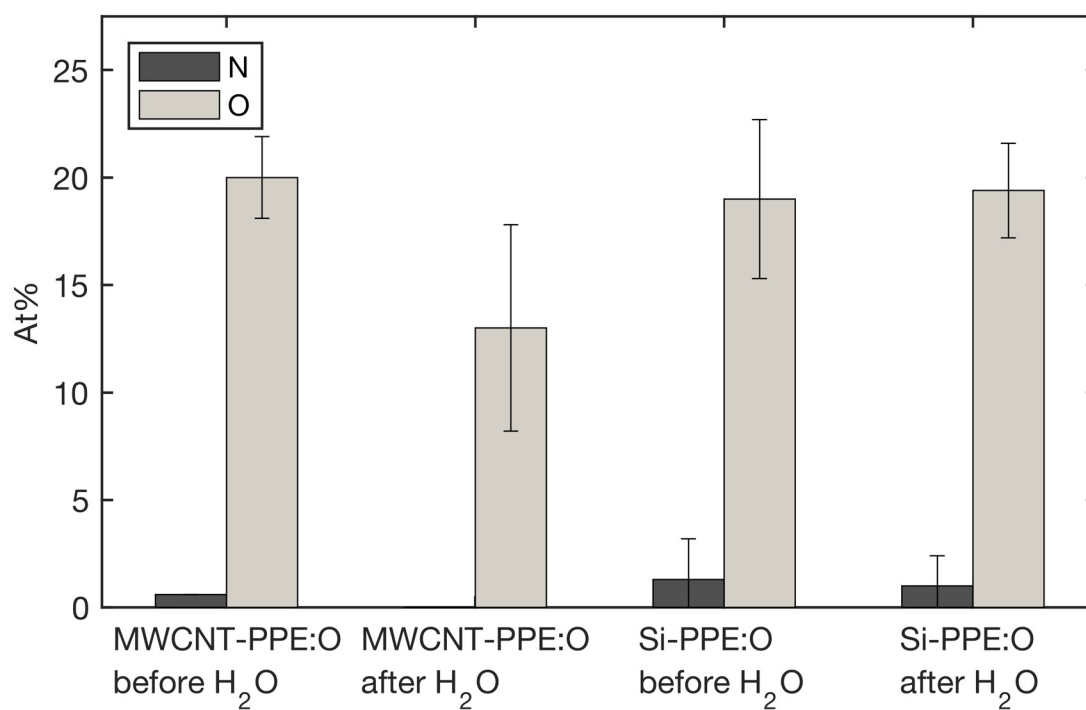


Figure 4.6: Elemental composition of MWCNT-PPE:O and Si-PPE:O before and after sonication in water.

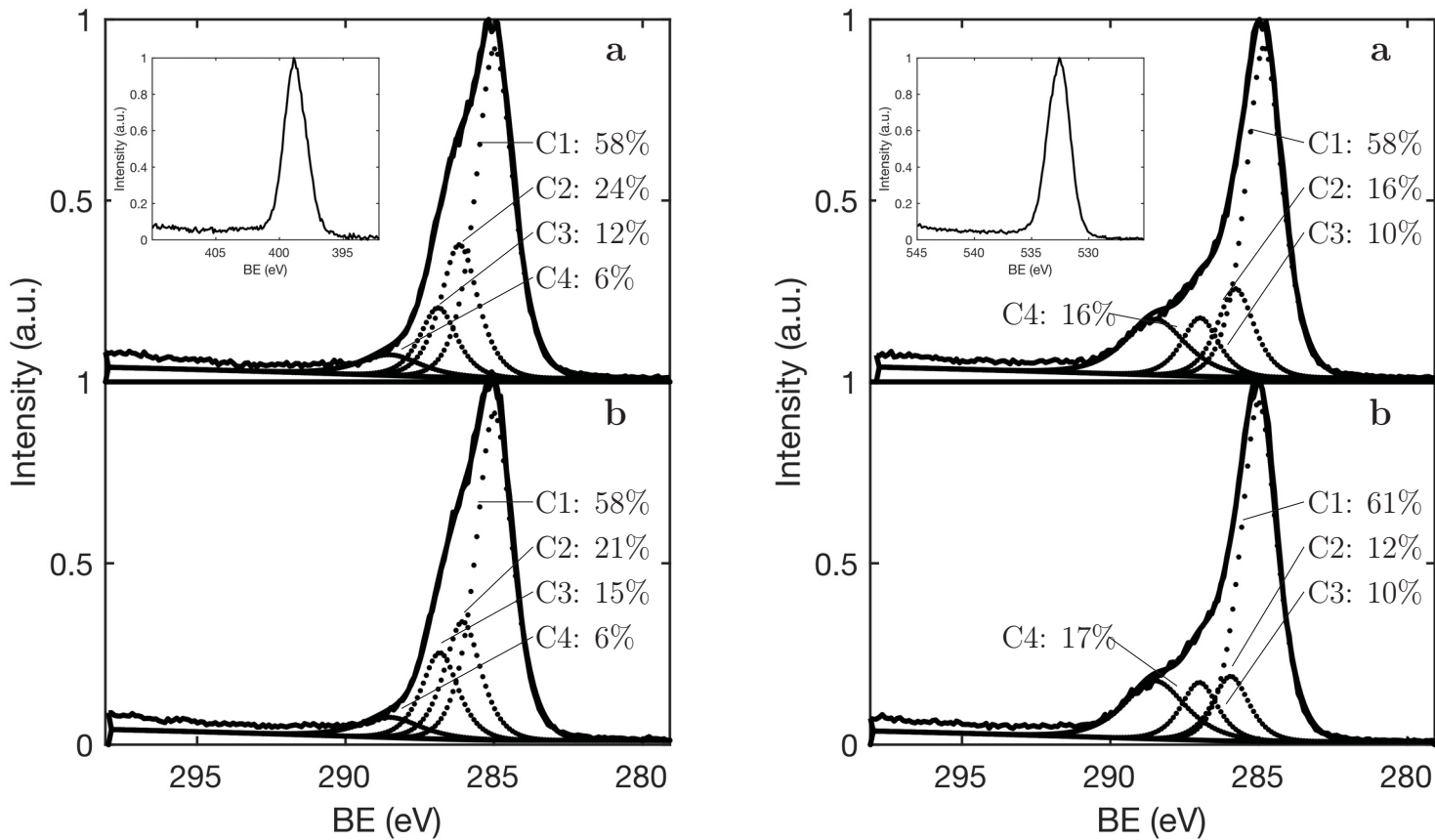


Figure 4.7: Experimental and fitted C 1s peaks for (a) as-synthesized Si-PPE:X, (b) after sonication, PPE:N on the left, PPE:O on the right. The component areas are also given as percentages. Insets show the high resolution N 1s peak for PPE:N (left) and O 1s peak for PPE:O (right).

C=N, amides, N-C=O, and amines, -NH₂ [32]. In PPE:O, the O 1s peak at 532 eV is typical of systems that contain contributions from single (between 532 and 533 eV) and double (between 531 and 532 eV) bonded oxygen to carbon [121, 122, 123].

4.4.2 Effect of pH on the stability of nanofluids

Figures 4.8 and 4.9 show the percentage loss of suspended MWCNT-PPE:X in aqueous nanofluids at different pH one week after production. All nanofluids were stable immediately after synthesis, except for MWCNT-PPE:N at pH 12 and MWCNT-PPE:O at pH 2. These two nanofluids presented visible agglomerates less than an hour after sonication. After one week, the agglomerates were completely settled leaving a perfectly clear solution on top. We can observe that for nanofluids containing MWCNT-PPE:N (Figure 4.8), changing the pH from 2 to 6 did not have a significant impact on the stability. Stability begins to be altered at pH ≥ 8 and complete sedimentation is observed at pH 12 as mentioned previously. We believe that the higher stability at acidic pH is due to the formation of charged groups such as amines which change from -NH₂ to -NH₃⁺ but also to the electron donicity of other nitrogen groups [124]. These functional groups act as Lewis bases in water and in an acidic environment preferentially attract water molecules and not other MWCNTs, therefore stopping agglomeration. At pH 12, PPE:N does not form charged groups and becomes in essence hydrophobic.

The reverse trend is observed for nanofluids with MWCNT-PPE:O (Figure 4.9). In this case, the PP contains carboxylic acid groups which, at pH 12, may be charged, going from -COOH to -COO⁻. Furthermore, in this case, oxygen-containing functional groups may act as good Lewis acids and therefore interact in a stabilising way with water at high pH. However, contrary to MWCNT-PPE:N, we did not observe a significant change in stability from pH 4 to 12. Xie et al. had also observed that for MWCNTs treated with acids, and

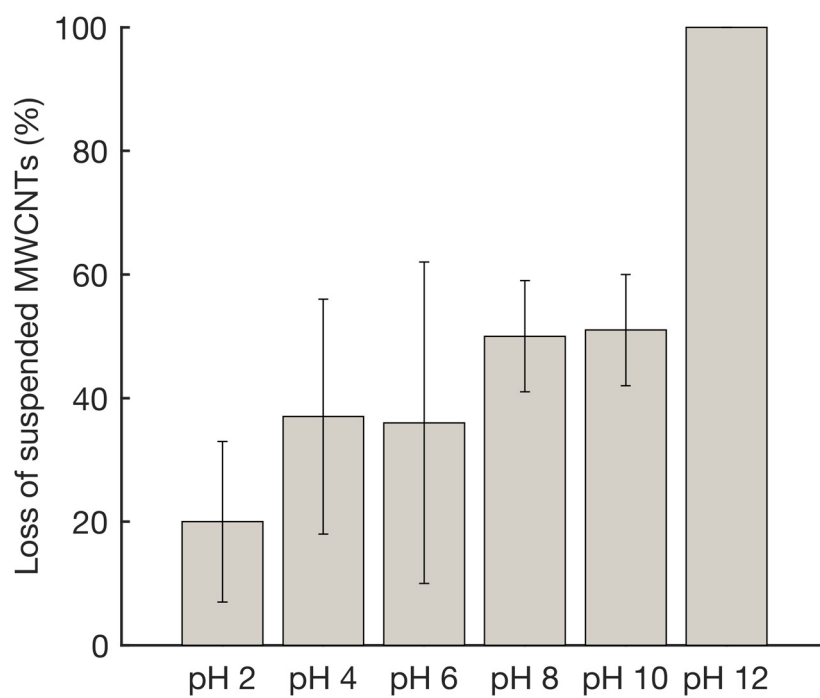


Figure 4.8: Stability of nanofluids prepared with MWCNT-PPE:N at different pH over a period of one week.

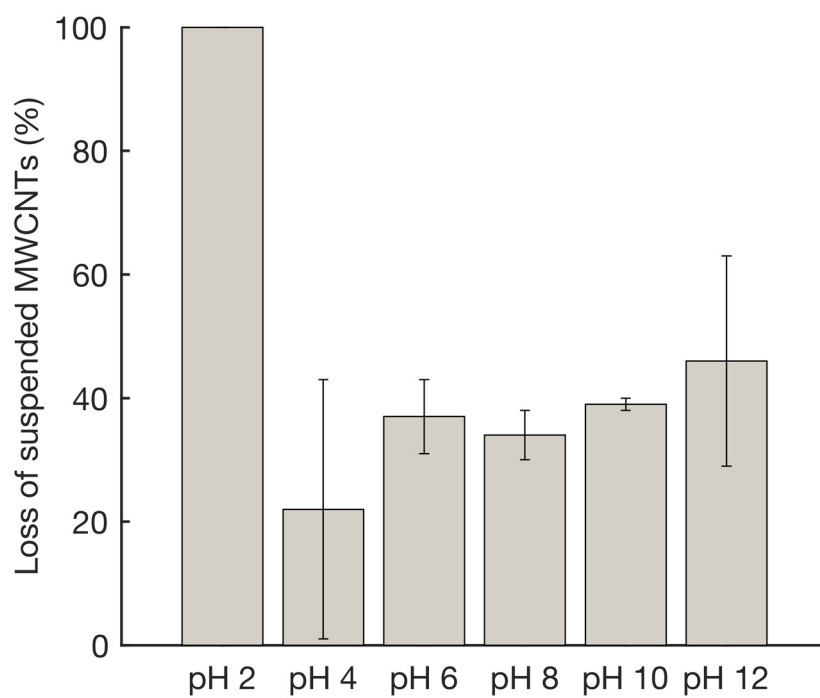


Figure 4.9: Stability of nanofluids prepared with MWCNT-PPE:O at different pH over a period of one week.

thus also containing oxygen functional groups, the nanofluid stability increased as the pH of the fluid was increased from 2 to 6 and then remained constant up to pH 12 [105].

Hordy et al. [47] had shown that grafting oxygen functional groups onto MWCNTs also led to stable suspensions at boiling temperature in different fluids. A simplified boiling experiment was conducted with these MWCNT-PPE:X in aqueous suspensions at different pH. Figure 4.10 compares the loss of stability of nanofluids prepared at the indicated pH or with pure RO water which is typically at a pH around 5.5. Adjusting the pH of the nanofluid containing MWCNT-PPE:N to a value of 2 makes the nanofluid more stable at boiling temperature. This correlates well with the trend seen previously where this nanofluid becomes increasingly more stable at room temperature going from pH 12 to 2. As for the nanofluid containing MWCNT-PPE:O, there is no significant change in its stability by increasing the pH to 12.

4.4.3 Destabilisation and dispersion of MWCNT-PPE:X through pH cycling

As shown before, a strongly basic nanofluid causes MWCNT-PPE:N to destabilise through the formation of agglomerates and a strongly acidic nanofluid has the same effect on MWCNT-PPE:O. However, the formation of these agglomerates is a reversible process. Figures 4.11 and 4.12 show that it is possible to cycle through at least seven destabilisation/dispersion steps by switching the pH from 2 to 12 and vice versa. The baseline decrease with time observed for both samples is due to the dilution of the nanofluid with each injection of NaOH or HCl, but also to the irreversible loss of MWCNTs through attachment to the stir bar and electrode or deposition in stagnation points in the cuvette.

When allowing the destabilisation step to run for longer times (Figure 4.13), it is possible to observe two processes. The first one, which takes between 130 to 160 s to complete, includes the mixing of the added acid or base and the agglomeration of the MWCNTs.

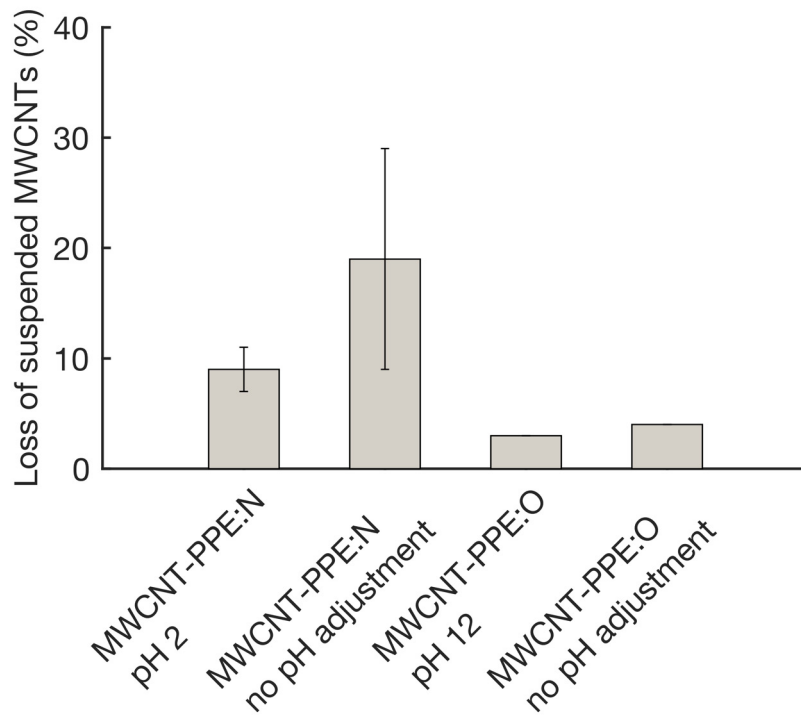


Figure 4.10: Stability of nanofluids prepared with either MWCNT-PPE:N or MWCNT-PPE:O at different pH after boiling for 3 min.

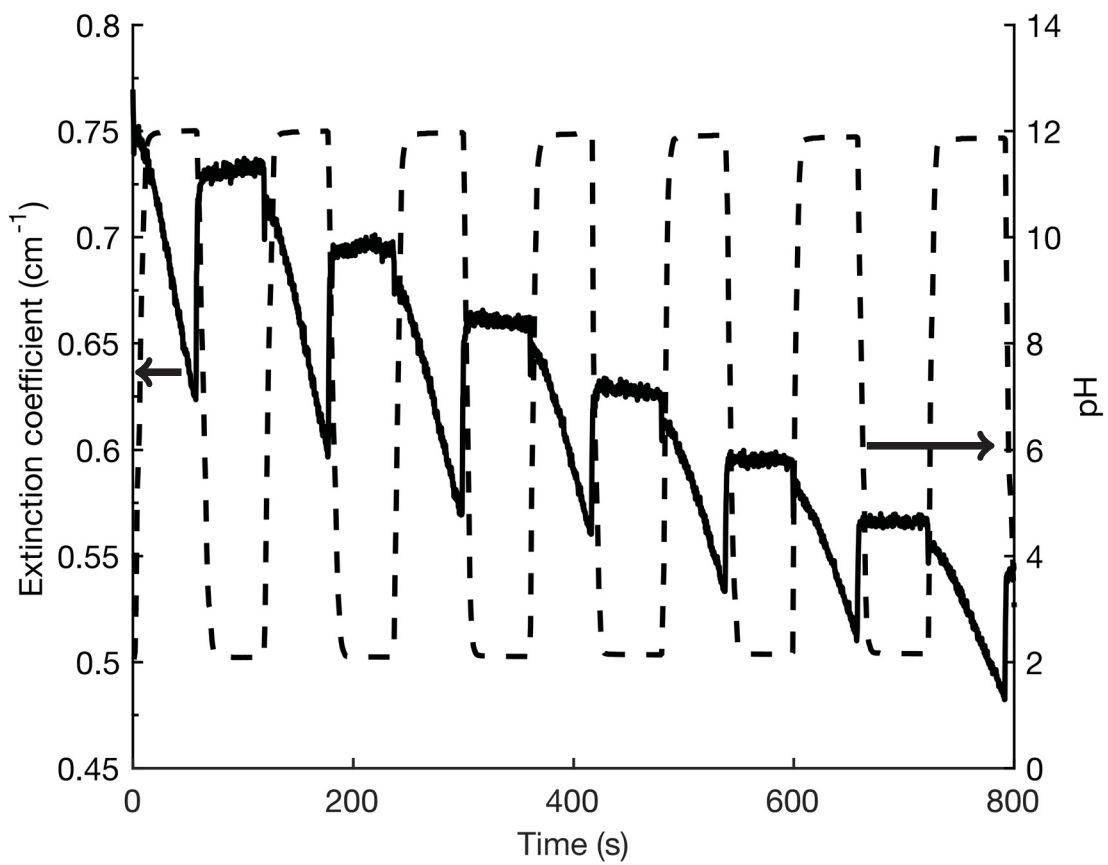


Figure 4.11: Cycles of destabilisation (decrease in extinction coefficient) and dispersion (increase) of a MWCNT-PPE:N nanofluid.

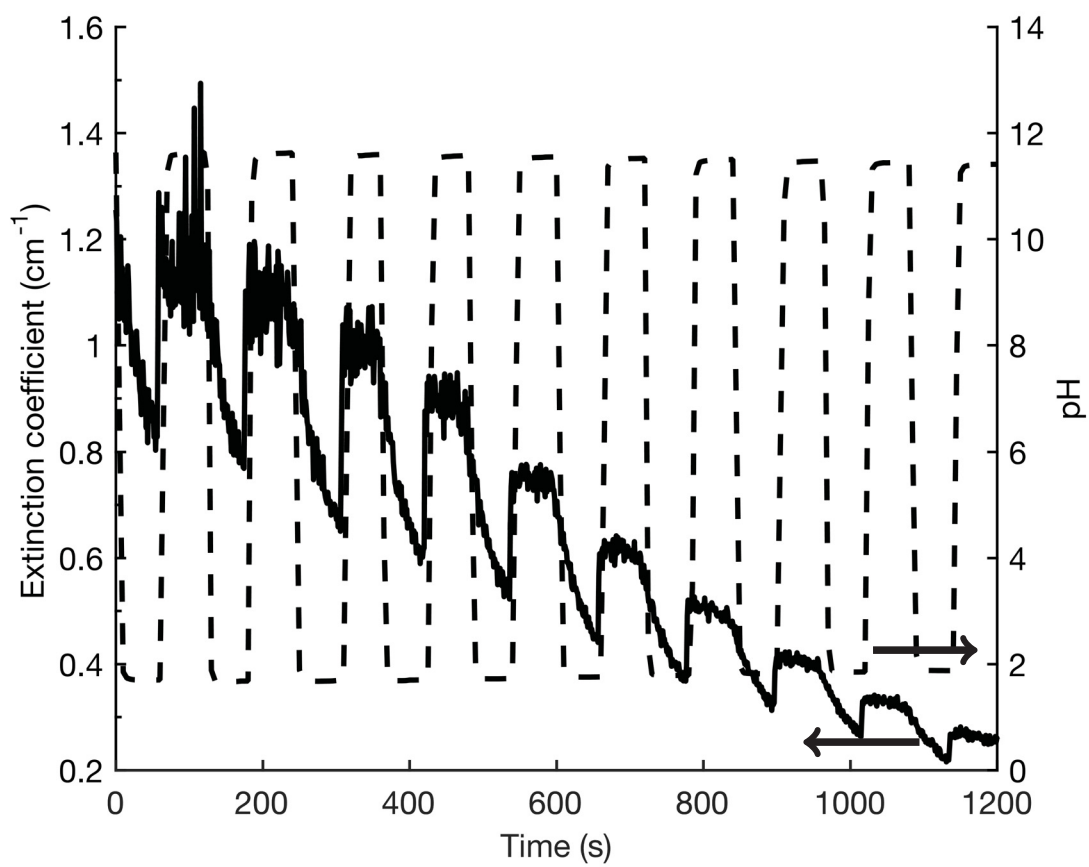


Figure 4.12: Cycles of destabilisation (decrease in extinction coefficient) and dispersion (increase) of a MWCNT-PPE:O nanofluid.

The pH switch from 2 to 12 (or vice versa for MWCNT-PPE:O) is completed after the first 40 s of this step. Although this first process seems to follow a first order mechanism, it is difficult to model it as both the concentration of agglomerates and their absorption coefficients are changing, and this data is not readily available. After the agglomerates have reached an equilibrium size, a second much slower process occurs where agglomerates deposit in stagnation points such as the corners of the cuvette and to the left of the stir bar as seen in the insert of Figure 4.13. This second process follows a first order mechanism that depends on the rate that the suspended agglomerates travel to the stagnation points [125].

It was also observed that the total concentration of ions added through the injections of NaOH and HCl had an impact on the MWCNTs' stability over time. After cycling the pH, the nanofluids were adjusted back to pH 2 for MWCNT-PPE:N or 12 for MWCNT-PPE:O, stirring of the nanofluid was stopped and they were stored at room temperature. Although the nanofluids were black (indicating that the MWCNTs were well dispersed) right after the cycling experiment, all MWCNTs had sedimented to the bottom of the vials in less than 24 hr. It is known that the pH as well as the ionic strength of the fluid have an impact on the stability and agglomeration of nanoparticles [43, 46]. By covering the surface of MWCNTs, ions from salts such as NaCl decrease the surface potential of the MWCNTs. Thus, there is less repulsion between the MWCNTs which leads to agglomeration [43]. In order to find the maximum permissible concentration of NaCl that does not affect the MWCNTs' stability, nanofluids with MWCNT-PPE:N or PPE:O and no pH adjustment were prepared and different quantities of NaCl were added. Their stability was then observed over time. When the concentration of NaCl was equivalent to 0.001 mol L^{-1} or less, the nanofluids were stable for at least 4 days. However, above 0.01 mol L^{-1} , the MWCNTs sedimented after one day, and above 0.5 mol L^{-1} , formation of agglomerates occurred immediately after salt injection. When comparing these salt concentrations to the concentration of NaCl in

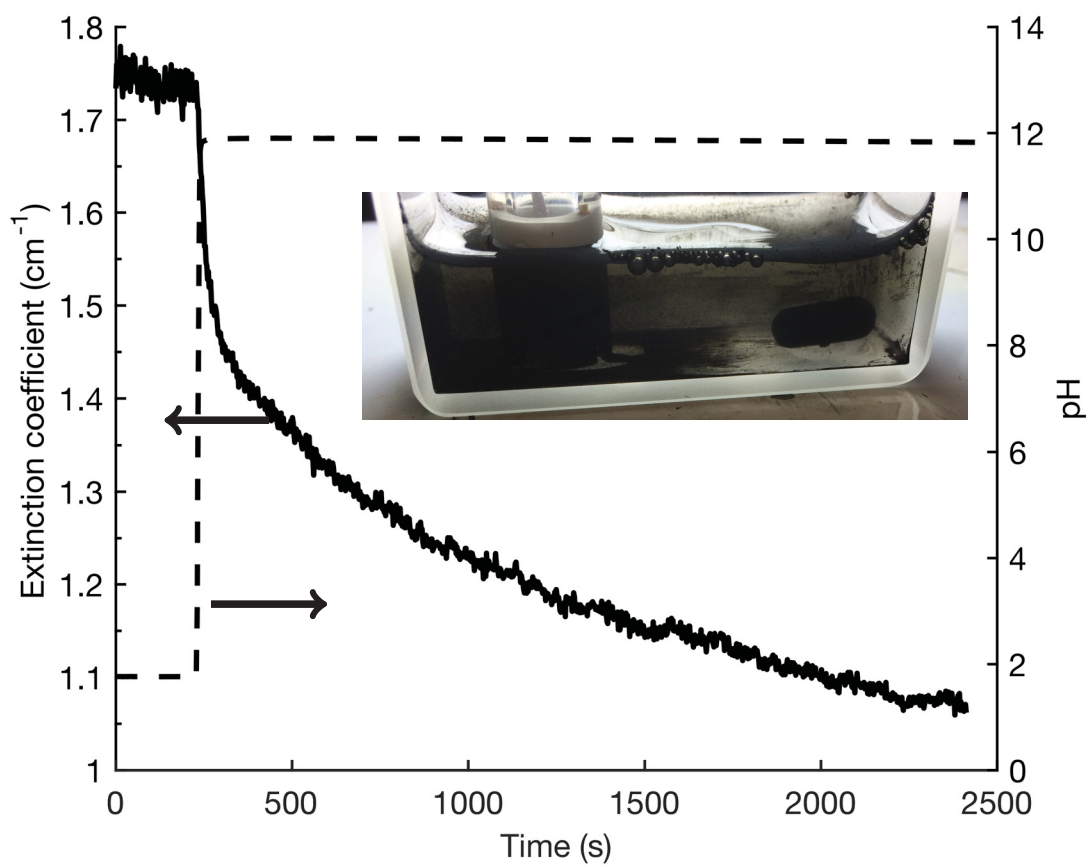


Figure 4.13: Loss of MWCNT-PPE:N in suspension at pH 12 over a time span of 40 min. Insert shows nanofluid at the end of the experiment.

the nanofluid after one cycle of pH changes, it is possible to understand why the nanofluids are destabilised. After a single cycle (i.e. injection of 300 μL of 1 M NaOH and then 300 μL of 1 M HCl for MWCNT-PPE:N), the NaCl concentration in the nanofluid is around 0.03 mol L^{-1} . This is more than 0.001 mol of NaCl L^{-1} , and as mentioned previously, a stable suspension of MWCNTs cannot be maintained regardless of the nanofluid's pH. Nevertheless, given that the ions from NaCl are not covalently attached to the MWCNTs, they can be removed. The unstable dispersions with high ionic strength can be regenerated by filtering the MWCNTs and washing with RO water. After redispersion in a solution at the appropriate pH (2 for MWCNT-PPE:N and 12 for MWCNT-PPE:O), the MWCNTs are once again stable for more than two weeks.

4.5 Conclusion

A simple and short PECVD treatment was used to deposit a PP coating containing either nitrogen or oxygen functional groups onto MWCNTs. Both PPs were shown to undergo only slight compositional changes after exposure to water.

The presence of these PPs on MWCNTs was shown to be sufficient to alter their chemistry and render them responsive to pH changes. MWCNTs coated with nitrogen-containing PP were unstable and agglomerated at pH 12 due to a decrease in charged functional groups on the MWCNT surface and decrease of electron donicity of nitrogen groups. The reverse effect was observed for MWCNTs coated with oxygen-containing PP which have carboxylic groups that are not charged at pH 2. The agglomerates formed can be broken by switching the pH to a range where the functional groups are charged. Destabilisation and dispersion cycles can be repeated at least seven times. However, complete redispersion is not achieved after each cycle. After destabilisation of the solution, agglomeration of the CNTs occurs over a period of 130 to 160 s until an equilibrium agglomerate size is reached. These agglomerates

then slowly deposit or attach to the available surfaces. The presence of more than 0.01 mol of NaCl L⁻¹ in the nanofluid also causes complete destabilisation even if the pH is amenable to dispersion. Washing the MWCNTs with RO water is sufficient to remove the added salt and regenerate stable suspensions of MWCNTs, therefore potentially enabling their use and reuse in applications of pollutant removal through agglomeration.

CHAPTER 5

Addition of APTS and TEPA on MWCNTs

5.1 Preface

This chapter presents an article submitted for publication in *Thin Solid Films*. The complete citation of the article is:

Jorge, L., Coulombe, S., & Girard-Lauriault, P. L.. (2018). APTS and TEPA Adsorbed on MWCNTs for Stable Water and Ethanol Nanofluids. *Thin Solid Films*.

The work was planned, executed, analyzed and written by L. Jorge (Ph.D. candidate). TEM images were taken by Dr. David Liu. Dr. S. Coulombe and Dr. P.-L. Girard-Lauriault were responsible for supervision of the work and reviewing of the manuscript.

In this chapter, the study of the PP coatings focuses on their structure and stability with respect to temperature. Since they are not damaged significantly up to 200 °C, it is therefore possible to expand the toolbox for modifying the surface chemistry of the MWCNTs to include vapor functionalization. With this technique, molecules with useful functional groups, such as tetraethylenepentamine (TEPA) which carries amine functional groups, can be adsorbed onto MWCNTs coated with oxygen-rich PP. Stable dispersions of these TEPA-treated MWCNTs were prepared at pH 5.5 and at pH 2, confirming the presence of TEPA onto the MWCNTs.

APTS and TEPA Adsorbed on MWCNTs for Stable Water and Ethanol Nanofluids

Larissa Jorge, Sylvain Coulombe, Pierre-Luc Girard-Lauriault

Plasma Processing Laboratory, Department of Chemical Engineering, McGill University,
Montreal, QC, Canada H3A 0C5

Abstract

Two solvent-free methods were combined to modify the surface of multi-walled carbon nanotubes (MWCNTs) with a high concentration of amine functional groups. First, an oxygen-rich plasma polymer (PP) coating was deposited on the MWCNTs. Second, either tetraethylenepentamine (TEPA) or (3-aminopropyl)triethoxysilane (APTS) were adsorbed on the surface of the MWCNTs by vapor functionalization. Results from thermogravimetric analysis of the PP coating reveal that it is composed of small oligomers, some of which are volatile at temperatures as low as 150 °C. Nevertheless, the PP coating can withstand the temperature required for vapor functionalization of the two chosen molecules. The APTS treated MWCNTs are not stable when dispersed in water, but stable in ethanol. As for TEPA treated MWCNTs, it is shown that they are stable in water at pH 2 and 5.5. This confirms that TEPA is adsorbed on the PP coating and completely shields this coating, allowing for the amines to stabilize the MWCNTs in an acidic environment.

5.2 Introduction

Aqueous carbon nanotube (CNT) nanofluids are extensively being studied for their use in drug delivery [126], dye and gas adsorption [66, 79], optical absorption of solar energy [47] and many other applications. CNTs cannot be used as-synthesized since, in their pristine state, they are hydrophobic and have limited interactions with other molecules. However, a

variety of chemical and physical methods can be used to modify their surface for the desired application. In particular, amine functionalized CNTs are highly sought after for carbon dioxide capture, epoxy polymer blends and capture of anionic dyes.

Wet chemical methods of adding amine functional groups onto CNTs include halogenation followed by amide bond formation with a diamine molecule [127, 128], or wrapping the nanotube with a polymer such as polyallylamine hydrochloride [129] to name only a few examples. However, difficulty in properly separating agglomerates of pristine CNTs in a solvent leads to partial functionalization of their surface. Given that CNTs are usually synthesized in dry conditions, it is advantageous to treat their surface also in a liquid free environment. The multi-walled CNTs (MWCNTs) used in this study are grown by thermal chemical vapor deposition (t-CVD) on a stainless steel (SS) mesh. Their surface chemistry is then modified by plasma enhanced chemical vapor deposition (PECVD), without having to expose the MWCNTs to any liquids.

To produce plasma polymer (PP) coatings containing amine functional groups, gas mixtures of a hydrocarbon with nitrogen, N_2 [115], or ammonia, NH_3 [29, 30, 31, 109], are typically used. However, achieving high quantities of and selectivity for amine groups on these coatings is difficult. First, a compromise must be made between nitrogen quantity in the PP coating and coating stability. Coatings with up to 40 N at% [29] have been produced, but they were soluble in water. In order to obtain a stable coating that remains on the substrate, lower quantities of nitrogen must be incorporated, which also means less amine groups. Second, the plasma breaks down the gaseous molecules and their recombination is random, thus not leading only to amines but to a variety of nitrogen containing functional groups. And although some parameters can be varied to preserve the original molecule, i.e. using lower power or pulsed plasma treatments, these changes usually cause a decrease in the coating's stability [25, 55].

It is possible to increase the density of the desired functional groups by vapor functionalization. The substrate is exposed to molecules carrying multiple functional groups, one of which is the desired amine and another one which can be used to covalently bind the molecules to the substrate's surface. Tetraethylenepentamine (TEPA) and (3-aminopropyl)-triethoxysilane (APTS) were chosen in the present study because they have a sufficient vapor pressure and are stable at the required reaction temperature. TEPA has two primary amine groups and may react with aldehydes [97] which can be found on oxygen-rich PP coatings [38, 130]. APTS has one primary amine and three ethoxy groups, which may react with hydroxyl groups [131, 132, 133] also found on oxygen-rich PP coatings [37, 38].

In this contribution, we combine plasma polymerization and vapor functionalization to produce amine-functionalized MWCNTs. First, the thermal stability of an oxygen-rich PP coating is presented using data obtained by thermal gravimetric analysis (TGA) to ensure it can withstand the temperature required for vapor functionalization. Then, composition analysis shows that APTS and TEPA are added onto the MWCNTs by vapor functionalization. Finally, we show that it is possible to disperse the functionalized MWCNTs in ethanol or water and obtain stable suspensions.

5.3 Experimental method

5.3.1 Synthesis of PPE:O and MWCNT-PPE:O

MWCNTs were produced in-house by t-CVD following a procedure described elsewhere [37] (Chapter 4). In short, a 316L stainless steel (SS) mesh (400 mesh series, TWP inc.), 3.5 x 7 cm² in size was inserted in a quartz tube (122 cm in length, 5.5 cm inner diameter) positioned inside a tube furnace. Air was removed from the tube by purging it with argon (99.999%, all gases were purchased from MEGS Specialty Gases). When the temperature inside the furnace reached 700 °C, acetylene, C₂H₂ (99%, dissolved in acetone), was injected

at 68 sccm for 2 min. The samples were then allowed to cool down under argon atmosphere before being exposed to air and stored in Petri dishes at room temperature.

PP coatings were deposited using a low-pressure capacitively-coupled RF (13.56 MHz, continuous) glow discharge described in detail by Kasparek et al. [92]. Carbon dioxide, CO₂ (99.99%), and ethylene, C₂H₄ (99.70%), were used to deposit an oxygen-rich coating named PPE:O hereafter. The flow rate of CO₂ was 30 sccm and 4 sccm for C₂H₄. The pressure was held at 80 Pa and RF power at 35 W. Deposition times were 60 min on glass Petri dishes (8.9 cm in diameter) in order to obtain sufficient material for TGA and 20 min on MWCNTs. The PECVD being located inside a nitrogen-filled glovebox (O₂ concentration < 0.1 ppm, model MB200B, MBraun), when samples were taken out of the PECVD, they were not exposed to air and therefore were not oxidized. Samples were stored in sealed bags (oxygen transfer rate 2.2 cc m⁻² day⁻¹, Duropac) filled with nitrogen. They were then used or analyzed in less than a week.

MWCNT-PPE:O samples were further modified by vapor functionalization with APTS or TEPA (both from Sigma-Aldrich). The samples were secured on the inner wall of a clean glass jar. A layer of glass beads lined the bottom of the jar. A volume of 150 μ L of TEPA was dripped onto the glass beads. For APTS treatments, 50 μ L was added to the jars. The jars were closed in a nitrogen-filled atmosphere, and put in an oven at 150 °C for 60 min for TEPA treatment, and 80 °C for 60 min for APTS treatment. After allowing the jars to cool down, they were opened in air and samples were either transferred to Petri dishes and stored in nitrogen-filled bags until further analysis, or immediately transferred to vials containing either reverse osmosis (RO) water or anhydrous ethanol. The pH of water was adjusted using 1 M HCl solution. It was measured using a pH meter (pHBasic+ series, Sartorius) equipped with a combination electrode (model 13-620-287A, Accumet). The vials were sonicated for 10 min to break off the MWCNTs from the mesh and disperse them into the liquid.

5.3.2 Characterization of PPE:O and MWCNTs

TEM

MWCNT-PPE:O still attached to the SS mesh were imaged using a transmission electron microscope (TEM, Tecnai G2 F20 200 kV Cryo-STEM). Images were taken of samples before and after heating at 150 °C for a period of 60 min.

TGA/DSC

The structure of the PPs was investigated by TGA and differential scanning calorimetry (DSC). The material deposited onto the glass Petri dishes was scraped from the substrate and loaded into alumina cups in the instrument (TGA/DSC 1 Star System, Mettler Toledo). Analysis was conducted under a flow of 60 mL min⁻¹ of N₂ to limit thermooxidative processes, at a heating rate of 10 °C min⁻¹ from 40 to 550 °C. The mass of the material remaining in the cup was recorded throughout the heating process, yielding the TGA curve. The DSC curve represents the difference in heat input between the reference cup (empty alumina cup) and the sample cup required to bring both cups to the same temperature.

XPS and CD-XPS

X-ray photoelectron spectroscopy (XPS) was used to determine the elemental composition of the samples. The analysis was conducted on a Thermo ScientificTM K-AlphaTM XPS. Details on how spectra were obtained and analyzed are presented in our previous publication [37] (see Chapter 4).

For chemical derivatization XPS (CD-XPS), samples were treated with 4-(trifluoromethyl) benzaldehyde (98%, TFBA, Sigma-Aldrich) in a similar fashion as described above for TEPA and APTS. Samples were treated for 3 hours, at 45 °C [29, 115]. Equations used to calculate

the total concentration of nucleophilic groups, $[\text{Nu}]_T$, and the selectivity of these groups with respect to all nitrogen containing groups, $[\text{Nu}]_S$, were presented in a previous publication [109] (see Chapter 6).

5.4 Results and discussion

5.4.1 Plasma polymer structure

The thermal behavior of the PP coating was investigated in order to better understand its structure. The TGA spectrum of PPE:O was compared to low density polyethylene, LDPE, and PPE, produced by plasma polymerization of ethylene gas only (Figure 5.1). The TGA curve shows that PPE:O starts losing mass at low temperature. Under nitrogen atmosphere, about 70% of the PPE:O's mass evaporates while the rest is converted into char after 500 °C. This behavior is very different from LDPE's which is thermally stable up to 400 °C and leaves no residue after 500 °C. PPE, which is a PP but containing no heteroatoms, is positioned between LDPE and PPE:O. These observations reflect the expected growth processes for LDPE and PPs.

In classic polymerization, all monomers react at the same unsaturated bond and form the same repeating bond with other monomers. By choosing the correct synthesis conditions and nature of monomers, it is possible to control the chain length size, and more specifically to produce very long chains by limiting the production of molecules that can cause chain termination (radical scavengers, impurities, etc.). When exposed to high temperature, polymers like LDPE undergo random chain scission, during which the breakage of bonds in the chains leads to the formation of a variety of smaller alkanes or alkenes [134, 135]. These compounds are volatile and thus, no char residue is left after the TGA experiment.

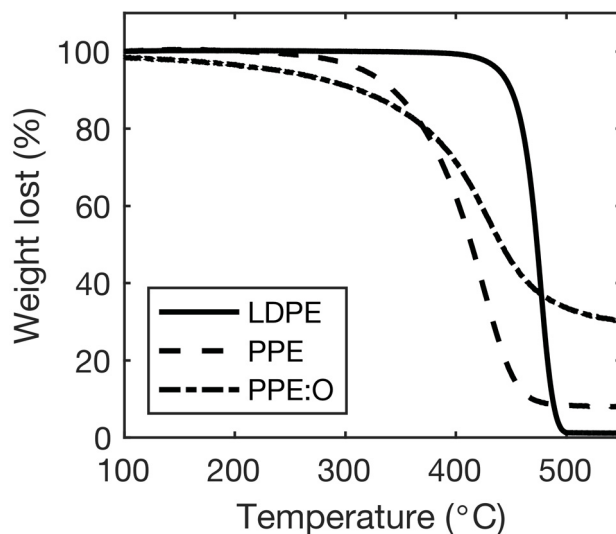


Figure 5.1: TGA spectra of LDPE, PPE and PPE:O.

During plasma polymerization, however, a variety of reactive species are generated. Table 5.1 lists the main possible breakdown products for CO_2 and C_2H_4 . Such products may then recombine with each other in the gas phase or on the substrate, leading to films that contain esters and carboxyls, COOR , hydroxyls and ethers, COR or carbonyls, $\text{C}=\text{O}$ in PPE:O [37]. It is not possible to control all the reactions happening in the plasma volume. Therefore, the formation of long carbon chains is rare and generation of oligomers is favored. These oligomers are volatile at low temperature.

Larger connected networks are formed when UV photons and ions bombarding the surface generate sites for crosslinking. Given that PPE:O formed char at high temperature, it suggests the presence of crosslinks. Although char formation mechanisms are still not

Table 5.1: Possible breakdown products (ions, radicals or excited species) of gases in the plasma.

C_2H_4	CO_2
C_2H_2 [136, 137]	CO [39, 41]
C_2H_6 [137]	O [39, 41]

completely elucidated, it has been observed that crosslinked networks and unsaturated bonds tend to form more char. These structures favor cyclization of the moieties in the coating instead of monomer and oligomer formation [134, 138, 139]. These cyclical structures can then undergo carbonization to finally form a black char residue [140].

DSC measurements confirm that the structure of the PPs is very different from that of actual polymers such as LDPE. DSC spectra reveal characteristic endothermic (negative heating rate) or exothermic (positive heating rate) reactions as the samples are heated as shown in Figure 5.2. For polymers, deviations from a straight line may indicate a melting point or a single degradation mechanism. LDPE has a melting point [25] as seen in Figure 5.2a whereas PPs don't. Also, due to their random structure [141], PPs decompose through a number of processes until complete pyrolysis whereas LDPE decomposes mainly by random scission [142] thus explaining the dip in Figure 5.2b as well as the sharp loss of mass around 450 °C.

5.4.2 Effect of heat on MWCNT-PPE:O

The TGA/DSC results presented above indicate that even very low temperature, such as the one used here for vapor functionalization, should have an impact on the structure of PPE:O. Therefore, TEM images of MWCNT-PPE:O (see Figure 5.3) were obtained after being heat treated at 150 °C for an hour. PPE:O forms a very uneven coating on MWCNTs [37], and therefore no changes of the coating thickness were observed.

Figure 5.4 shows the nitrogen and oxygen contents of MWCNTs and MWCNT-PPE:O before and after heat treatment at 150 °C in nitrogen-filled atmosphere using the same setup as the one used for vapor functionalization. The coating composition does not change significantly. The small changes observed are probably due to normal variations of the coating from sample to sample.

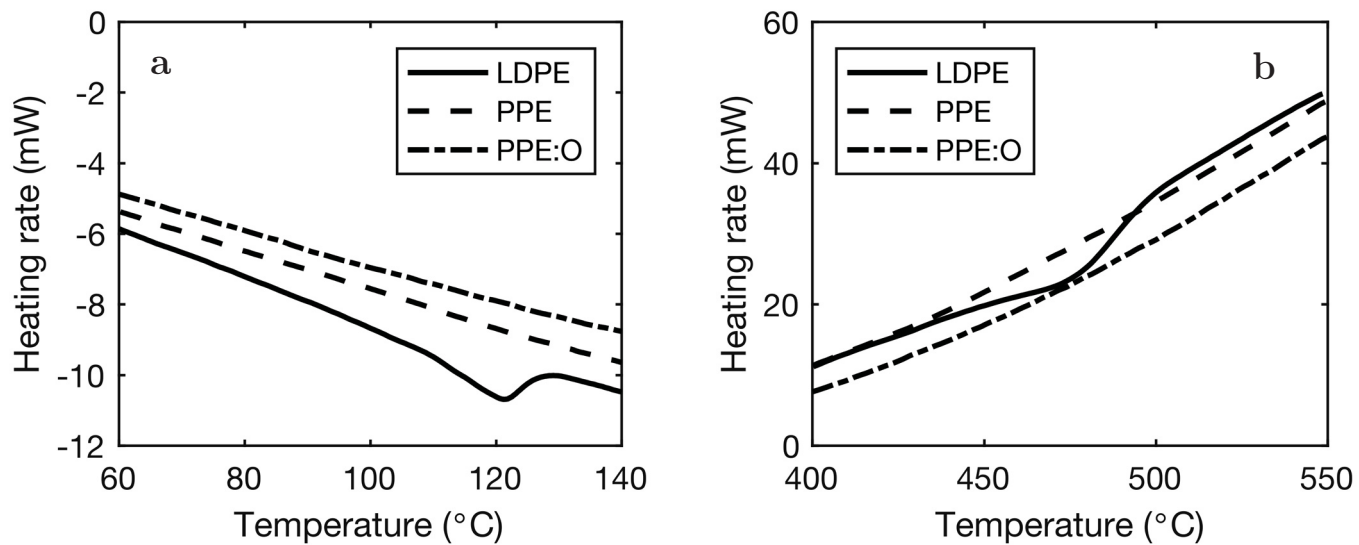


Figure 5.2: DSC spectra of LDPE, PPE and PPE:O.

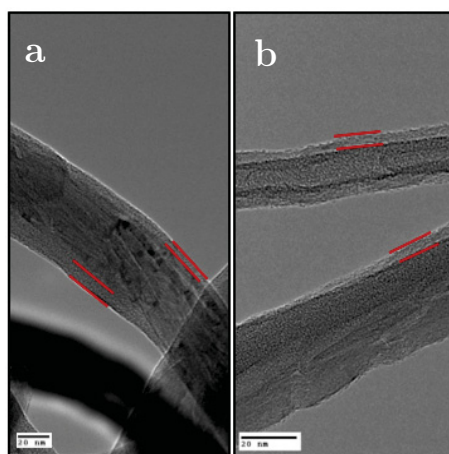


Figure 5.3: TEM images of MWCNT-PPE:O before (a) and after (b) heating at 150°C for one hour in argon.

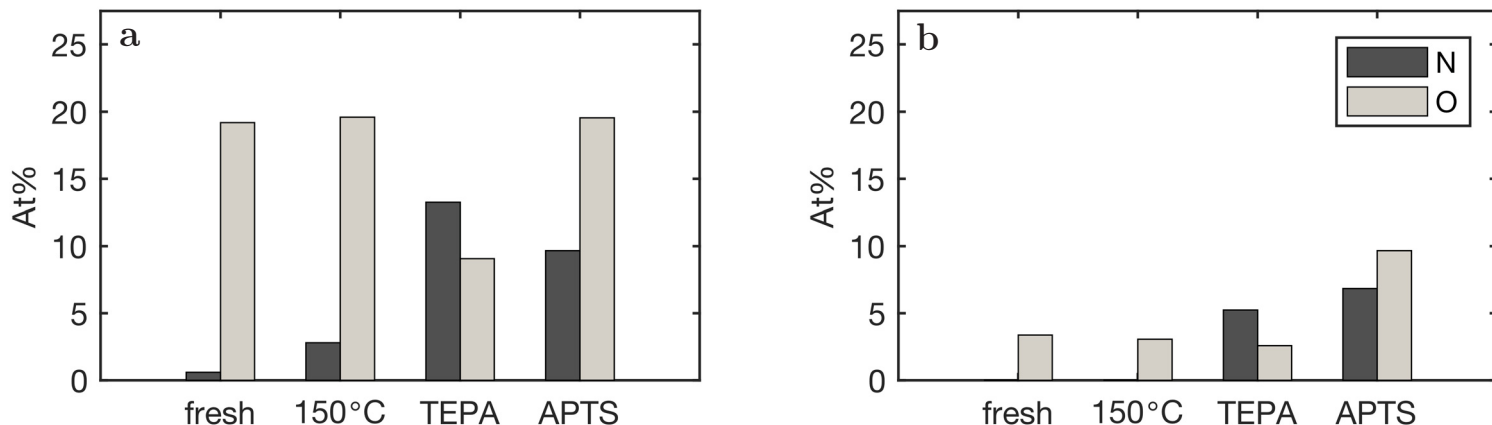


Figure 5.4: Composition of (a) MWCNT-PPE:O and (b) MWCNT, freshly prepared, after heating at 150 °C, after vapor functionalization with TEPA at 150 °C or APTS at 80 °C.

These results show that the PPE:O coating on MWCNTs is not affected significantly by the conditions for vapor functionalization and it should thus provide anchoring sites for APTS or TEPA.

5.4.3 APTS on MWCNT and MWCNT-PPE:O

Figure 5.4a shows the composition of MWCNT-PPE:O samples after vapor functionalization with APTS. The same treatment procedure was performed with bare MWCNT samples as well to determine if the PPE:O coating does have an impact on the attachment of APTS (see Figure 5.4b). An increase in nitrogen content at the surface of both samples is observed. The presence of Si (for which the only source is APTS) at ~ 7 at% for MWCNT-PPE:O-APTS and ~ 5 at% for MWCNT-APTS confirms the presence of APTS on the surface.

Although XPS has shown that the molecules are present on the MWCNT samples, the next step was to determine how APTS was attached to the substrate and if functional groups present on PPE:O could indeed covalently react with APTS under the chosen treatment

conditions. The desired reaction scheme for APTS is shown in Figure 5.5 where, after losing the ethoxy groups through hydrolysis, the remaining silanols can react with available hydroxyl groups on the substrate [143, 144, 145, 146]. Determining if these new bonds are present on the substrate based on XPS spectra is difficult, since the spectra only change slightly after addition of the new molecules. Fourier transform infrared spectroscopy (FTIR) could provide a little more insight given that it probes functional groups and not individual atoms but its interpretation remains complex and leaves much to the experience of each researcher. In lieu of a better method to characterize the bonding strength of newly added molecules on a substrate, many researchers opt for assessing the stability of their samples in the conditions for their desired application. In this work, we assessed the stability of MWCNTs treated with APTS dispersed in water and ethanol by visual observation of the nanofluids produced over a period of two weeks.

As can be seen in Figure 5.6, both dispersions of APTS treated MWCNTs were unstable in water. MWCNT-APTS was temporarily stable in ethanol and only MWCNT-PPE:O-APTS was stable over a longer period of time in ethanol. These observations suggest that APTS is simply adsorbed onto MWCNT and MWCNT-PPE:O and that no covalent bonds have formed between APTS and the nanoparticles. A more detailed look at the surface chemistry of the nanoparticles and the reactivity of APTS in water and ethanol helps to better understand these results.

If we look at bare MWCNTs, they contain very little oxygen and therefore it was expected that no reaction would occur with APTS. The lack of stability of MWCNT-APTS in water confirms that. When dispersing MWCNT-APTS by sonication in water, the adsorbed APTS undergoes hydrolysis to form a trisilanol group. Being hydrophilic, the trisilanol molecule is repelled by the hydrophobic MWCNT surface. The MWCNTs are then left with no coating and quickly agglomerate and sediment.

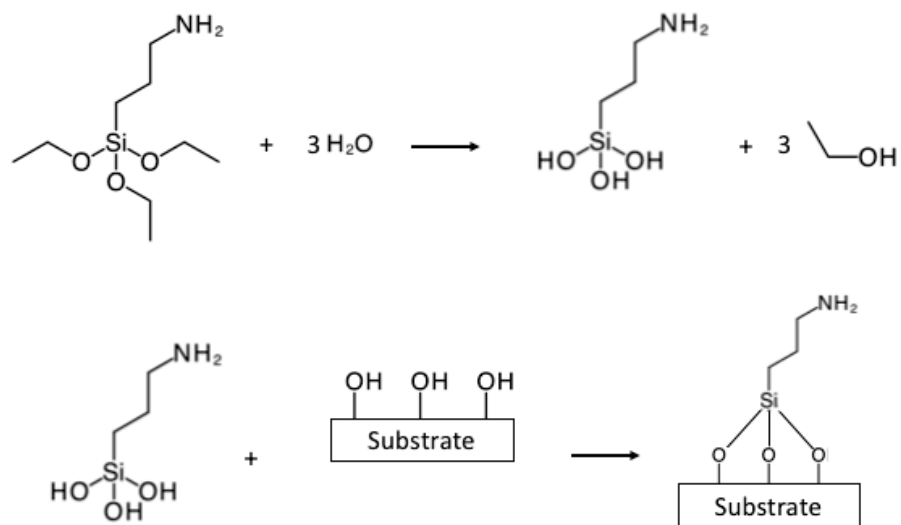


Figure 5.5: APTS hydrolysis and reaction with hydroxyl terminated surface.

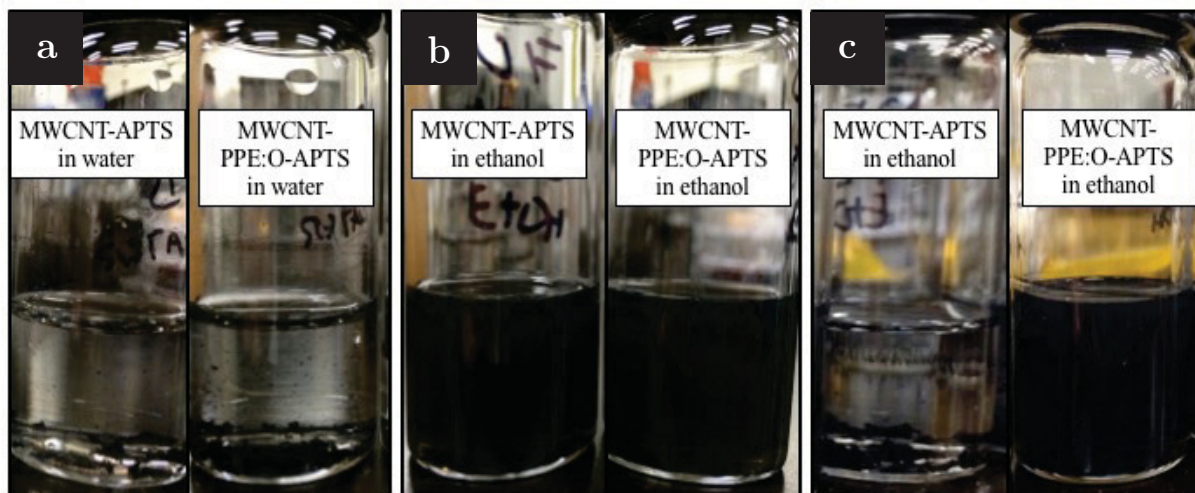


Figure 5.6: Aqueous (a) and ethanol (b,c) dispersions containing APTS functionalized MWCNTs after (a, b) 24 hr, (c) 2 weeks.

In the case of MWCNT-PPE:O, without APTS, these nanoparticles are stable in water [37], but with APTS they are unstable. This suggests that APTS is interfering with the charged moieties on the surface of MWCNT-PPE:O that keep the nanoparticles separate from each other [37]. This could be explained by the formation of insoluble oligomers of neighbouring APTS molecules on the surface of MWCNT-PPE:O [147].

The temporary stability of MWCNT-APTS dispersions in ethanol also supports the idea that APTS is only adsorbed on the nanoparticles during the vapor functionalization step. In ethanol, APTS remains intact and cannot hydrolyse. Therefore, instead of forming a trisilanol it remains as a triethoxy. This hydrophobic group may interact through van der Waals forces with the bare MWCNTs, leaving the more polar amine group pointing outwards towards the ethanol and thus helping stabilize the MWCNTs [148]. However, the amount of stabilizing groups was not enough to provide long term stability and the MWCNT-APTS agglomerated after three days. The MWCNT-PPE:O-APTS on the other hand remained stable for two weeks. The adsorbed APTS cannot react to form oligomers and therefore, it simply detaches from the nanoparticle's surface leaving behind an intact PPE:O coating which can stabilize the MWCNTs in ethanol.

There are two possible reasons that explain why APTS did not attach covalently to MWCNT-PPE:O: a low density of hydroxyl groups and a lack of water vapor during vapor functionalization. PPE:O contains hydroxyl groups but other groups as well such as carboxylic acid groups [38, 130]. Other researchers were able to covalently attach APTS to nanoparticles only when these particles were covered with numerous hydroxyl groups [149, 150], such that all three silanols of each APTS molecule reacts with the surface. Control of the amount of water vapor during vapor functionalization also greatly impacts the formation of bonds between APTS and a desired substrate. In the case presented here, no water vapor was added. Therefore APTS could not form silanol groups and only adsorbed on the surface.

However, when detaching MWCNT-PPE:O-APTS from the mesh, there was enough water to convert all ethoxy groups to silanols, but not enough hydroxyl groups on the surface for them to attach to. This led to oligomerization of APTS. Similar observations were made by other researchers. For example, Fiorilli et al. [143] showed through FTIR measurements that reacting a hydroxyl-rich silicon surface with only APTS vapor led to its adsorption. Injection of water vapor as a second step in the functionalization process was necessary to observe bonding between APTS and the substrate. Zhuang et al. [133] observed the negative impact of too much water vapor when preparing self-assembled monolayers. High quantities of water vapor led to the oligomerization of the organosilane before it interacted with the surface, thus leading to the deposition of undesirable agglomerates. Based on the results from these other groups and the results presented above, it is suggested that for a better functionalization of MWCNTs with APTS, a PP coating with more hydroxyl groups is necessary and water vapor is needed during the vapor functionalization step.

5.4.4 TEPA on MWCNT and MWCNT-PPE:O

TEPA functionalization also led to an increase in nitrogen content for both MWCNT and MWCNT-PPE:O (see Figure 5.4). The addition of TEPA on the MWCNTs had a clear impact on their stability when dispersed in water at pH 2 or 5.5. As-synthesized MWCNTs immediately form large agglomerates in water that are completely settled in only a few hours. MWCNT-TEPA behaved differently. At pH 2 and 5.5, they were stable, although agglomerates did form from the moment the nanoparticles were dispersed in water. These agglomerates can be seen at the edge of the liquid. Furthermore, the pH of the nanofluid has an impact on the stability of MWCNT-TEPA. After 2 weeks, most of the solid material from MWCNT-TEPA at pH 5.5 has settled but at pH 2, the mixture is still opaque (there is solid material settled at the bottom of the vial but it is not visible in the picture). This difference is due to the increased formation of positively charged groups, such as amines $-NH_2$ being

protonated to $-\text{NH}_3^+$ at pH 2 [37]. These charged groups repel neighboring MWCNTs, thus avoiding agglomeration and sedimentation.

As for MWCNT-PPE:O-TEPA in water, they are still stable after 2 weeks as shown in Figure 5.7. MWCNT-PPE:O, without TEPA, is stable at pH 5.5 however it is immediately unstable at pH 2. As shown in Figure 5.7, coating MWCNT-PPE:O with TEPA seems to mask the PPE:O and allows the nanoparticles to remain stable in water at pH 2. This is contrary to what had been observed by other groups that had reacted CNTs or graphene oxide with TEPA and saw these particles settling in less than 24 hr [151, 152, 153, 154]. The combination of PPE:O and TEPA is therefore an improvement on these other attempts at functionalizing MWCNTs with amine-containing molecules.

CD-XPS measurements show high levels of nucleophilic groups on TEPA-modified samples (see Figure 5.8). Although similar total nucleophilic concentration and selectivity have been reported by others using only PPs [29, 30], PPs contain a variety of functional groups that can react with TFBA, not just amines. TEPA, on the other hand, does not degrade at the temperature used during vapor functionalization and the nitrogen atoms being added on the MWCNTs are primary and secondary amine groups only. Thus, vapor functionalization is an easy method for enrichment of amine groups specifically, without having to resort to classical wet chemistry.

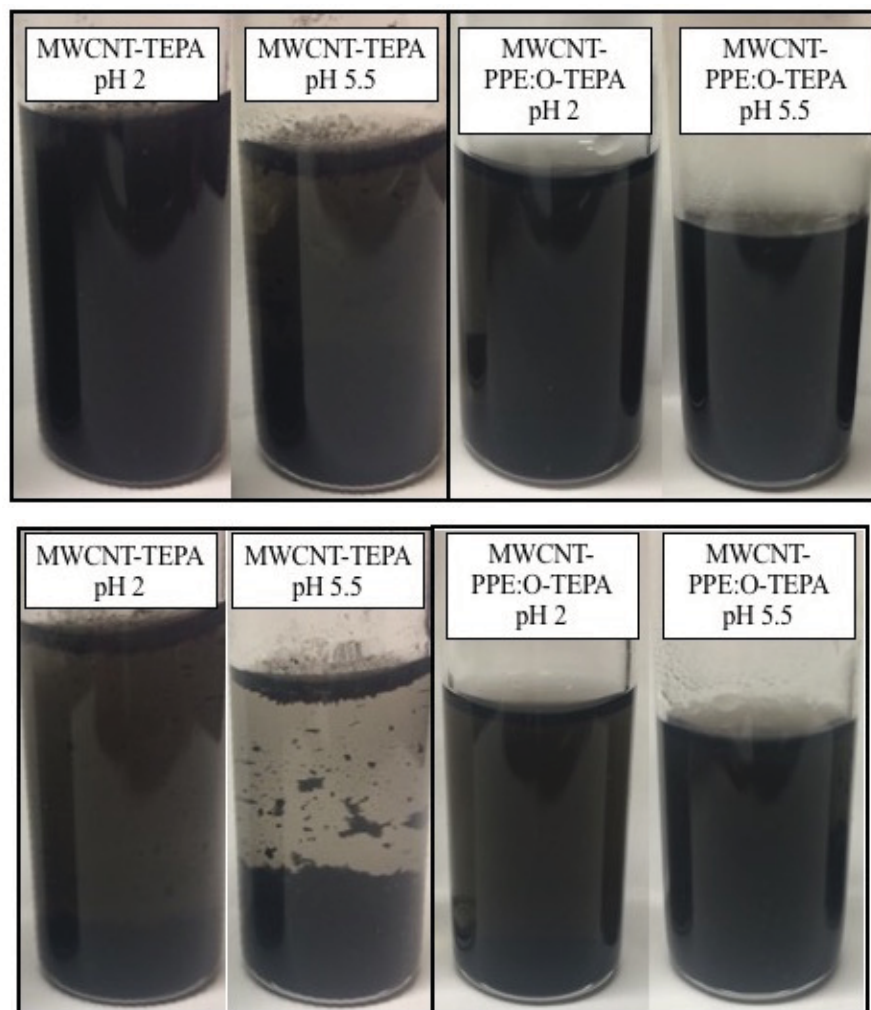


Figure 5.7: Nanofluids containing TEPA functionalized MWCNTs after 48 hr (top) and 2 weeks (bottom).

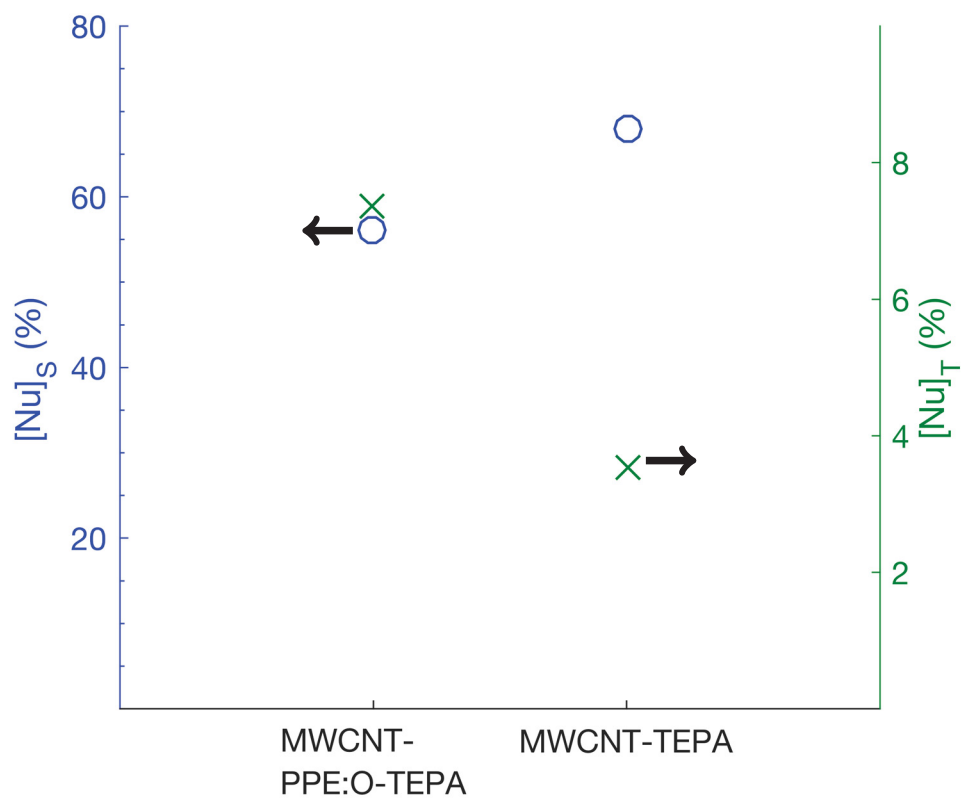


Figure 5.8: Selectivity of nucleophilic groups $[Nu]_S$ (circles), and total nucleophilic groups concentration $[Nu]_T$ (crosses).

5.5 Conclusion

PPE:O coating on MWCNTs in combination with vapor functionalization using TEPA or APTS produce amine-covered MWCNTs that can be dispersed in water or ethanol to form stable suspensions. TGA and DSC measurements showed that PPE:O is thermally unstable starting at 100 °C. However, this is expected due to the conditions used in this work for PP deposition which favor oligomer formation. Vapor functionalization of the MWCNTs at 150 °C or less allowed for the deposition of TEPA or APTS on their surface without degradation of the PP coating. When dispersed in water, MWCNT-PPE:O-APTS were shown to be unstable due to the reaction of APTS with itself forming insoluble oligomers. In all other cases, addition of TEPA or APTS either did not interfere or improved the stability of the nanoparticles. With such simple methods of enriching the surface of MWCNTs with a single functional group, it is possible to develop materials with more targeted interactions with desired molecules in aqueous dispersions.

5.6 Supplementary information

This section presents data not to be submitted with the remainder of Chapter 5. It presents additional information about the structure of PPE:X¹ obtained by analyzing the char residue after complete pyrolysis of the samples.

Figure 5.9 shows that the composition of both PPs slightly changes after moderate heating at 150 °C. A loss of about 2 at% of nitrogen is observed for PPE:N on Si wafer and 2 at% of oxygen for PPE:O on the same substrate. As for the char residue left after heating at 600 °C, it contains only about half of the original content of the desired heteroatom.

¹ Information on nitrogen-rich coating PPE:N can be found in Chapter 4.

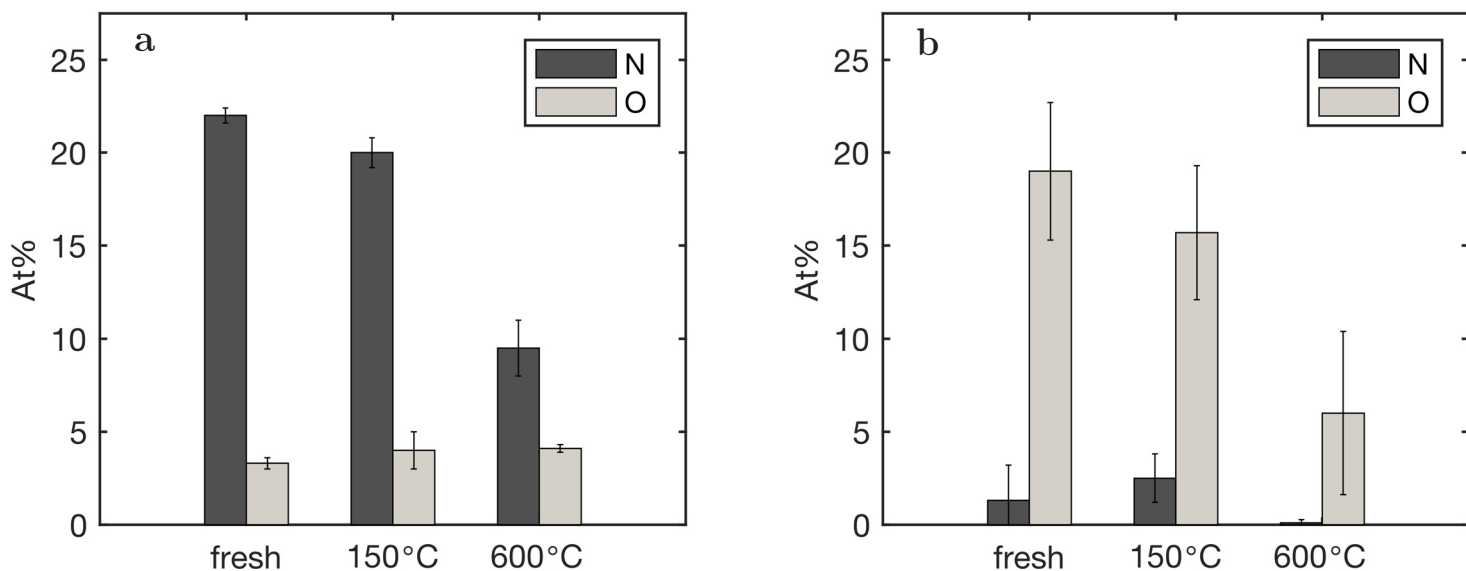


Figure 5.9: Elemental composition of (a) Si-PPE:N and (b) Si-PPE:O.

Comparison of the shape of the C 1s peaks of the PPs also reveals information on the changes in structure of the material. Figure 6.7 shows the C 1s peaks with fitted components for both PPs deposited on Si. The peaks were fitted with four components, C1 to C4, and their properties are presented in Table 4.2 (see Chapter 4). When comparing the peaks for as-synthesized PPE:N and after treatment at 150°C, a certain ordering of the structure is observed through an increase of the C1 component. As for PPE:O, mild heat exposure led to a slight decrease in the C2 component and an increase in C1 with respect to the original PPE:O.

As for the C 1s peak of the PPs heat treated at 600°C, they are shown in Figure 5.11. For these peaks it was necessary to add a component at 292 eV and with a full width at half maximum (FWHM) of 6. This component, attributed to a π - π^* transition, is commonly observed in the tail of the C 1s peak of graphitic materials [98, 155]. The FWHM of the C1

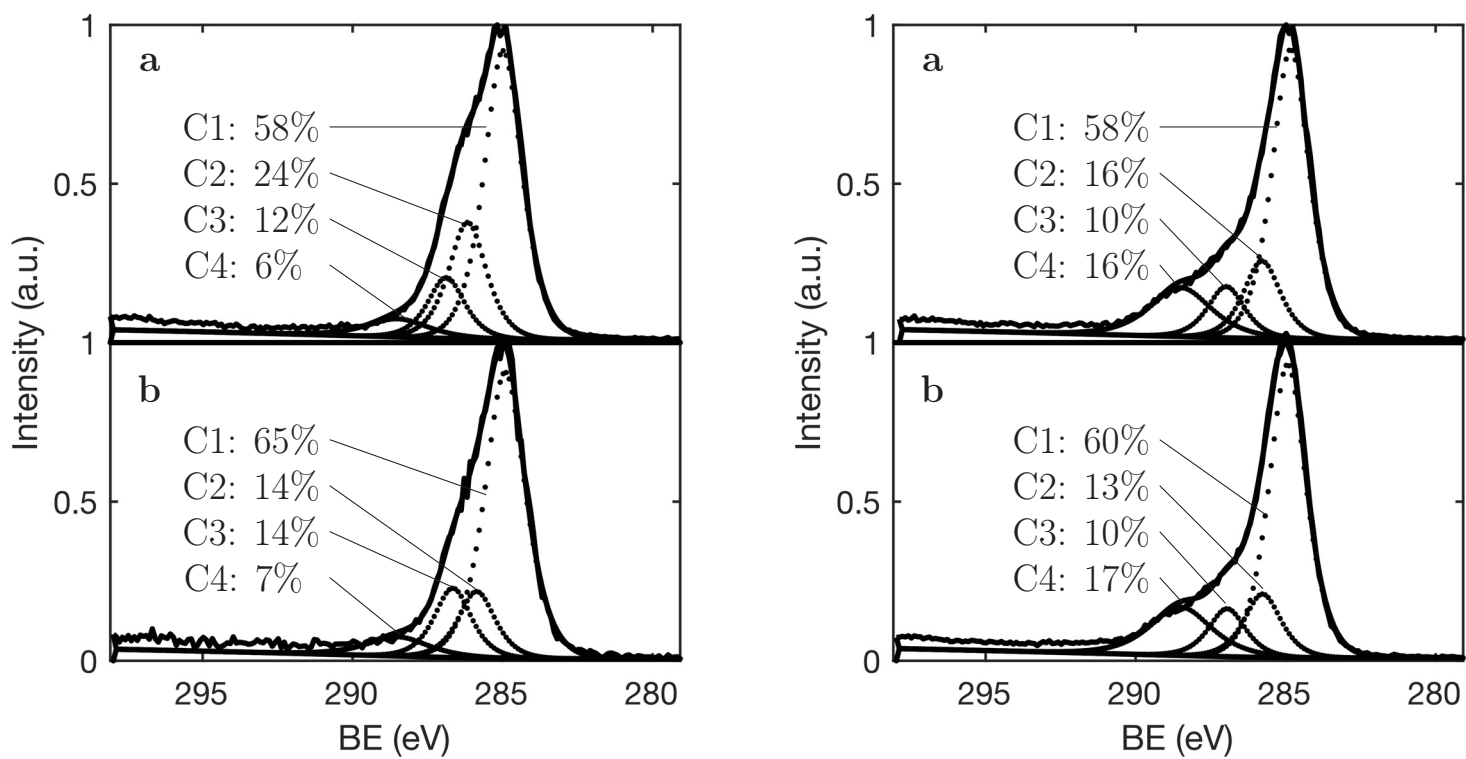


Figure 5.10: Experimental and fitted C 1s peaks for (a) as-synthesized Si-PPE:X, (b) after heating at 150 °C, PPE:N on the left, PPE:O on the right. The component areas are also given as percentages.

component for PPE:O also decreased to 1 which is indicative of a graphitization of the PP film.

The changes in the N 1s peaks for PPE:N before and after pyrolysis (Figure 5.12) also indicate graphitization of the sample. PPE:N as-synthesized has a N 1s peak at 399 eV which is usually assigned for imines, C=N, amides, N-C=O, and amines, -NH₂ [32]. After pyrolysis, the N 1s peak contains a component at 398 eV which is assigned to pyridinic (6 member ring) nitrogen, and another component at 400 eV for pyrrolic (5 member ring) nitrogen [32, 156]. Table 5.2 lists the characteristics of the components used to fit the N 1s peak [32]. As-synthesized PPE:O has a O 1s peak at 532 eV which is typical of systems that contain contributions from single (between 532 and 533 eV) and double (between 531 and 532 eV) bonded oxygen to carbon [121, 122, 123]. After pyrolysis, the O 1s peak has changed shape and now has contributions from two components at 531 and 533.5 eV (see Figure 5.13).

For XRD measurements, two samples (one of PPE:N and another of PPE:O) were pyrolyzed. A black powder was obtained in both cases. However, the slower deposition rate of PPE:O produced a smaller amount of sample and after pyrolysis, there wasn't enough for XRD measurement. Therefore only the XRD spectrum of PPE:N is presented in Figure 5.14. The diffraction peak at 25° corresponds to the graphite (002) lattice plane which is associated with the distance between stacked hexagonal structures. The peak at 43° is the (100) lattice plane and is associated with a hexagonal repetitive structure [158, 159]. All coals exhibit these peaks and a thinning of the peaks indicates formation of a larger crystal. Analysis of the shape of the peaks allows for calculation of the graphitic interplanar distances and the degree of crystallinity but this usually requires a study of a series of similarly prepared samples where only one treatment variable is changed [160, 161]. Such analysis would be relevant if future experiments using pyrolyzed PPs were to be investigated.

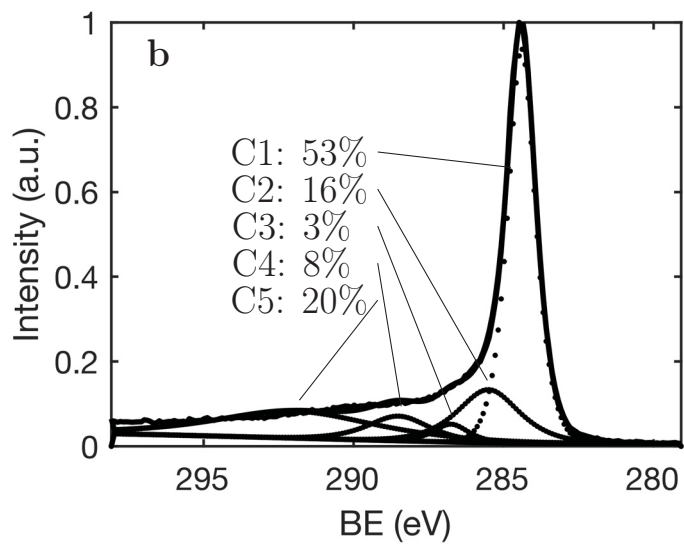
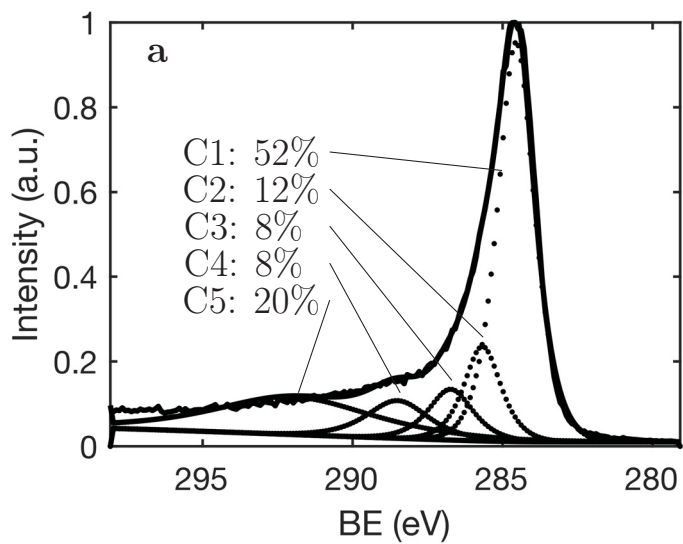


Figure 5.11: Fitted components for C 1s peaks of (a) Si-PPE:N and (b) Si-PPE:O after heating at 600 °C. The component areas are also given as percentages.

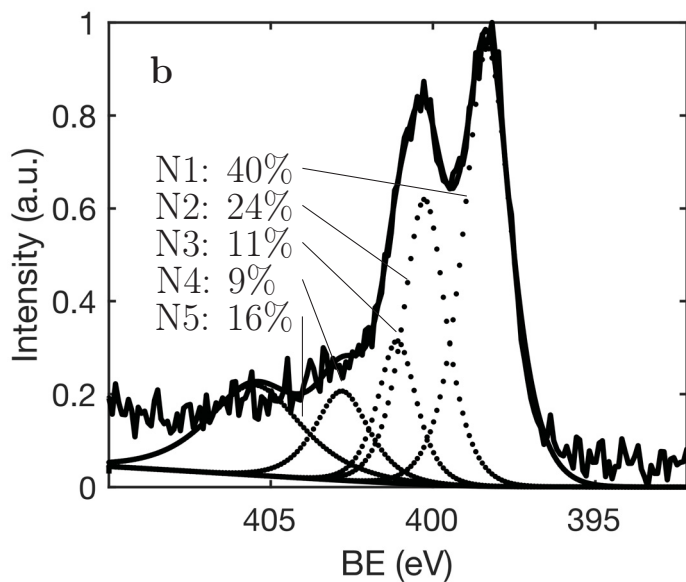
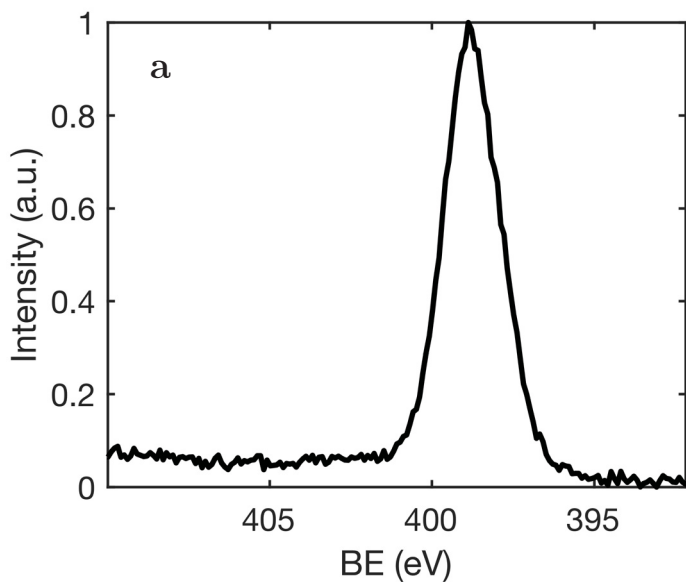
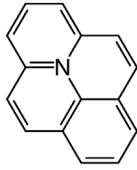


Figure 5.12: Fitted components for N 1s peaks of Si-PPE:N (a) before and (b) after heating at 600 °C. The component areas are also given as percentages.

Table 5.2: Characteristics of XPS fitted components for N 1s [32, 157].

Component name	BE (eV)	FWHM (eV)	Chemical assignment
N1	398	~1.5	pyridinic N 
N2	400	~1.5	pyrrolic N 
N3	401	~1.5	quaternary N 
N4, N5	402, 405	~1.5, ~3	various nitrogen oxides

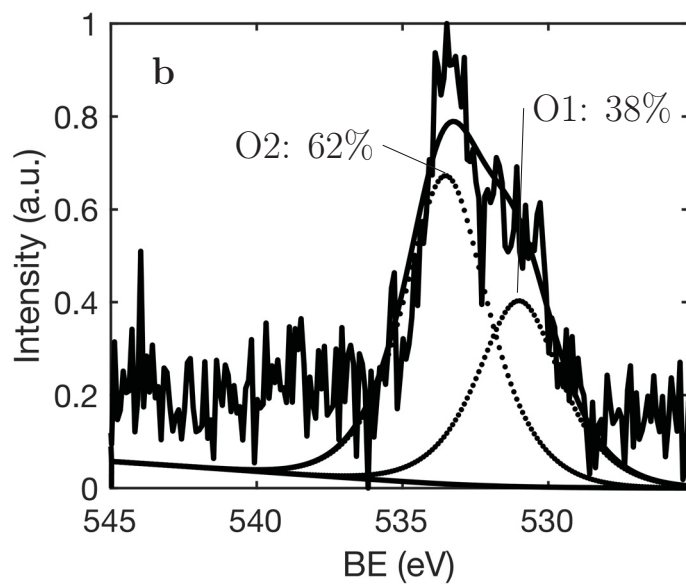
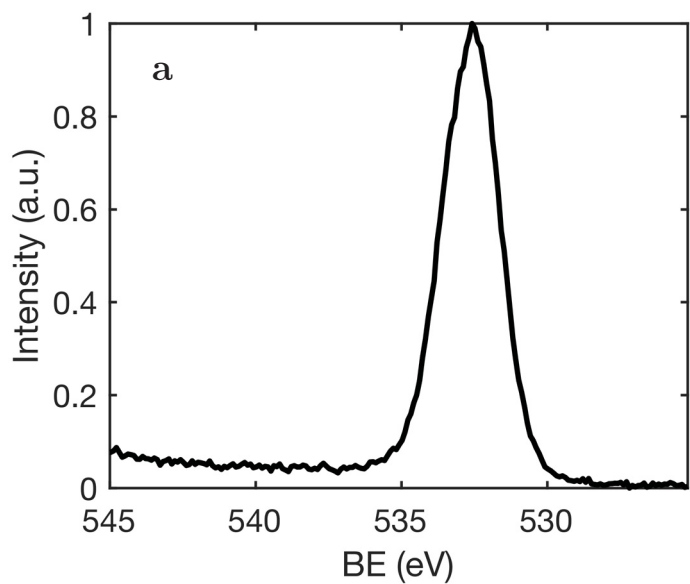


Figure 5.13: Fitted components for O 1s peaks of Si-PPE:O
 (a) before and (b) after heating at 600 °C.
 The component areas are also given as percentages.

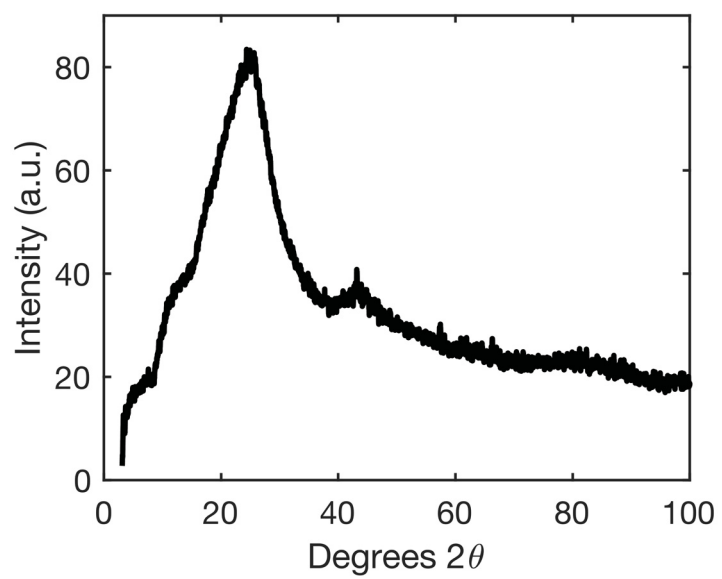


Figure 5.14: XRD of PPE:N after heating at 600 °C.

CHAPTER 6

Carbon dioxide capture

6.1 Preface

This chapter presents an article that was published in *Plasma Processes and Polymers*. The complete citation of the published article is:

Jorge, L., Coulombe, S., & Girard-Lauriault, P. L.. (2015). Nanofluids Containing MWCNTs Coated with Nitrogen-Rich Plasma Polymer Films for CO₂ Absorption in Aqueous Medium. *Plasma Process. Polym.*, 12(11), 1311-1321.

The work was planned, executed, analyzed and written by L. Jorge (Ph.D. candidate). TEM images were taken by Dr. David Liu. Data acquisition on the NEXAFS was performed by M. Andreas Lippitz, Dr. Paul Dietrich, and Dr. Wolfgang E.S. Dr. S. Coulombe and Dr. P.-L. Girard-Lauriault were responsible for supervision of the work and reviewing of the manuscript.

Chapters 4 and 5 established the main properties of the PP coatings and the behaviour of plasma-treated MWCNTs in water. The current chapter and the next focus on the use of these nanofluids for capture applications. In this chapter, the use of nanofluids for CO₂ capture in a gas bubble column is presented. Four plasma treatments are tested on the MWCNTs, three with increasing nitrogen quantity and a fourth with oxygen. The highest absorption capacity is observed for the MWCNTs carrying the largest quantity of amine functional groups. Nanofluids containing oxygen-treated MWCNTs also show some enhancement in absorption capacity but not as much as with the nitrogen-treated MWCNTs. This

proves that both the nanoparticle and its surface chemistry tailored for the desired gas are necessary for improvement of gas absorption capacity.

A different naming convention for plasma-treated MWCNTs was used in this chapter. Note that MWCNT-10:10 presented here is the same as MWCNT-PPE:N presented in the rest of this thesis.

Nanofluids Containing MWCNTs Coated with Nitrogen-Rich Plasma Polymer Films for CO₂ Absorption in Aqueous Medium

Larissa Jorge, Sylvain Coulombe, Pierre-Luc Girard-Lauriault

Department of Chemical Engineering, Plasma Processing Laboratory, McGill University,
Montréal, QC, Canada H3A 0C5

Abstract

Amine-functionalized multi-walled carbon nanotubes (MWCNTs) dispersed in water are investigated as CO₂ absorbents. MWCNTs grown by chemical vapor deposition on stainless steel meshes form open forests that can be coated via a RF capacitively coupled glow discharge. When treating the MWCNTs in an atmosphere containing either pure ammonia or mixtures of ammonia and ethylene for 5 min, grafting of nitrogen functional groups or deposition of a nitrogen-rich plasma polymer layer occurs. In particular, for a 1:1 mixture, a 10 nm thick plasma polymer layer coats the MWCNTs. This layer contains about 19 N at%, and 12% of these nitrogen atoms are nucleophilic sites (such as amines) that may react with CO₂. These functional groups not only enhance the absorption of CO₂ but also increase the hydrophilic character of the MWCNTs, allowing them to stay suspended in water for at least three months at room temperature. The CO₂ absorption capacity of this nanofluid is 36% higher than that of water, with a MWCNT concentration of about 40 mg L⁻¹.

6.2 Introduction

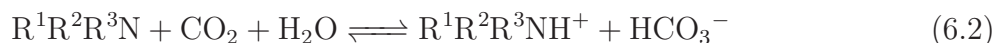
Among the numerous technologies for green house gas mitigation, CO₂ capture is deemed one of the most promising in the short term efforts to control climate change [56]. Current technologies, which for the most part include the use of an aqueous alkanolamine solution [162], capture a fraction of the CO₂ present in the flue gases after fuel combustion.

However, there are still important energy costs associated with frequent equipment repairs due to the corrosive nature of the CO₂ absorbing fluid and flue gas cooling to decrease evaporation of the aminated molecules. These problems deter industries from installing CO₂ reduction systems. For this reason, investigation of new CO₂ absorbents is technologically relevant.

Nanofluids (NFs), which are engineered dispersions of nanoparticles (NPs) in a desired host fluid, have been shown to enhance the mass transfer of gaseous species into a liquid phase and are thus promising candidates as absorbents. A variety of NPs have been added to water such as Al₂O₃ [64], SiO₂ [60], and Fe₃O₄ [58]. For example, Kim et al. observed an overall 76% increase in CO₂ absorption rate (and 24% increase in absorption capacity) for an aqueous NF of silica NPs with respect to water in a gas bubble column [60]. They attributed this increase to both the adsorption of CO₂ onto the NPs as well as the ability of the NPs to induce bubble “cracking”, which increases the available contact area between the gas and liquid phases. NPs have also been mixed with solutions containing aminated molecules. Jiang et al. observed an enhanced CO₂ absorption rate when Al₂O₃ and SiO₂ were added to aqueous solutions of monoethanolamine, one of the most used alkanolamines for CO₂ capture [163].

One of the main difficulties associated with the synthesis and use of NFs is the stability of the NPs in the host liquid. Ultrasonication is usually the method of choice to disperse the NPs but most often the resulting NFs are only stable for a few days [163, 164, 165]. Functional groups added to the surface of NPs can help stabilize them and, if chosen appropriately, may also participate in the gas absorption process. For example, Olle et al. reported the use of oleic acid-functionalized Fe₃O₄ NPs in water for the absorption of O₂. For CO₂ capture, different types of amine functional groups can be mixed to tailor the properties of the absorbent suspensions such as the loading capacity or absorption kinetics. Two primary

or secondary amines can react with one molecule of CO₂ to form a carbamate (Equation 6.1) whereas one tertiary amine, in the presence of water, can lead to the formation of a bicarbonate ion by reacting with a single CO₂ molecule (Equation 6.2) [166, 167, 168]. Therefore, primary and secondary amines have smaller loading capacities compared to tertiary amines, but their CO₂ absorption kinetics is much higher [166]. To the best of our knowledge, there have been no reports of NFs with amine-functionalized NPs for the capture of CO₂.



Multi-walled carbon nanotubes (MWCNTs) have large surface areas amenable to grafting or coating with many amine groups. Our laboratory has developed a methodology to grow MWCNTs directly on a stainless steel mesh, forming an open forest that can be fully functionalized. The ability to treat all the MWCNTs before they agglomerate in a liquid or in powder form allows these NPs to stay stable in the host liquid for a period of months [10]. In this contribution, we present the use of an aqueous NF containing plasma-functionalized MWCNTs for the sorption of CO₂ in a simple bubble column gas-liquid contactor. For this application, nitrogen functional groups are either grafted to the MWCNTs surface or a nitrogen-rich plasma polymer layer is deposited onto the MWCNTs in order to combine both the hydrophilic stabilization effect and a chemical affinity for CO₂. It is hypothesized that well-dispersed MWCNTs would enhance the absorption of CO₂ in water by favoring the formation of smaller bubbles, offering a large surface for CO₂ adsorption and offering amine functional groups where CO₂ may react.

6.3 Experimental method

6.3.1 Nanofluid synthesis

MWCNTs were produced in-house following a method described in detail elsewhere [10]. Briefly, MWCNTs were grown by chemical vapor deposition (CVD) on a 3.5 x 6 cm² piece of 316 grade stainless steel (SS316) mesh (400 series, McMaster-Carr) in a tube furnace. A 30 min heat treatment at 700 °C under Ar¹ (99.999%) produced the required growth sites on the mesh. A mixture of acetylene, C₂H₂ (99%), at 68 sccm and Ar at 600 sccm was then injected in the tube furnace at atmospheric pressure for 2 min. The furnace was kept at 700 °C for another two minutes to allow for MWCNT growth and then turned off to cool down.

The MWCNT-covered stainless steel meshes were functionalized using a low-pressure capacitively-coupled RF (13.56 MHz, continuous) glow discharge with either pure ammonia, NH₃ (99.99%), or a mixture of ethylene, C₂H₄ (99.70%) and a source of nitrogen (NH₃) or a source of oxygen (O₂). The sample was positioned directly on the live electrode and the chamber walls acted as the ground electrode. Process gases were injected inside the chamber at the desired flowrates for about 5 min to ensure a homogeneous atmosphere, which was maintained at a pressure of 80 Pa with a throttling gate valve. Samples were treated for 5 min at 35 W RF power, and then left in the chamber at base pressure (<2 mTorr) for 10 min before being exposed to air. Samples were stored in non-permeable high barrier bags filled with N₂, and put in the freezer until further use to limit ageing of the samples [112]. Three different combinations of gas flow rates, Q, were used, shown in Table 7.1. Each sample was

¹ Gases were purchased from MEGS Specialty Gases.

named as MWCNT-x-y where x and y are the flowrates of NH_3 and C_2H_4 respectively (with the exception of the sample where O_2 replaces NH_3).

Reverse-osmosis (RO) water produced in-house with the use of a $0.22 \mu\text{m}$ filter and containing a total organic content of less than 10 ppb and a conductivity of $10 \mu\text{S}$ was used as the host liquid for the NF. Vials each containing one MWCNT-covered SS316 mesh and 25 mL of RO water were put in an ultrasonic bath for 15 min. This highly energetic process breaks off the MWCNTs from the growth substrate. The meshes were then removed from the vials and disposed of. The NFs were stored at room temperature. The concentration of MWCNTs in the NF was obtained by measuring the weight of the MWCNT-covered mesh before and after sonication to determine the mass of MWCNTs removed in a given volume of RO water. In these experiments, the concentration of MWCNTs in the NF is approximately 40 mg L^{-1} .

6.3.2 Characterization of the MWCNTs

SEM and TEM

To investigate the MWCNTs morphology before and after plasma treatment, MWCNTs on the mesh were imaged by scanning and transmission electron microscopy (SEM, Hitachi SU-3500, and TEM, Tecnai G2 F20 200 kV Cryo-STEM).

Table 6.1: Gas flow rates during plasma functionalization.

Sample name	$Q_{\text{NH}_3 \text{ or } \text{O}_2}$ (sccm)	$Q_{\text{C}_2\text{H}_4}$ (sccm)
MWCNT-10:10	10	10
MWCNT-10:10- O_2	10	10
MWCNT-20:4	20	4
MWCNT-20:0	20	0

OES

The main species present in the plasma were determined by collecting optical emission spectra (OES) with a fiber optic cable (Solarization-Resistant Multimode Patch Cables for UV, Thorlabs) connected to a portable spectrometer (OceanOptics USB2000). The fiber optic cable was positioned outside the vacuum chamber on the glass viewport. The acquisition range was limited to 300-850 nm, and the spectral resolution of the system was 1 nm. The average of three spectra, each obtained with an integration time of 1000 s, was recorded. The spectra were normalized with respect to the peak at 337 nm, corresponding to N₂ species, found in all the spectra recorded.

XPS, CD-XPS and NEXAFS

The chemical composition of the samples was analysed on a Thermo Scientific™ K-Alpha™+ X-ray photoelectron spectrometer (XPS). Monochromatic Al K α excitation with a 400 μ m X-ray spot size was used. Survey spectra were recorded at a pass energy of 200 eV and 1 eV resolution and a 90° take-off angle. High resolution spectra of C 1s, N 1s and O 1s were recorded at a pass energy of 50 eV and 0.1 eV resolution. The spectra recorded were analyzed using the CasaXPS software (version 2.3.16) which uses the following relative sensitivity factors for C, N, O and F: 1, 1.8, 2.93, 4.43. Peak fitting was performed according to a procedure described by Girard-Lauriault et al. [98] and Estrade-Szwarczkopf [155]. A Tougaard background was applied to all the spectra and a mixed Gaussian/Lorentzian peak shape was used for all components.

Chemical derivatization XPS (CD-XPS) using 4-(trifluoromethyl)benzaldehyde (98%, TFBA, Sigma-Aldrich) was used to estimate the amount of nucleophilic functional groups added by plasma treatment. Non-functionalized and functionalized samples were put in a vacuum chamber at base pressure, 2.25 Torr. Samples were treated for 4 hours in vapors

of TFBA at room temperature. After derivatization, samples were stored again in N₂-filled bags in the freezer until characterization with the XPS. Equations 6.3 and 6.4 show how the total nucleophilic group concentration, $[Nu]_T$, and their selectivity, $[Nu]_S$, are linked to the total nitrogen concentration, where $[X]$ is the atomic percentage of a given atom, and subscripts “nd” and “d” are for the non-derivatized and derivatized samples, respectively [98].

$$[Nu]_T = \frac{[F]_d}{3[N]_d} \cdot [N]_{nd} \quad (6.3)$$

$$[Nu]_S = \frac{[F]_d}{3[N]_d} \quad (6.4)$$

CD-XPS with TFBA has generally been considered a method to estimate the concentration of primary amines on a given surface. A recent investigation of the reaction of plasma prepared surfaces with TFBA is suggesting that TFBA does not react selectively with amines and might also be reacting with imines [97]. Given that plasma treatment of MWCNTs may introduce a number of chemical functional groups on the surface, including both amines and imines, all results regarding CD-XPS will be reported as concentrations of nucleophilic groups, and not amines exclusively.

For a more in-depth study of unsaturated functional groups, near edge X-ray absorption fine structure spectroscopy (NEXAFS) was performed on a HE-SGM monochromator dipole magnet beam line at the BESSY II synchrotron radiation source (Berlin, Germany). The spectra of the C, N and O K-edges were taken in total electron yield mode. The spectra were taken at an angle of 55° which had been shown in the past to provide the most information on the samples analysed. More details on the data acquisition method can be found elsewhere [98]. Spectra shown have been normalized. For peak fitting, a two-step

background was used, with one step at the edge of the $1s \rightarrow \pi^*$ (285.3 eV) transition and another one at the $1s \rightarrow \sigma^*$ transition (291.7 eV) [169], with its height corresponding to the magnitude of the spectra at 330 eV.

6.3.3 Gas bubble column

A gas bubble column was used to measure the CO_2 absorption capacity of the NFs (Figure 6.1). The setup consisted of a glass column (16 mm diameter, 150 mm in length, MDC Vacuum), a gas diffuser (4 μm pores sintered metal filter, Ideal Vacuum Products) at the bottom of the column, an injection port that brings CO_2 (bone dry, 99.9%, Praxair Technology) and Ar to the gas diffuser, an injection port for Ar at the top of the column, and a mass spectrometer (MS, Pfeiffer GSD 301 O2) for the determination of the gas composition. Gas flow rates were controlled by two mass flow controllers (Brooks Instrument 5850E for Ar and Qualiflow AFC80MD for CO_2). The total volume from the gas diffuser to the MS sampling capillary was 32 mL. Experiments were carried out at a room temperature of about 17°C. At the beginning of each day, the MS was baked to condition the analysis chamber and recalibrated with a known gas mixture. The glass column was loaded with 25 mL of RO water or NF. For all experiments, a few cycles of CO_2 desorption and absorption were performed. Each cycle would begin with Ar being injected from the bottom of the column to purge the liquid from CO_2 . Then, CO_2 was injected at 10 sccm from the bottom of the column and Ar was injected from the top of the column at 80 sccm. The Ar input was positioned just above the liquid and helped transport the CO_2 to the mass spectrometer while keeping a low concentration of CO_2 on top of the liquid. Equation 6.5 was used to calculate the amount of CO_2 absorbed by the NF, where $V_{\text{CO}_2}^{\text{max}}$ is the total volume of CO_2 absorbed, Q_{CO_2} is the flowrate of CO_2 going into the column, C_t is the concentration of CO_2 in the outgoing gas stream at time t , C_{max} is the maximum concentration of CO_2 in the outgoing gas stream, and t_{eq} is the time required to reach a pseudo equilibrium in the

system. It was assumed that the CO_2 absorption process reached equilibrium when the CO_2 concentration recorded with the MS remained constant for at least ten minutes.

$$V_{\text{CO}_2}^{\text{max}} = \int_0^{t_{\text{eq}}} \frac{Q_{\text{CO}_2}(C_{\text{max}} - C_t)dt}{C_{\text{max}}} \quad (6.5)$$

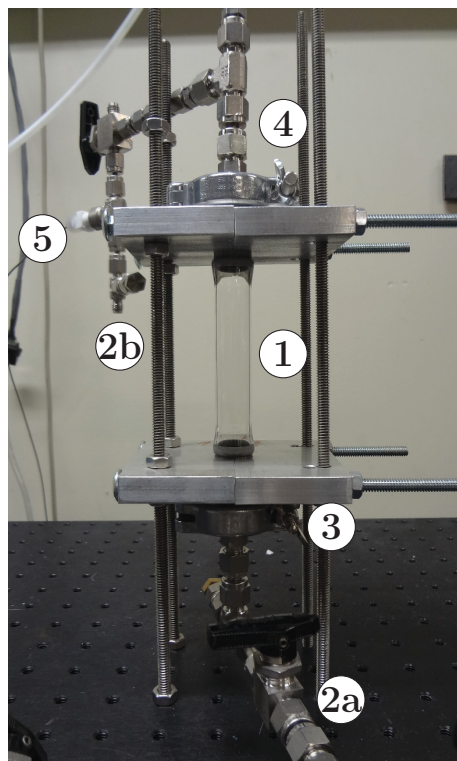


Figure 6.1: Gas bubble column for absorption of CO_2 by NFs. 1) column, 2) gas inlet (a) and outlet (b), 3) gas diffuser, 4) argon inlet, 5) connection to mass spectrometer.

6.4 Results and discussion

6.4.1 MWCNTs morphology

As-synthesized MWCNTs form an entangled network that cover the entire mesh (Figure 6.2a-b). Plasma functionalization of MWCNTs under the conditions presented above

does not alter their physical aspect as seen by comparing images of as-synthesized MWCNTs and MWCNTs-10:10 (Figure 6.2c-d). The duration of the treatment is short enough that there is no observable degradation of the MWCNTs.

TEM images show no visible changes to the MWCNT-20:0 samples after functionalization (Figure 6.3a). However, for samples MWCNT-20:4 (Figure 6.3b), a fraction of the surface area of the tubes is covered with a plasma polymer layer no thicker than 5 nm. This layer grows to about 10 nm in thickness and covers all tubes for samples MWCNT-10:10 (Figure 6.3c).

6.4.2 Gas-phase species in the plasma

Figure 6.4 shows the emission spectra of the plasma produced to treat the MWCNTs. Ammonia decomposes sequentially into NH_2 , NH and then recombines into N_2 [27]. Molecular bands for these species can be observed in all three spectra with the exception of NH_2 which cannot be detected by our low-sensitivity OES setup [22]. Another molecular band around 388 nm due to CN species is found for the MWCNT-10:10 plasma. The intensity of this band decreases for MWCNT-20:4 given the lower concentration of C_2H_4 in the chamber. The absence of the CN emission for the MWCNT-20:0 plasma, where no C_2H_4 was used, is a good indication that the plasma treatment did not degrade the MWCNTs [22]. Emission from CN species was also observed by Choukourov et al. [170] when doing plasma polymerization, whereas samples treated with NH_3 , N_2 and H_2 and no hydrocarbons usually lead to grafting of molecules onto the surface [171]. From these spectra and the images obtained by TEM, it is hypothesized that for sample MWCNT-20:0, grafting of functional groups occurs and for the MWCNT-10:10 sample, the deposition of a plasma polymer is the main mechanism of functionalization. Samples MWCNT-20:4 would therefore be a combination

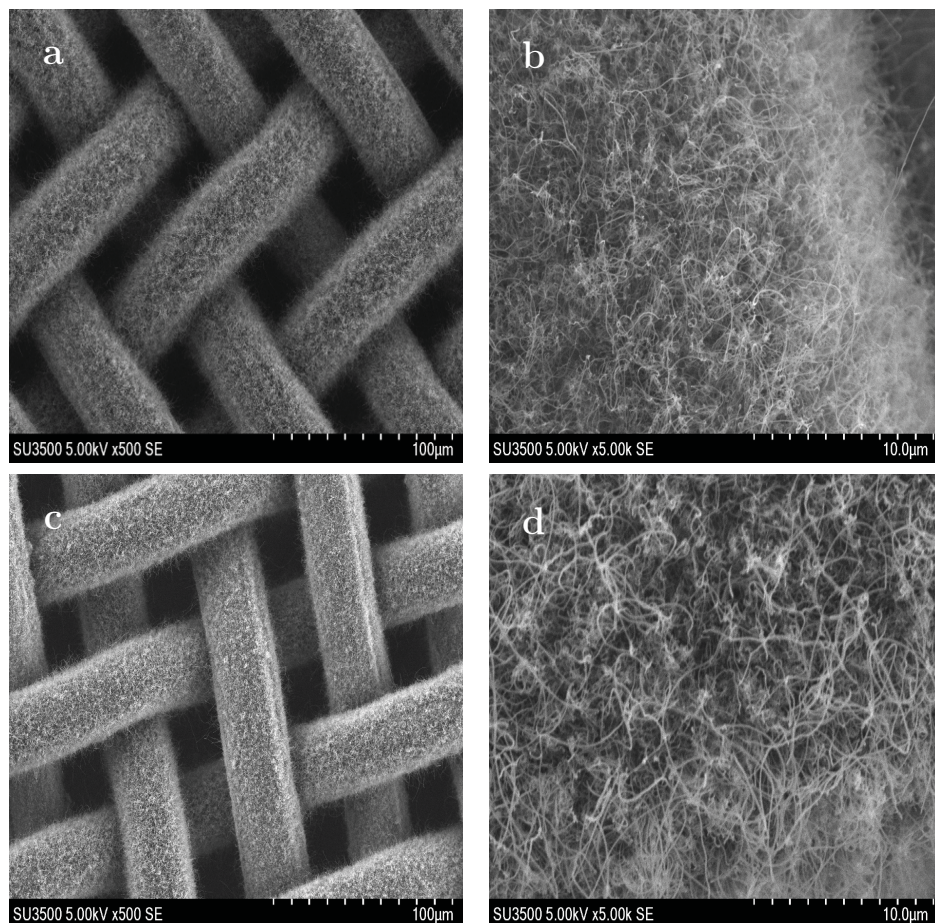


Figure 6.2: SEM images of as-produced MWCNTs (a and b) and MWCNTs-10:10 (c and d).

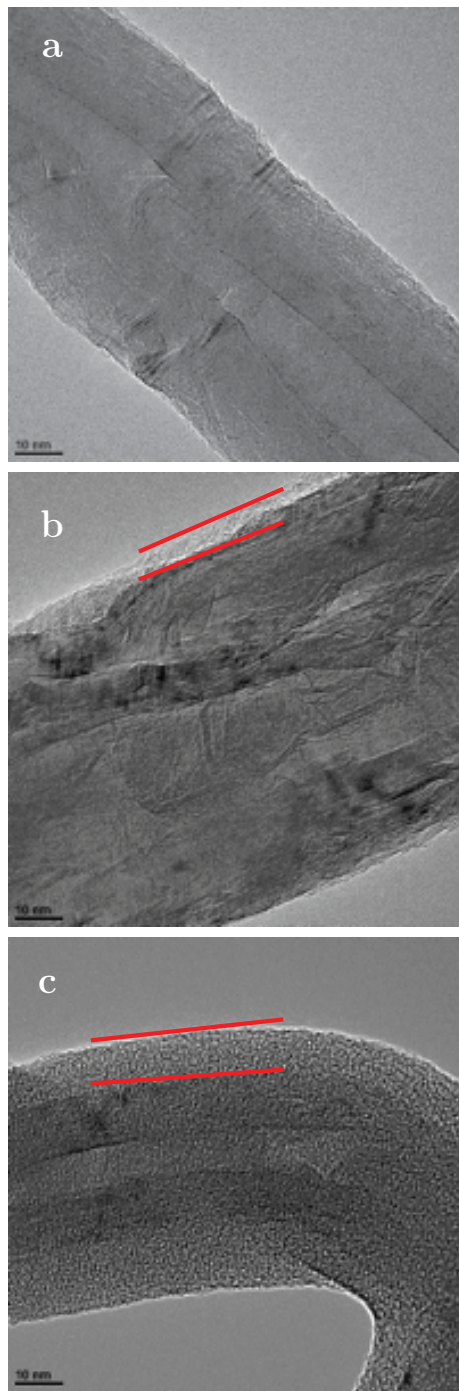


Figure 6.3: TEM images of a) MWCNT-20:0, b) MWCNT-20:4, c) MWCNT-10:10. The plasma deposited organic macromolecule layer is found between the two red lines.

of both processes given that only a fraction of the MWCNTs surface area is covered with a thin plasma polymer layer.

6.4.3 MWCNTs chemical composition

We are interested in integrating nitrogen, and more specifically amine functional groups on the surface of the MWCNTs for better chemical affinity for CO₂. Figure 6.5 shows the atomic percentage of nitrogen as well as the concentration of nucleophilic functional groups found in the treated samples by XPS and CD-XPS. MWCNT-20:0 samples with grafted nitrogen groups contained about 8 N at%, whereas the deposited plasma polymer on sample MWCNT-10:10 had about 19 N at%. As for sample MWCNT-20:4, its incorporation of nitrogen comes from both grafting and deposition of a plasma polymer layer, leading to a total of about 12 N at%. Also note that although the total concentration of nucleophilic sites is higher for the MWCNT-10:10 sample, the selectivity of the nitrogen atoms for nucleophilic sites remains relatively constant for all samples (Figure 6.6).

Other researchers have found that increasing $R = Q_{\text{NH}_3}/Q_{\text{C}_2\text{H}_4}$ yields coatings with higher nitrogen contents [115, 116, 117]. In our case, only two samples had plasma polymer coatings, MWCNT-20:4 and MWCNT-10:10. Therefore, we expected that the former sample would have a larger nitrogen content than the latter. However, we observed the opposite as seen on Figure 6.5. Since the plasma polymer layer in sample MWCNT-20:4 is thinner than the XPS information depth, the reported nitrogen atomic concentrations can be significantly lower than the actual atomic concentrations in the plasma polymer layer.

Peak fitting was performed on the C 1s peaks of as-synthesized and functionalized MWCNTs (Figure 6.7). The two main components used are an asymmetric graphene component centered at 284.5 eV (sp²), and a “defects” component at 283.9 eV (sp). Defects are an important part of MWCNTs as these are favorable sites for grafting of molecules [172]. Other

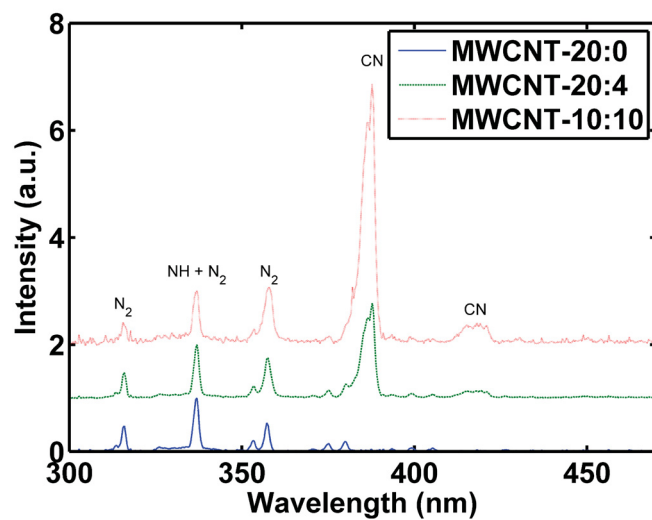


Figure 6.4: OES spectra of the plasma used to functionalize the MWCNTs.

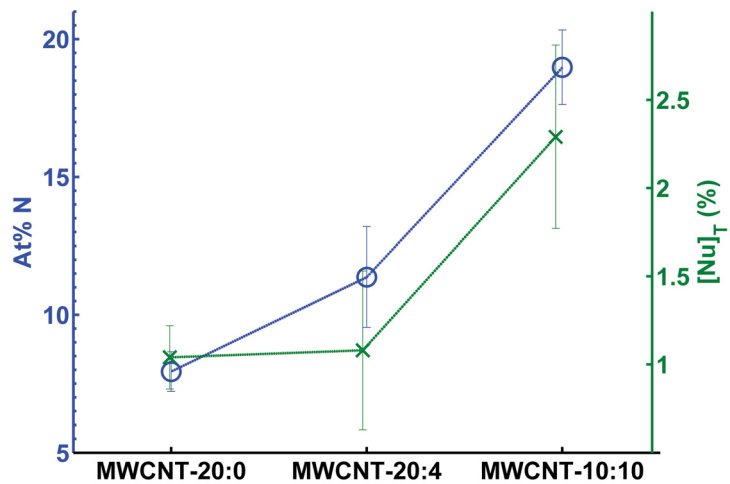


Figure 6.5: Nitrogen content (o) and total concentration (x) of nucleophilic groups on the surface of functionalized MWCNTs.

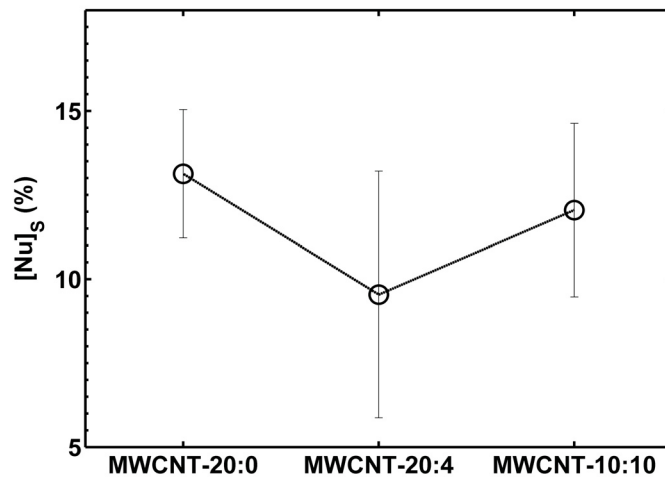


Figure 6.6: Selectivity of nitrogen functional groups for nucleophilic groups.

components that allow the description of the C 1s tail are found at 291.7 eV (π -plasmon) and at 294.2 eV (bulk loss). A component at 285 eV is attributed to sp^3 bonds. For the treated samples, 4 components are added, from 286.5 to 289.5 eV, and they are labeled C1, C2, C3, C4. These components correspond to functional groups added to the surface of the MWCNTs with increasing electronegativity going from low to high binding energies (BE). The possible functional groups are: amines C-N<, hydroxyls or ethers C-O, imines C=N, nitriles C \equiv N, carbonyls C=O, amides N-C=O and N-C-O [21, 173]. Note that it is not possible to attribute specific functional groups to the C1 to C4 components given the complexity of the C 1s peak for a functionalized MWCNT. Fitting these 4 components only allows us to qualitatively observe the changes in functionalization between samples. All the components and their positions are shown in Table 6.2.

Functional groups containing oxygen atoms were added to the list of possible functional groups as there is about 1 at% of oxygen found in all samples. Oxygen can be incorporated in the samples both on the grafted functional groups or the plasma polymer coating through

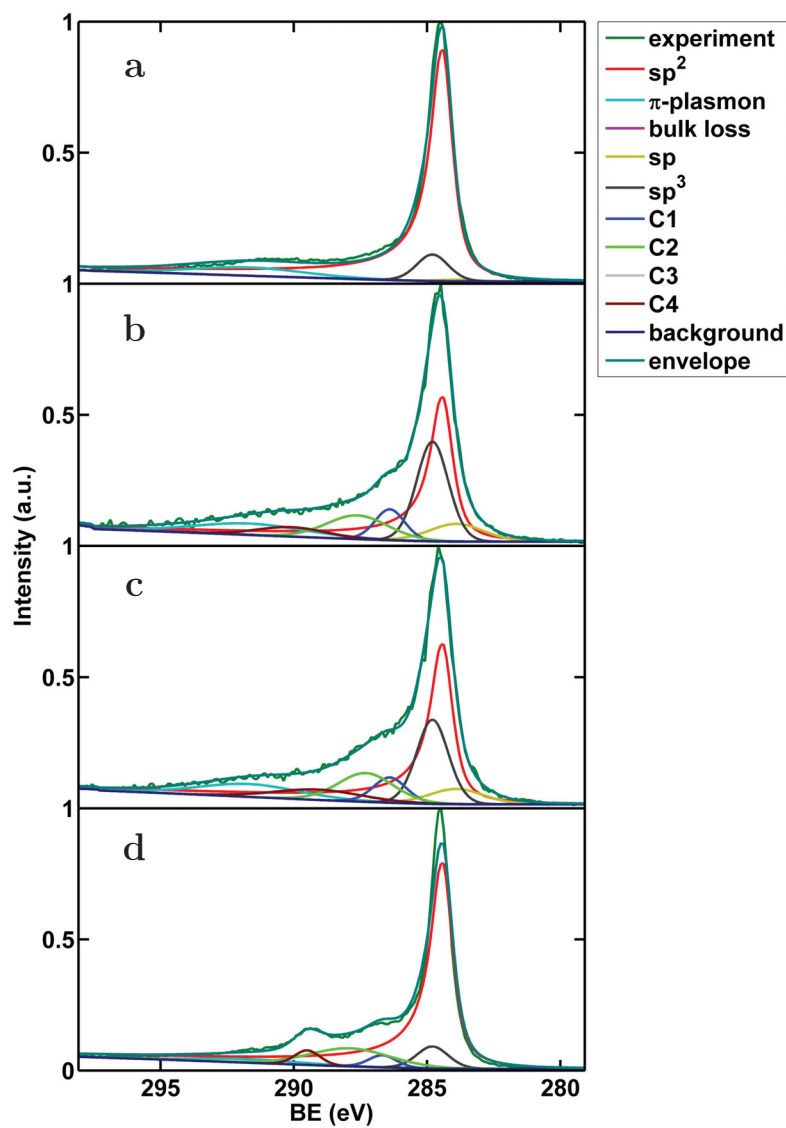


Figure 6.7: Experimental and fitted C 1s peaks for a) as-synthesized MWCNTs, b) MWCNT-20:0, c) MWCNT-20:4, d) MWCNT-10:10- O_2 .

Table 6.2: XPS fit component positions [21, 173].

Component name	BE (eV)	FWHM (eV)	Chemical assignment
sp	283.9	~3	defects in the graphitic structure
sp ²	284.5	~1	
sp ³	285	~1.5	graphitic structure
C1 to C4	286.5, 287.5, 288.5, 289.5	~2 per component	
π -plasmon	291.7	~5	N and O functional groups with increasing electronegativity
bulk loss	294.2	~6	

reactions between the fresh sample and components of atmospheric air, a phenomenon generally referred to as “ageing” [22, 112]. This process is limited by the storage of samples in the freezer in inert atmosphere. However, sample handling during preparation for various analyses led to an unavoidable 20 min exposure to air, on average.

When comparing pure MWCNTs to ammonia plasma-treated samples, we can already observe a decrease in the graphene component and an increase of the defect and C1 to C4 components. Given the very small changes between samples MWCNT-20:4 and MWCNT-20:0, these changes may be attributed to the newly deposited plasma polymer on MWCNT-20:4 and not to grafting of more functional groups. As for sample MWCNT-10:10, fitting of the C 1s peak was not performed given that XPS measurements on this sample yielded information on the plasma polymer alone. As we do not have a set of similar samples to compare to each other, it is not possible to deduce meaningful conclusions about its different components.

Figure 6.7d shows the C 1s peak for the MWCNTs-10:10-O₂ sample. About 16 O at% was measured for this sample and no nitrogen nor fluorine, after treatment with TFBA, were detected. Peak fitting on this sample suggests that the main moieties added to the surface

of the MWCNTs are hydroxylic and carboxylic groups (components C1 and C4 around 286 and 289 eV) [10].

The first peak seen on the NEXAFS spectra of the carbon K-edge around 285 eV is attributed to C 1s transitions to π^* orbitals (Figure 6.8) [115]. Other peaks typical of MWCNTs and graphitized structures are those seen above 291 eV [115, 174], present on all samples except MWCNT-10:10. As with the XPS measurements, the NEXAFS measurements for MWCNT-10:10 only report information on the plasma polymer layer over the MWCNTs and not the nanotubes themselves. The added functional groups to the MWCNTs can be found between 285 and 289 eV. More specifically, the peak at 285 eV includes contributions from C=N. Peaks seen around 286.8 eV on samples MWCNT-20:4 and MWCNT-10:10 are assigned to nitriles (C \equiv N) [115]. The small peaks between 287.5 and 289 eV can be attributed to nitrogen in conjugated systems, such as N=C-N and N \equiv C-N [175]. In our case, since oxygen was also found on these samples, these peaks may have contributions from oxygenated surface functional groups as well [176].

Peak fitting was also performed for a part of the NEXAFS spectra (Figure 6.9). Two components at 285.3 and 291.7 eV were used for the main transitions to the π^* and σ^* orbitals. Components labelled A and B represent the added nitrogen and oxygen groups. The increase in area of these two components when comparing samples MWCNTs-20:0 and MWCNTs-20:4 to the as-synthesized MWCNTs reflect the incorporation of nitrogen groups measured by XPS and the deposition of a plasma polymer that was observed through TEM. Only one other component labelled C was used to fit the spectra between 291 and 293 eV (not shown here). The rest of the available range of the spectra was not fitted since no information on the attribution of the multiple components could be found for MWCNTs modified with both oxygen and nitrogen groups.

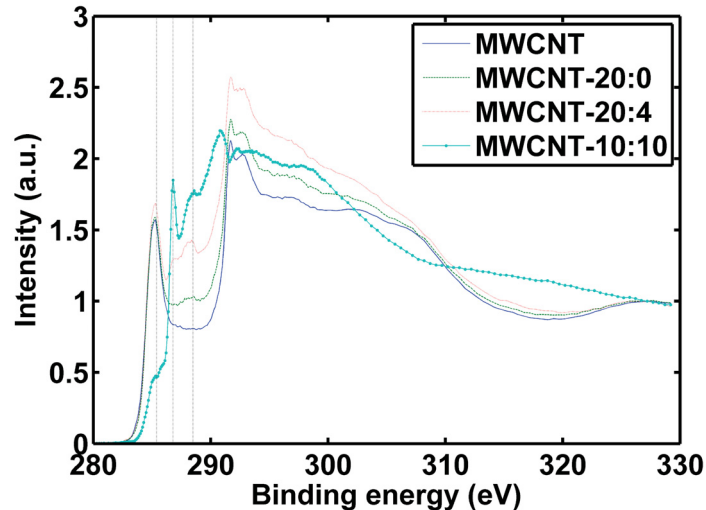


Figure 6.8: NEXAFS spectra of the C K-edge for as-synthesized MWCNTs and all functionalized MWCNTs.

Figure 6.10 presents the NEXAFS spectra of the nitrogen K-edge. The shoulder at 399 eV corresponds to imines and the larger peak at 400 eV is attributed to nitriles. Other researchers have also often observed nitriles when plasma polymerizing molecules containing amine functional groups. Shard et al. explained this phenomenon through a reaction scheme which favored nitriles instead of conservation of the original amines in the molecules [177]. Another feature of interest in this graph is the presence of a small peak at 401 eV in samples MWCNT-20:0 and MWCNT-20:4 which could be attributed to substitutional nitrogen atoms inside the graphitic structure of the tubes. The broadening of the large peak found after 401 eV is also an indication of the presence of defects.

6.4.4 Stability of nitrogen functionalization after water immersion

It has been reported that plasma polymers synthesized from ammonia and ethylene can be unstable in water [115, 116, 117]. In order to investigate this, SS meshes covered with plasma-treated MWCNTs were placed in water for 24 h and then dried in argon. The composition of the samples was analysed by XPS. It was observed that for all three samples, there

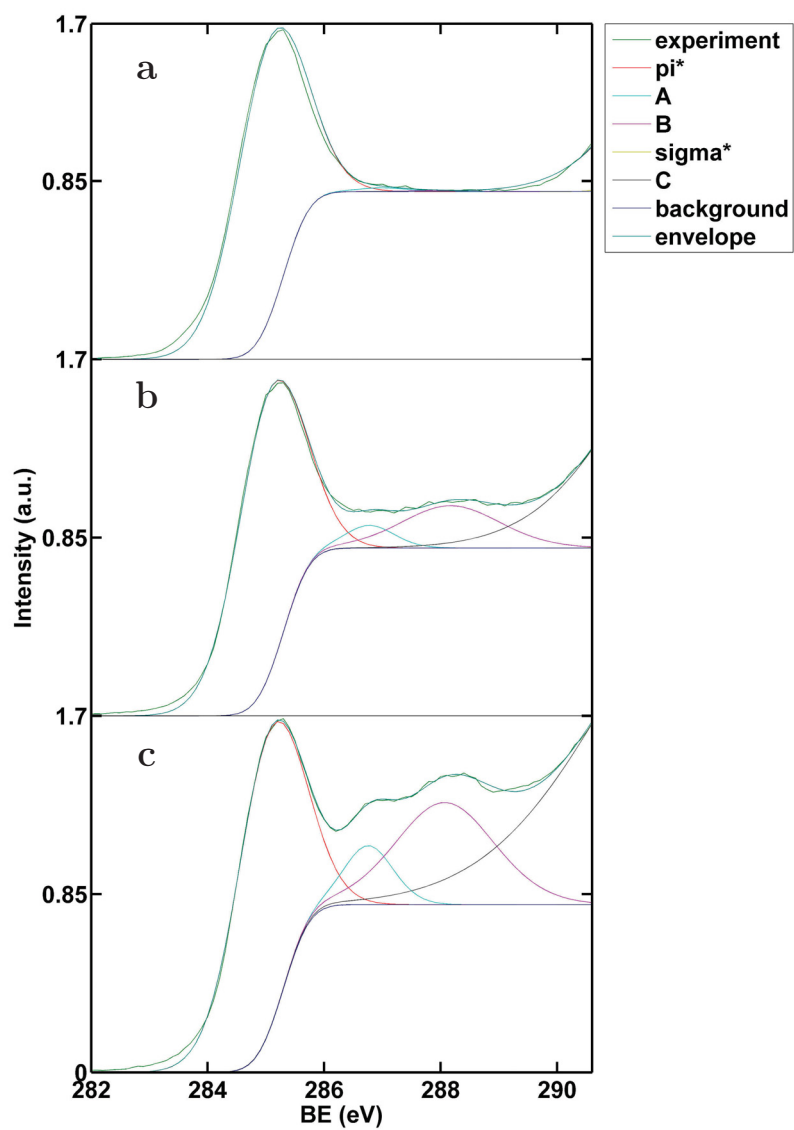


Figure 6.9: Experimental and fitted carbon peaks for a) as-synthesized MWCNTs, b) MWCNT-20:0, and c) MWCNT-20:4.

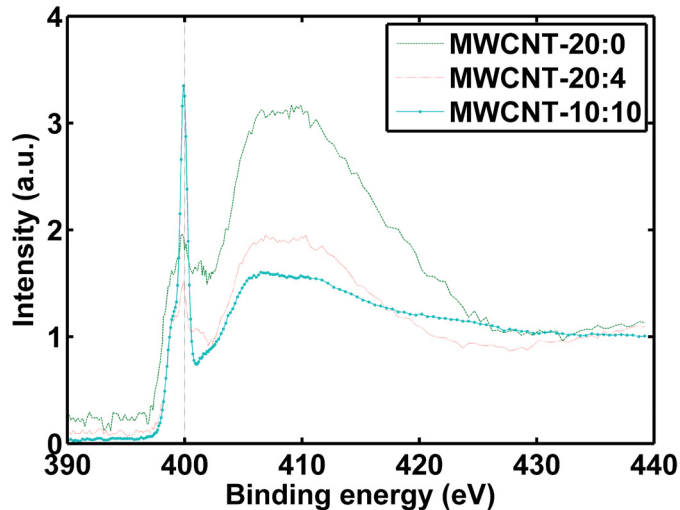


Figure 6.10: NEXAFS spectra of the N K-edge for all functionalized MWCNTs.

was an increase in oxygen content from about 1 to 3 at% and a loss in nitrogen content as shown in Figure 6.11. For samples MWCNT-20:4 and MWCNT-10:10, the loss in nitrogen could be attributed to solubilization of the plasma polymer layer. Truica-Marasescu et al. explained that low power input and pressure conditions during synthesis led to poorly cross-linked plasma polymers that are soluble in polar solvents such as water [115]. Hydrolysis reactions that convert imines and amines into hydroxides, carboxylic acid and carbonyls could be responsible for the degradation of the plasma polymer coating [178]. As for sample MWCNT-20:0, although its nitrogen functional groups are directly grafted to the MWCNTs, the same hydrolysis reactions could be responsible for the observed loss in nitrogen. Nevertheless, on all three samples, a functional layer with nitrogen groups remains as was also observed by other researchers [115, 116, 117].

6.4.5 NFs CO₂ absorption capacity

Figures 6.12 and 6.13 show the absorption capacity and rates of CO₂ by RO water and the three different NFs. Sample MWCNT-10:10, which has the most nucleophilic sites that

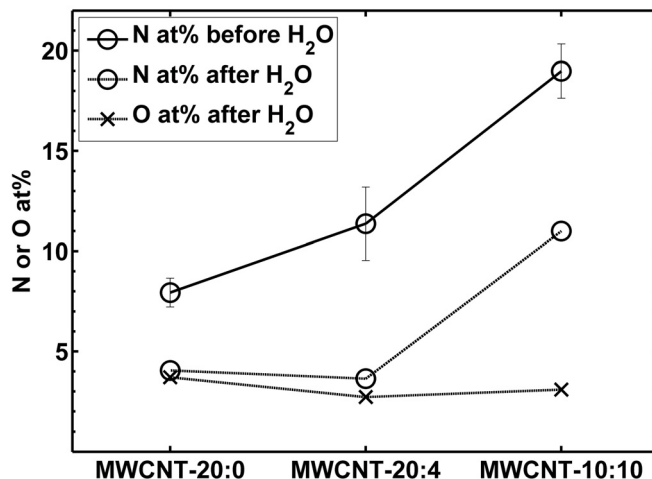


Figure 6.11: Nitrogen content (o), and oxygen content (x) before (solid line) and after (dashed line) immersion of the MWCNTs in water.

may interact with CO₂, has the largest gas absorption capacity, at 1.67 mL of CO₂ g⁻¹ of NF, corresponding to a 36% increase with respect to water. Kim et al. reported similar total absorption capacities with an aqueous SiO₂ NF [60]. Note however that their NP concentration was an order of magnitude higher than the one used in our experiments. A discrepancy between our absorption capacity of CO₂ in water and theirs also exists and is probably due to experiments being run at different temperatures: Kim et al. did not specify their room temperature.

The highest CO₂ absorption capacity was registered during the first absorption cycle for sample MWCNT-10:10. In subsequent cycles, the absorption capacity was smaller but remained fairly constant (Figure 6.14). One explanation for this behavior is that flowing Ar through the column might not be enough to remove all the CO₂ present in the NF. For common alkanolamines, it is usually necessary to heat them to dissociate the product of the reaction between CO₂ and amines [59]. For example, Liu et al. observed that N₂ purging and

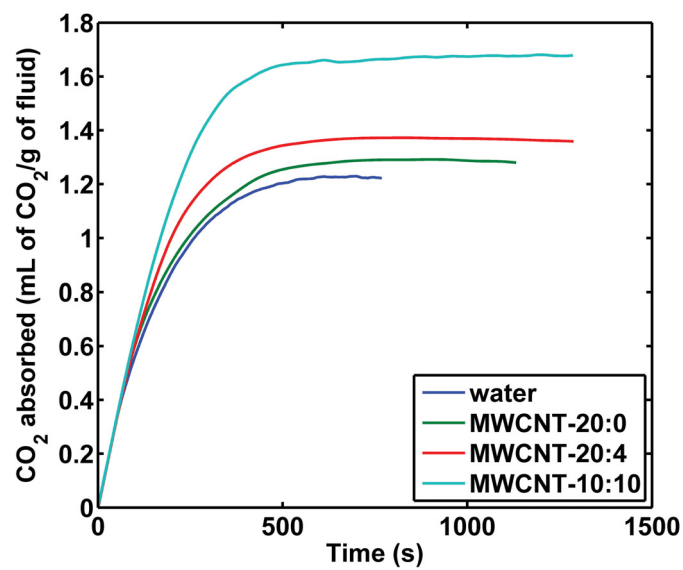


Figure 6.12: Total amount of CO₂ absorbed by RO water and aqueous MWCNT NFs as a function of time.

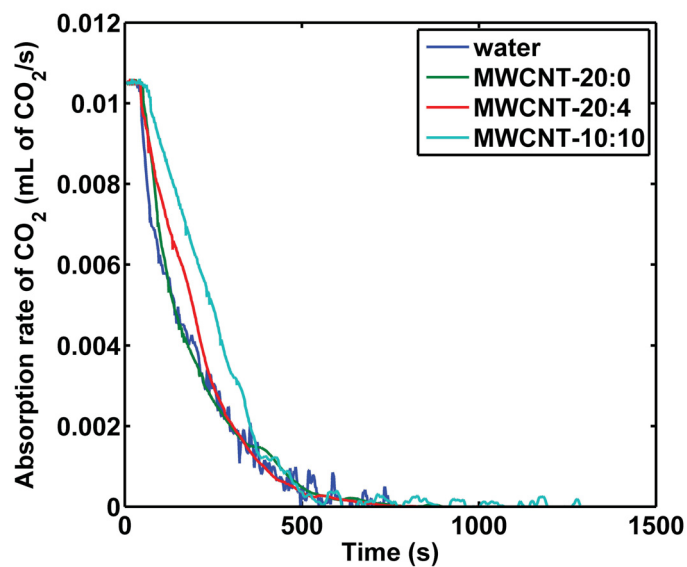


Figure 6.13: Absorption rate of CO₂ in RO water and aqueous MWCNT NFs.

a temperature 40 °C higher than the CO₂ adsorption temperature was necessary for efficient recovery of their original material [179].

There was no agglomeration of MWCNTs during the experiments on the gas bubble column. MWCNT-10:10 NFs that were stored at room temperature after being tested remained stable. However, nanotubes in MWCNT-20:0 and MWCNT-20:4 would agglomerate and drop to the bottom of the vial less than 24 h after the end of their use in the gas bubble column. When these NFs were not tested and left untouched, visual inspection of the suspensions for evidence of MWCNT agglomeration and settling showed none, thus indicating that they were stable for at least three months. The agitation of the NFs by the passing of the bubbles may accelerate the formation of larger MWCNT agglomerates. For poorly stabilized samples as observed with MWCNTs containing less nucleophilic sites, this possibly may be all that is necessary to cause the loss of NP stability in the host fluid.

In order to demonstrate that the addition of nucleophilic groups is important, a sample was treated with a O₂/C₂H₄ mixture rather than NH₃/C₂H₄. In this way, the MWCNTs were stable in water but they do not react with CO₂. As shown in Figure 6.15, the oxygen functionalized sample did not perform as well as sample MWCNT-10:10. Its performance is comparable to that of the two samples with the smallest amount of nucleophilic sites.

The absorption capacity of these NFs is low compared to other technologies available. Common solutions of alkanolamines can go up to 4 mol of CO₂ L⁻¹, with concentrations of 5 mol L⁻¹ of the alkanolamine [180]. In the current study, the maximum obtained is 0.067 mol of CO₂ L⁻¹ of NF. Although, the added nitrogen functional groups to the surface of the MWCNTs have a noticeable impact on both their stability in RO water and CO₂ absorption capacity, this latter effect is small. Olle et al. experiments also suggested that the impact on absorption for the oleic acid used to stabilize the NPs was minimal since its

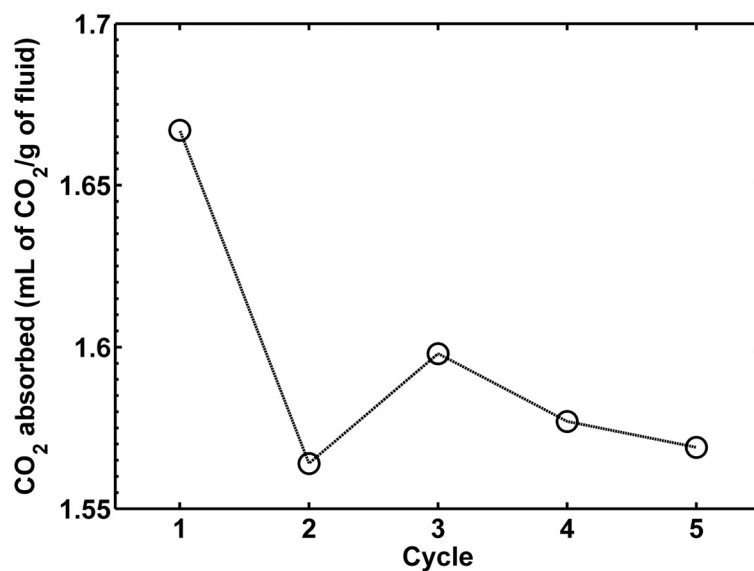


Figure 6.14: Maximum CO₂ absorbed by NF MWCNT-10:10 through multiple absorption/desorption cycles.

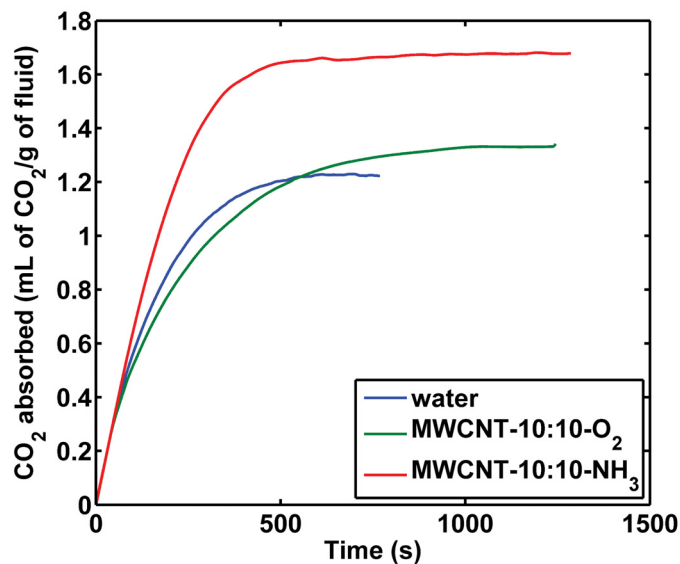


Figure 6.15: Total amount of CO₂ absorbed by two NFs with MWCNTs treated with oxygen or ammonia.

concentration could account for only a very small portion of the total oxygen uptaken by the NF [181]. This may also be the case in this work as the quantity of nucleophilic groups added to the MWCNTs is very small compared to the large concentrations of alkanolamines used in absorbing fluids.

6.5 Conclusion

MWCNTs plasma-functionalized with ammonia and ethylene were shown to have an enhanced CO₂ absorption capacity with respect to water. Modification of the surface chemistry of MWCNTs fulfilled two goals: ensure stability of the MWCNTs in the host liquid (RO water) and enhance their interaction with CO₂. Grafting of functional groups onto the MWCNTs using a pure NH₃ plasma was seen to yield low quantities of added nucleophilic groups. Addition of ethylene in the plasma allowed for the deposition of a nitrogen-rich plasma polymer layer on the MWCNTs. Aqueous nanofluids prepared with these MWCNTs showed a 36% increase in CO₂ absorption capacity with respect to water. However, this enhancement is not sufficient to compete with common aqueous solutions of alkanolamines which have much higher concentrations of amines compared to our NFs.

Nevertheless, the combined addition of nitrogen functional groups and enhanced stability of these NPs in water make them interesting candidates for biological applications. It has been shown that amine and imine functional groups can provide anchoring points for biomolecules [126]. Given their high level of functionalization, the MWCNTs will not tend to agglomerate inside the body allowing for easy biodegradation and elimination [182]. Future work will focus on increasing the density of nucleophilic functional groups on the MWCNTs and exploring their potential use in biological applications.

CHAPTER 7

Dye capture

7.1 Preface

This chapter presents the results from a study on the interaction between MWCNTs and MWCNT-PPE:X with dyes.

The work was planned, executed, analyzed and written by L. Jorge (Ph.D. candidate). Dr. S. Coulombe and Dr. P.-L. Girard-Lauriault were responsible for supervision of the work and reviewing of the chapter.

By being able to tune the surface charge of the MWCNTs using the two different types of plasma polymer coatings at different pH values, this chapter shows that they can be used to preferentially adsorb dyes of opposite charge.

7.2 Introduction

Some soluble molecules found in wastewater cannot be filtered, degraded or coagulated. However, they might be removed by adsorption [183, 184]. Among the materials being developed for wastewater treatment, carbon nanomaterials such as graphene and carbon nanotubes make interesting adsorbents. They have large surface areas and their surface chemistry can be easily modified to enhance interaction with the desired molecules. In particular, they can make very strong adsorbents for dyes. The hexagonal structure of the carbon nanomaterials provides bonding interactions with the conjugated systems of the dyes, while addition of functional groups onto the adsorbent allows for electrostatic interactions with the charged moieties of the dyes.

As shown in Chapter 4, multi-walled carbon nanotubes (MWCNTs) modified with nitrogen or oxygen-rich plasma polymer (PP) coatings form stable suspensions in water. There are no visible agglomerates and a maximum of surface area is available for interaction with other molecules. Furthermore, the choice of nitrogen or oxygen-containing functional groups on the coating makes it positively or negatively charged, thus determining the type of dye that it interacts with more favorably.

This chapter presents a study on adsorption of an anionic dye, methyl orange (MO), and a cationic dye, methylene blue (MB, see Figure 7.1), onto MWCNTs and plasma treated MWCNTs. The impact of pH on the adsorption capacity and the dye desorption is investigated. However, low quantities of MWCNTs available limited the types of experiments that could be conducted. These experimental limitations are discussed and suggestions for improvement are offered.

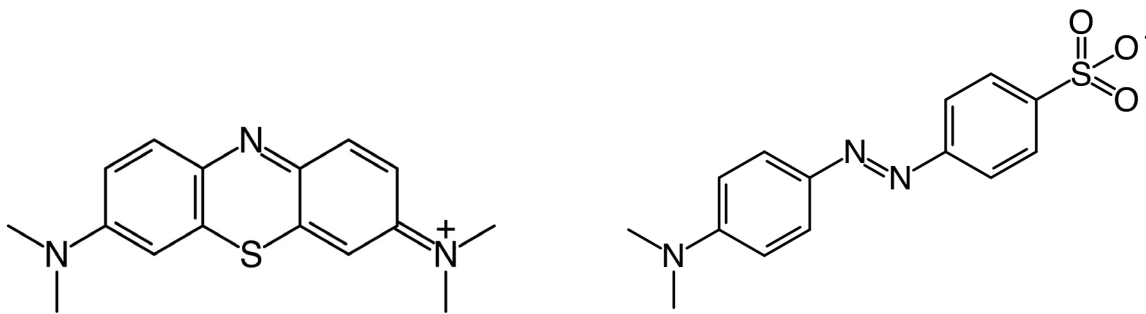


Figure 7.1: Methylene blue (left) and methyl orange (right).

7.3 Experimental method

7.3.1 Nanofluid synthesis

MWCNTs were produced in-house using a method developed by Hordy et al. and explained in detail elsewhere [37](see Chapter 4). Briefly, in a tubular furnace kept at 700 °C, MWCNTs are grown on the surface of a stainless steel mesh (316 grade, 400 mesh, TWP Inc.) by thermal chemical vapor deposition (t-CVD) of acetylene gas C₂H₂ (99%, dissolved in acetone).

MWCNTs were then covered with a PP coating in a low pressure RF glow discharge (13.56 MHz, continuous) described elsewhere [92]. Coatings containing nitrogen functional groups were produced when using a mixture of ammonia, NH₃ (99.99%), and ethylene, C₂H₄ (99.70%). These coatings are referred to as PPE:N. Coatings with oxygen functional groups were obtained when using a mixture of carbon dioxide, CO₂, and C₂H₄ and are referred to as PPE:O. The deposition conditions as well as the nitrogen and oxygen content of these coatings is presented in Table 7.1.

Each mesh sample (size 3.5 x 7 cm²) was then sonicated for 10 min in 6 mL of reverse osmosis (RO) water (pH ~5.5) or water at pH 4.0±0.1 or 9.9±0.1 (adjusted using solutions

Table 7.1: Operating conditions for plasma polymer deposition.

	MWCNT-PPE:N	MWCNT-PPE:O
$Q_{\text{NH}_3\text{orCO}_2}$ (sccm)	10	10
$Q_{\text{C}_2\text{H}_4}$ (sccm)	30	4
Deposition time (min)	4	20
N at% [37]	17.4	0.6
O at% [37]	1.3	20.0
Pressure (mTorr)	600	
Power (W)	35	

of 1 M HCl or 1 M NaOH). These pH values are referred to as pH 5.5, 4 and 10 respectively for the rest of this chapter.

7.3.2 Interaction of MWCNT-PPE:X with dyes

Adsorption and reuse

For adsorption experiments (see Figure 7.2 for schematic), 5 mL of the desired nanofluid were mixed with 5 mL of the dye solution, at 25 mg L⁻¹, in a glass vial. The capped vials were then stored in the dark for 24 hr. The nanofluids were transferred to 15 mL Falcon tubes and centrifuged at 3500 RPM for 30 min. When MWCNTs would not settle after centrifugation, 500 μL of 4.3 mol L⁻¹ NaCl solution was added and then nanofluids were centrifuged again. The dye concentration in the supernatant was then measured by visible absorption spectroscopy (Evolution 300, Thermo), using disposable polystyrene cuvettes (Fisher). Spectra were recorded from 400 to 800 nm. When necessary, the sample was diluted in order to obtain an absorbance between 0 and 1.4 absorbance units. The remaining liquid mixture was then filtered onto a pre-weighed nitrocellulose membrane filter (porosity 0.22 μm , 47 mm diameter, Merck Millipore) and the mass of MWCNTs was measured by weighing the filter with MWCNTs after it had completely dried in air.

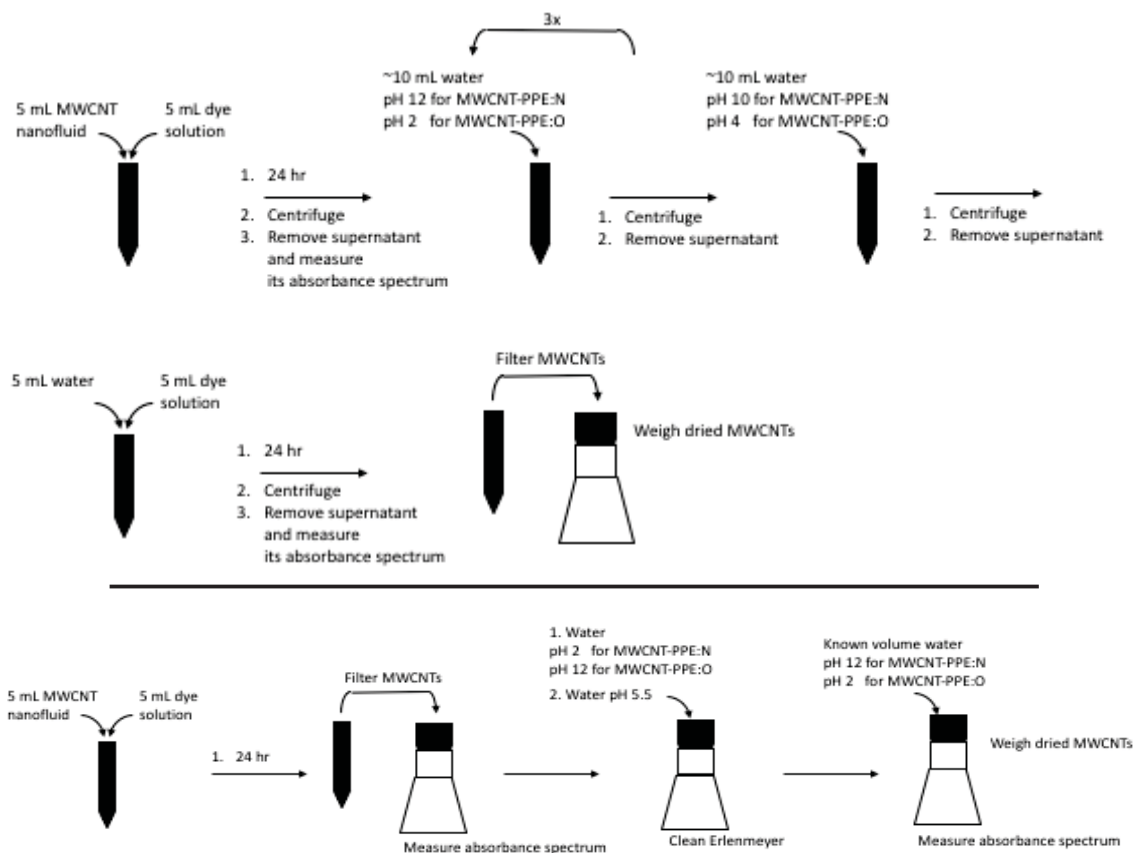


Figure 7.2: Schematic of the adsorption and reuse (top) and release experimental procedures (bottom). MWCNT here refers to both MWCNTs and MWCNT-PPE:X, unless specified otherwise.

The first step in treating the data obtained was to bring all baselines to zero. MWCNTs absorb in the same wavelength range as the dyes, and in some samples, centrifugation was not enough to settle all MWCNTs. Their presence in the supernatant caused an offset of the spectrum to higher absorption values, thus requiring an adjustment of the baselines before performing further calculations. The second step was to calculate the concentration of the dye, c (mg L^{-1}), using Beer-Lambert's law (see Equation 7.1). Table 7.2 presents the wavelength and the absorption coefficient, ϵ ($\text{cm}^{-1} \text{mg}^{-1} \text{L}$), used for the two dyes. The path length of the cuvette, l , was 1 cm and A is the absorbance measured.

$$A = c\epsilon l \quad (7.1)$$

The adsorption capacity, q_t (mg g^{-1}), was then calculated according to Equation 7.2

$$q_t = \frac{(c_0 - c_a)V}{m} \quad (7.2)$$

where c_0 and c_a are, respectively, the initial and final dye concentration after adsorption, V is the volume of solution in L and m is the mass of MWCNTs in g.

A few samples were selected to test for reusability of the adsorbent. At the end of the first adsorption cycle, samples were in Falcon tubes, with the solid adsorbent at the bottom and the remaining dye solution on top. The supernatant was removed and about 10 mL of water at pH 12 for MWCNT-PPE:N or pH 2 for MWCNT-PPE:O was then added into the Falcon tube to release the dye from the MWCNTs. The MWCNTs were redispersed in the liquid and then underwent another centrifugation step. This washing technique was repeated until the supernatant was clear and contained no more dye (usually three or four cycles were necessary). One more washing cycle was then performed using water at pH 10

for MWCNT-PPE:N and water at pH 4 for MWCNT-PPE:O. The supernatant was removed and the remaining concentrated mixture of MWCNTs was redispersed in water at the desired pH value. As previously done for the first adsorption test, 5 mL of the MWCNTs nanofluid was mixed with 5 mL of fresh dye solution. After 24 hr in the dark, they were centrifuged again and the absorption spectrum of the supernatant was recorded.

Release

In order to quantify the amount of dye released by washing the adsorbent, the nanofluids with dye were filtered over a nitrocellulose membrane filter. The absorption spectrum of the filtrate was measured. The solid MWCNTs were then washed with water at pH 2 for MWCNT-PPE:N and water at pH 12 for MWCNT-PPE:O in order to remove any loosely attached dye. When no more dye was observed in the filtrate, the solid residue was washed with RO water and a new clean collection cup was positioned under the filter. Then, a known volume of water at pH 2 was used with MWCNT-PPE:O or water at pH 12 with MWCNT-PPE:N to release the dye from the solid residue. This solution was collected and its absorption spectrum measured. The results are presented as a percentage of dye recovered, d , as shown in Equation 7.3

$$d = \frac{c_r V_r}{(c_0 - c_a)V} = \frac{m_r}{m_a} \quad (7.3)$$

where c_r is the concentration of dye released and V_r is the known volume of water used to release the dye. In other words, d is the fraction of mass of dye released, m_r , with respect to the mass of adsorbed dye m_a .

7.4 Results and discussion

7.4.1 Effect of pH, concentration and time on MO and MB

The most common method of detection for studies involving colored dyes is the use of visible absorption spectroscopy given its ease of use and fast sample throughput. The concentration of the dye can be quickly determined through Beer's law (see Equation 7.1) as long as we know the molecule's absorption coefficient at a given wavelength. However, a molecule's structure, and therefore its absorption coefficient, may change with its concentration or the pH of the solution. In dye adsorption studies, where both these parameters change, not considering their effect on the absorption coefficient may lead to errors in analysis of the spectra obtained. Values for absorption coefficients are not readily available in the literature and therefore they needed to be determined for our desired experimental conditions.

Starting from stock solutions of MO and MB, solutions at different pH values and concentrations were prepared. From the visible absorption spectra obtained for these solutions, the wavelength at the peak of maximum absorption, λ_{max} , was recorded. Using the absorption intensity at this wavelength and the known concentration of the sample, the absorption coefficients, ϵ , were calculated.

Figure 7.3a shows the effect of pH on both ϵ and λ_{max} for MO. As can be seen, λ_{max} is between 461 and 463 nm and ϵ fluctuates from 0.077 to 0.079 L mg⁻¹ cm⁻¹ for a pH between 4 and 12. Figure 7.3b also confirms that at pH 5.5, λ_{max} and ϵ are not functions of concentration. However, at pH 2, the values for both properties are different. An apparent change in ϵ (see Figure 7.3b) is observed with a change in dye concentration. A white precipitate forms when the solution is brought to pH 2. Furthermore, from pH 2 to 3.7, the absorption peak of MO shifts from 463 to 505 nm, as the dye solution visually changes from orange to red. This indicates that the solution is actually a mixture of MO in its

anthraquinone and azo forms [185], each one having its own absorption coefficient. To simplify the data treatment, it was decided not to use MO solutions with pH below 4.

Figure 7.4a shows that λ_{max} or ϵ for MB do not change from pH 2 to 10. However, at pH 12, MB changes its structure gradually with time. As can be seen in Figure 7.5, a fresh solution of MB at pH 12 already has a different absorption spectrum compared to a fresh solution of MB at pH 5.5. MB continues to change over time at pH 12 as shown by its very different absorption spectrum 11 days after preparation of the solution. At pH 2 and 5.5 the absorption spectra remain the same after 11 days.

Figure 7.4b also shows that concentration has an important impact on the dye. Given the cell path length used, the upper limit for the concentration of MB that can be measured with this spectrometer is 25 mg L⁻¹. Below that concentration, the absorption coefficient constantly changes from 0.14 L mg⁻¹ cm⁻¹ at 19 mg L⁻¹ of MB to 0.23 L mg⁻¹ cm⁻¹ for 0.8 mg L⁻¹. The explanation for this change in absorption coefficient is not precipitation of the dye as was observed for MO. Rather, it is that MB exists as monomers, dimers, trimers or even larger oligomers in solution, each one having a different absorption spectrum. Many researchers have tried developing models to separate the absorption spectrum of the mixture into its individual components with little success [186]. Therefore, for this study, an empirical method was used to determine the apparent absorption coefficients at $\lambda_{max} = 660$ nm, based on the regression line correlating measured absorption coefficient and absorbance intensity of MB solutions (see Figure 7.6). Every MB solution analyzed was diluted to an absorbance value below 1.4 and its apparent absorption coefficient was then calculated using the equation from Figure 7.6.

In order to work with both dyes at the same conditions, it was decided that further experiments would be limited to pH 4, 5.5, and 10. The initial dye concentration after being

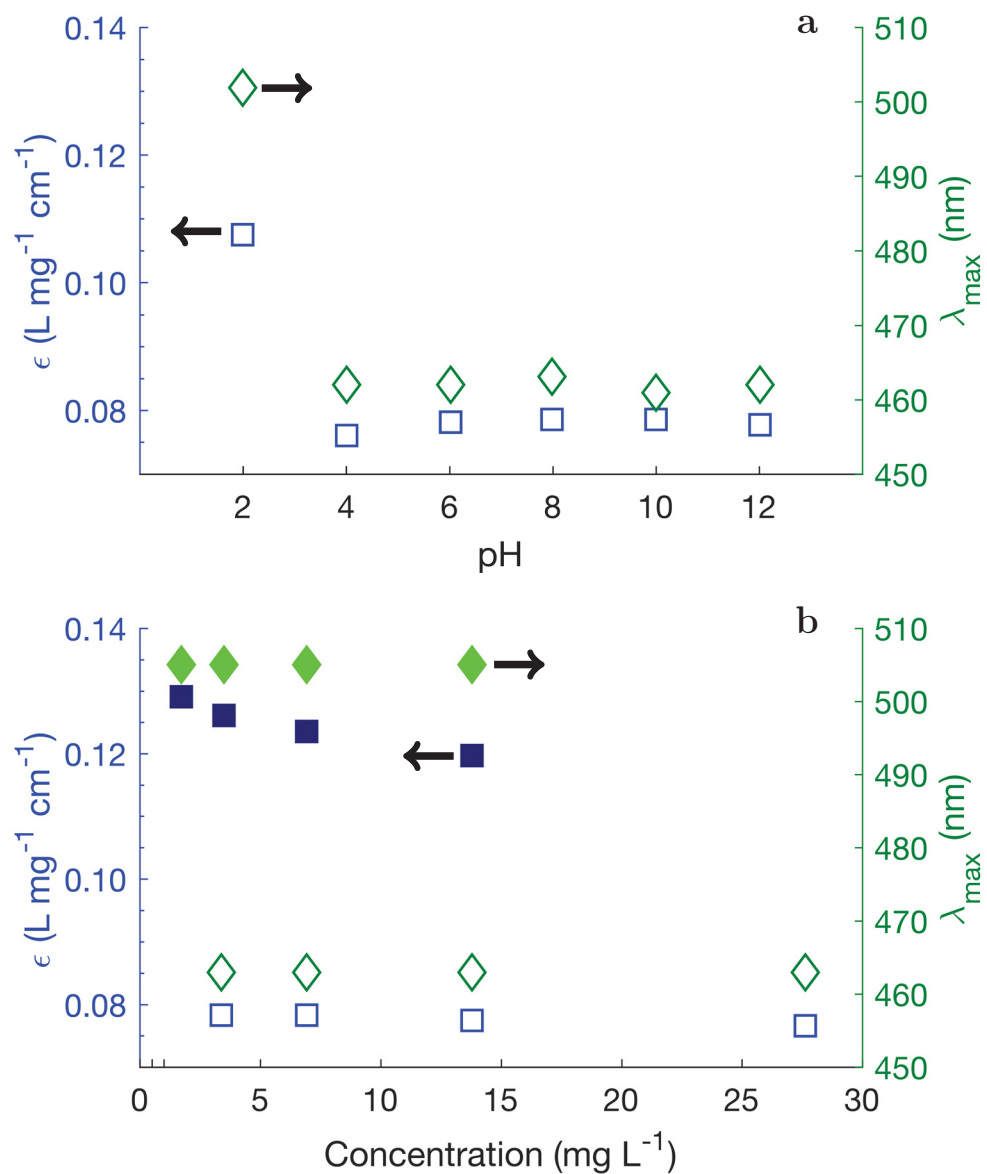


Figure 7.3: Absorption coefficient (squares) and wavelength of maximum absorption (diamonds) of MO with respect to (a) pH (28 mg L⁻¹) and (b) concentration (filled markers at pH 2, empty markers at pH 5.5).

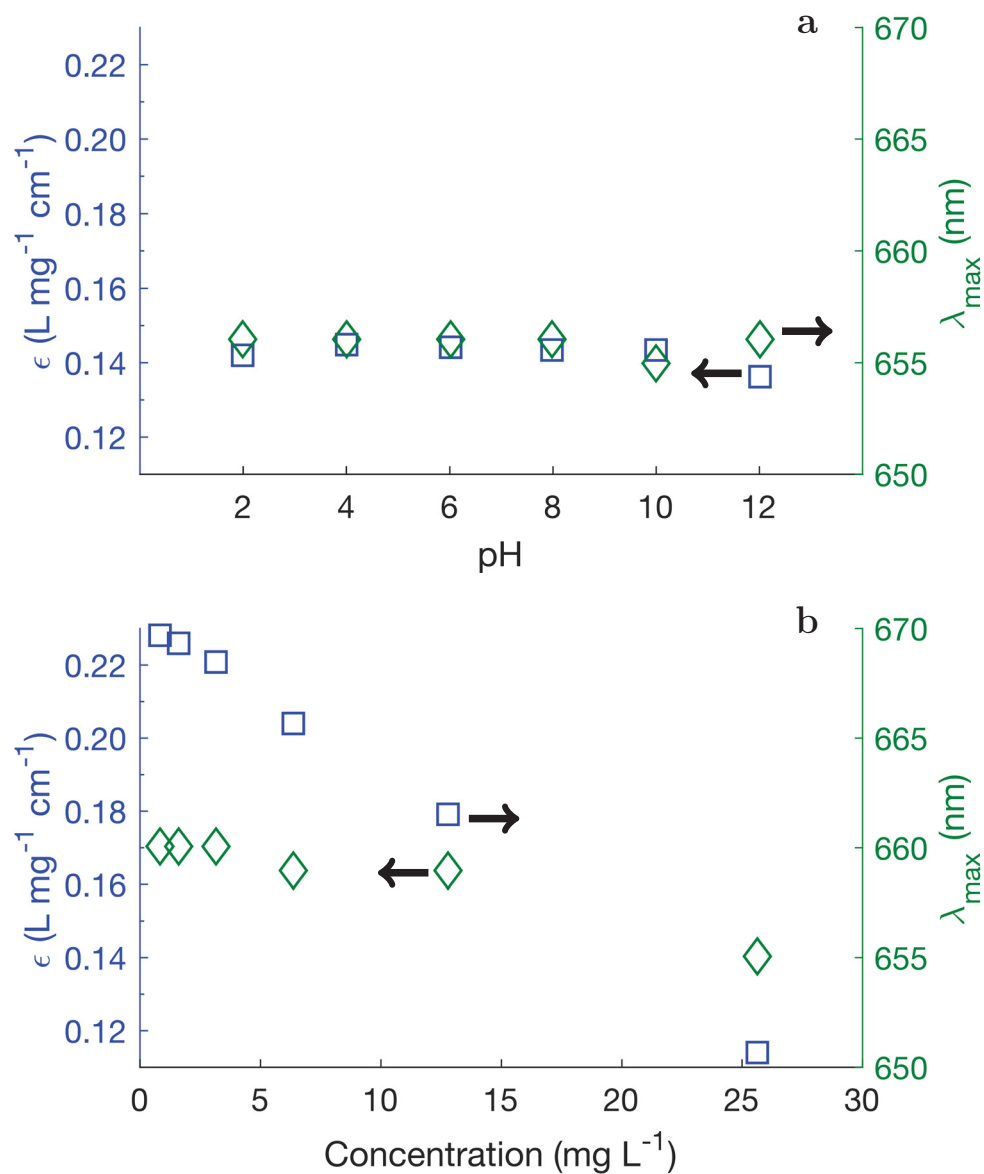


Figure 7.4: Absorption coefficient (squares) and wavelength of maximum absorption (diamonds) of MB with respect to (a) pH (19 mg L^{-1}) and (b) concentration (pH 5.5).

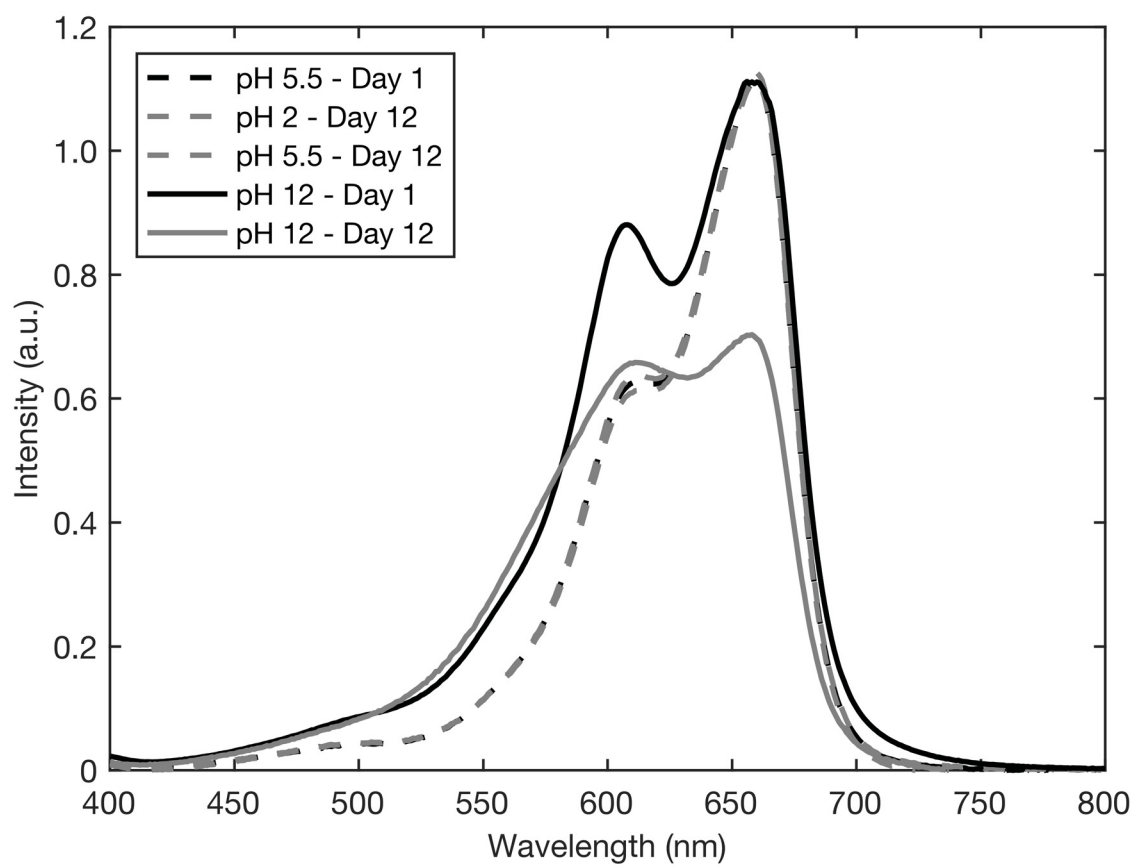


Figure 7.5: Absorption spectrum of MB at different pH values and time since preparation.

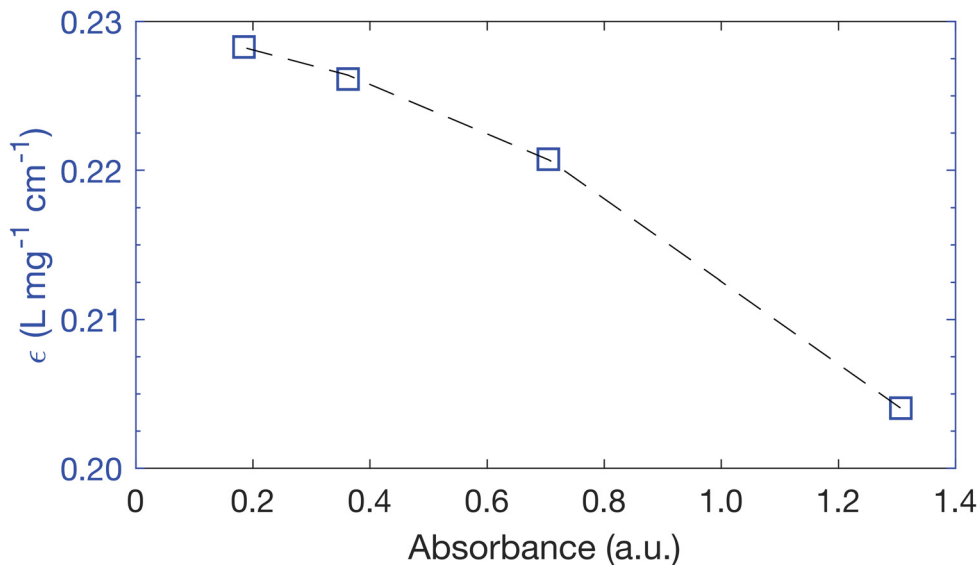


Figure 7.6: Absorption coefficients of MB with respect to absorbance units. The dashed line corresponds to the regression line with equation: $-0.118x^2 - 0.004x + 0.229$.

mixed with the MWCNT nanofluid was chosen as 12.5 mg L^{-1} . The values for λ_{max} and ϵ for each dye are presented in Table 7.2.

7.4.2 Adsorption, reuse and release

Figure 7.7 shows the MO adsorption capacity of MWCNTs and MWCNT-PPE:X. The main observation is that MWCNT-PPE:N increases its adsorption capacity as the pH becomes more acidic. A much smaller adsorption capacity was measured when using MWCNT-PPE:O or MWCNT. Figure 7.8 shows the MB adsorption capacity. Contrary to adsorption

Table 7.2: Properties of MO and MB.

	MO	MB
$\epsilon \text{ (L mg}^{-1} \text{ cm}^{-1}\text{)}$	0.078	0.20 to 0.23
$\lambda_{max} \text{ (nm)}$	463	660

of MO, adsorption capacity for MB increases with more basic pH not only for MWCNT-PPE:O but also for MWCNT-PPE:N and MWCNT. The adsorption capacity of samples that were washed and then reused for a second adsorption experiment are shown with stars as markers.

The main adsorption mechanism for dyes on MWCNT-PPE:X is electrostatic forces [78, 83, 187, 188, 189, 190, 191]. As had been shown in our previous work [37] (Chapter 4), MWCNT-PPE:N is more stable at acidic pH values due to the formation of positive charges on the nitrogen-containing functional groups. MWCNT-PPE:O is more stable at basic pH values due to negatively charged oxygen-containing groups. This explains an increase in MO adsorption, which is an anionic dye, on the positive surface of MWCNT-PPE:N at acidic pH. The same effect is observed for MB, a cationic dye, which adsorbs more at basic pH values on the negatively charged surface of MWCNT-PPE:O. On MWCNT, given that there are no functional groups, adsorption occurs most likely through π - π interactions. MO and MB may interact with the π system of the MWCNTs pristine surface since they are planar molecules with conjugated systems [78].

Given that electrostatic forces are the strongest interactions determining the adsorption of the dyes, a pH switch that decreases the amount of charged functional groups on the surface of MWCNT-PPE:X was used to cause dye desorption. An increase in the amount of dye released when switching the water pH was observed as shown in Figure 7.9. The spectrum shown with a dashed line corresponds to the last 10 mL of water used to wash MWCNT-PPE:O (a total of 80 mL of water was used). After switching to water at pH 2, more MB could be removed (solid line in Figure 7.9). The desorption method used here allowed for recovery of 51% of MO adsorbed on MWCNT-PPE:N, and 58% of MB on MWCNT-PPE:O. This low recovery of the dyes suggests that other forces, in addition to electrostatic forces, govern their adsorption. Other researchers have used a pH switch in conjunction with other

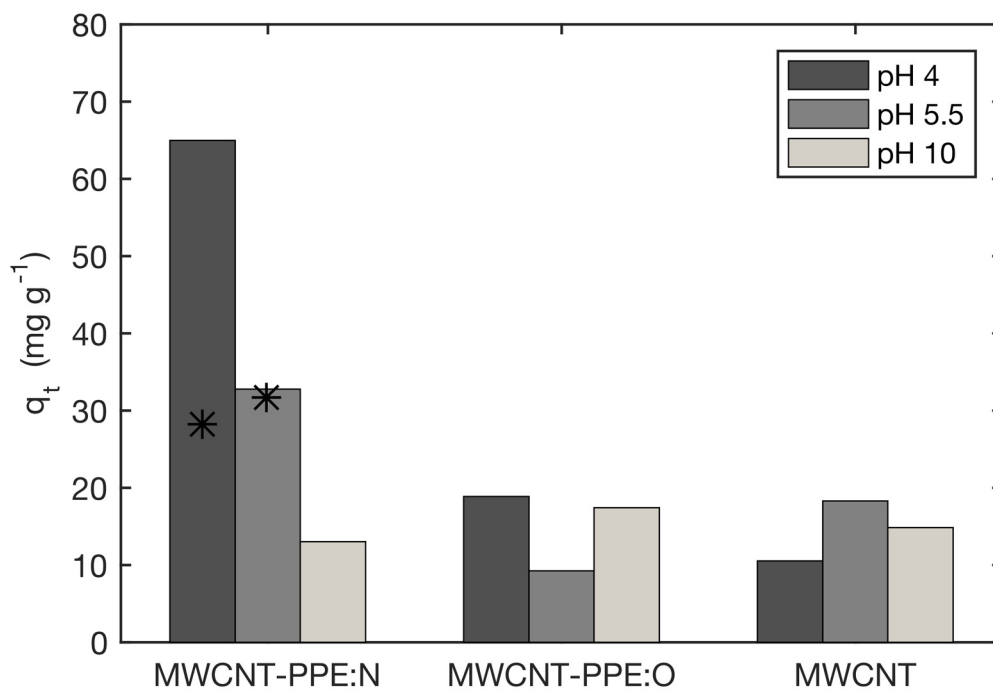


Figure 7.7: Adsorption capacity of MO on MWCNT-PPE:X and MWCNT after 24 hr. The asterisks correspond to the adsorption capacity after adsorbent reuse.

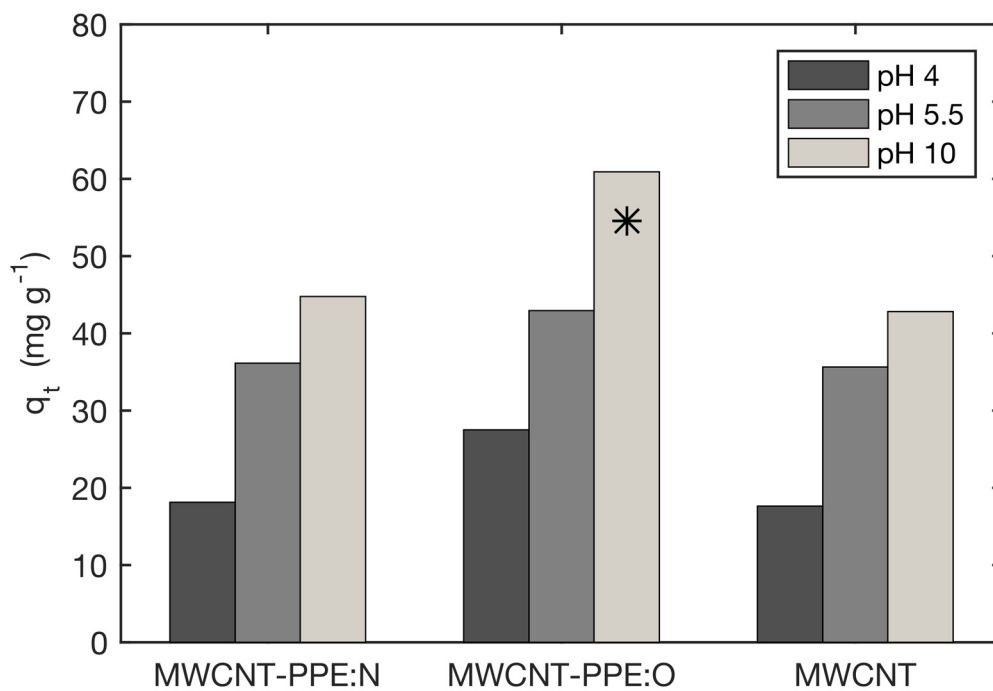


Figure 7.8: Adsorption capacity of MB on MWCNT-PPE:X and MWCNT after 24 hr. The asterisk corresponds to the adsorption capacity after adsorbent reuse.

solvents such as ethanol or acetone for dye desorption. Although both of these solvents are polar like water, the presence of methyl groups allows for hydrophobic interactions and less hydrogen bonding, thus increasing the number of ways that they may interact strongly with the dyes.

7.4.3 Experimental limitations

The results presented above clearly show an interaction between the chosen dyes and coated or non-coated MWCNTs. The functional groups present on the PPE:X coating help keep the MWCNTs stable and, at the correct pH, they interact more strongly with the dye of opposite charge. However, further tests would have been necessary to better understand the properties of MWCNT-PPE:X as a dye adsorbent. For example, other studies found in the literature on dye adsorption usually report the adsorption capacity with respect to contact time, the effect of initial dye or adsorbent concentration, and most importantly the kinetics of adsorption. However, when designing the experimental plan for the study presented here, a number of limitations related to the production method of the adsorbent made it impossible to perform these other tests. This section provides some information about the experimental choices made for this study and offers some suggestions for improvement.

The main problem in trying to conduct these dye adsorption experiments was the very low quantity of MWCNTs available. When using our in-house MWCNT production method as described in the experimental section, each piece of mesh of size 3.5 x 7 cm² contains between 0.5 and 2 mg of MWCNTs. Producing about 10 mg of MWCNTs (which is the lowest quantity typically used in other studies in the literature [87, 88, 192, 193]) for each nanofluid sample would be too time-consuming. Therefore, it was decided that smaller quantities of MWCNTs had to be used. More specifically, one or two pieces of MWCNT-covered mesh were used per nanofluid sample.

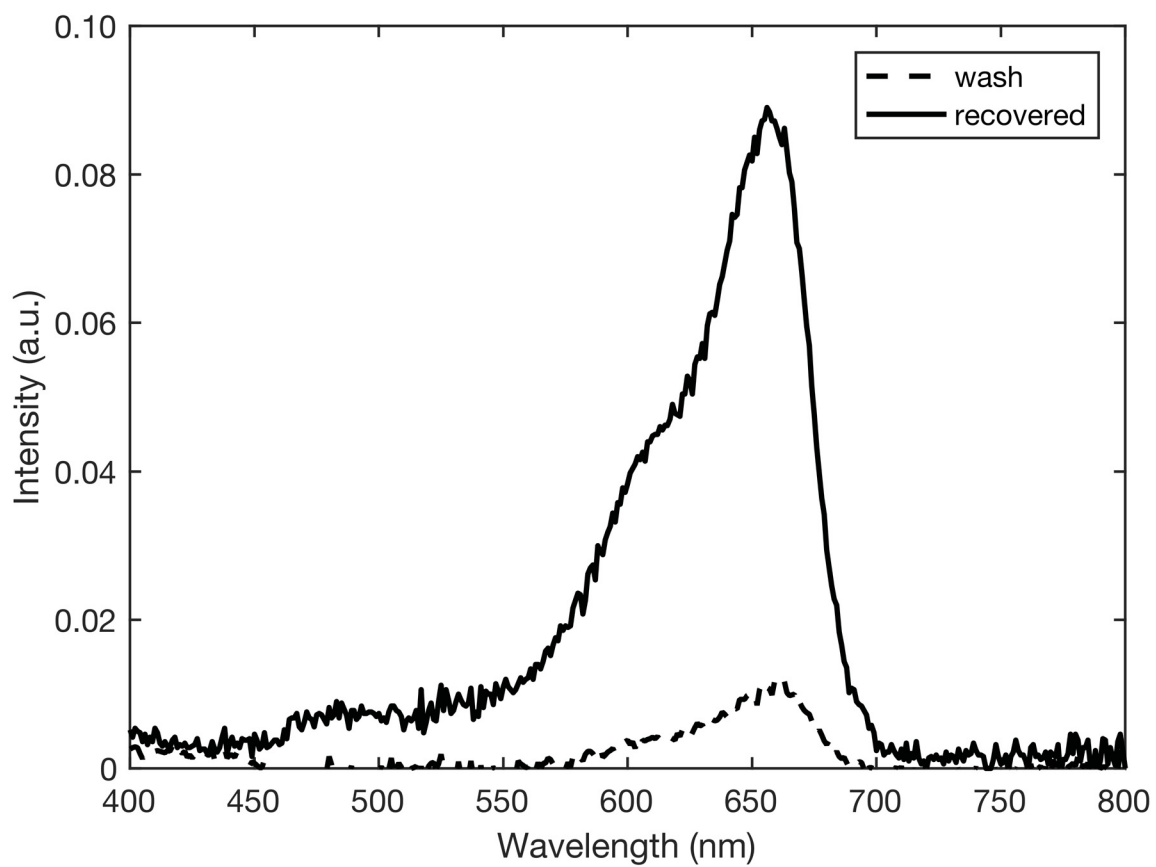


Figure 7.9: Absorption spectra of last wash solution and recovered dye.

Although this choice allowed for more experimental conditions to be tested, it meant that other types of studies, such as kinetic studies, couldn't be performed. In a kinetic study, aliquots of a sample are removed at pre-determined times and the adsorption capacity of each aliquot is measured. Given the very small quantity of MWCNTs used for each sample in this study, each aliquot would contain so little MWCNT that it wouldn't be possible to accurately measure its mass. The weight of MWCNT and MWCNT-PPE:X couldn't be estimated because the amount removed from the mesh by sonication changed from sample to sample.

Small quantities of MWCNT and MWCNT-PPE:X also meant that typical methods for quantification of functional groups or surface area of the nanoparticles could not be used. Titrations are the method of choice to determine quantities of carboxylic acid groups, amine groups, pK_a , pK_b or points of zero charge of nanoparticles [194, 195, 196]. However, all these techniques require large quantities of material, minimally around 25 mg, which are not available with our production methods. Nitrogen gas adsorption for surface area measurements also cannot be performed given that these instruments require at least 100 mg of material. Consequently, much needed information to better understand the interaction between the dyes and the adsorbents is not available.

It is important to note however that working with powders of commercial MWCNTs, available in much larger quantities, is not necessarily the solution. In powders, MWCNTs are already agglomerated and treatment methods in the liquid phase that are used to modify the MWCNTs' surface chemistry do not ensure their proper separation. Therefore, not all available MWCNTs are functionalized. Treatment methods in the gas phase, such as PECVD, only treat the top of any powder sample put in the chamber. Some groups have shown that mixing the powder during plasma treatment increases the quantity of sample treated. However, improvements are still necessary. For example, Trulli et al. [197] showed

that mixing during plasma treatment allowed for large quantities of oxygen treated CNTs to remain stable in water for at least a month. However, about 30% of the CNTs in suspension settled after 24 hr, which suggests that even though the sample was mixed during plasma treatment, about 30% was not properly treated [197]. When comparing with similar oxygen-treated MWCNTs using our in-house MWCNTs on the stainless steel mesh, Hordy [47] was able to show stability of the suspensions in water for 8 months with only a 5% decrease in suspended material per month. Therefore, although commercial powders of MWCNTs can be easily and relatively inexpensively obtained, some material is lost due to poor surface treatment. Any agglomerated material is not available for dye adsorption which would lead to lower adsorption capacities.

For future development of the PPE:X coated MWCNTs for dye adsorption, it will be necessary to evaluate if the gain obtained from proper separation of the MWCNTs during plasma treatment and thus a better functionalization of the samples outweighs the disadvantage incurred by the labor intensive preparation of the samples. This material would need to be compared to adsorbents that may be easier to produce in larger quantities, but where more material will be lost due to agglomeration when dispersed in water.

In conjunction with this work, it would be necessary to design a setup to scale up the MWCNT production. For example, roll-to-roll t-CVD would be suitable for increasing production yields. Using a PECVD chamber with large surface area but minimal height, larger quantities of mesh could be treated with minimal increase of pumping capacity. Such equipment, albeit expensive and not simple to automate, is available commercially. The major difficulty in this scale-up of the MWCNT production would be the design of a plasma chamber that limits the deposition of a heterogeneous coating (see appendix for more information on the coating deposition across the entire surface of the MWCNT covered mesh).

7.5 Conclusion

Two dyes were shown to adsorb on MWCNTs and MWCNT-PPE:X. Increased adsorption capacity was observed between the cationic dye, methylene blue, and the negatively charged MWCNT-PPE:O, or the anionic dye, methyl orange, and the positively charged MWCNT-PPE:N. Changing the pH of the mixtures has an impact on the amount of charge on the adsorbent and consequently on the adsorption capacity. This property of the adsorbent was used to show that it was possible to desorb the dyes and reuse the adsorbents.

Low production yields of the adsorbent limited this study to adsorption and reuse experiments. Future work would require investigating options to scale up the MWCNT production method as well as determining which applications justify the use of these easy to functionalize and non-agglomerated MWCNTs.

CHAPTER 8

Conclusion

8.1 Summary

With this thesis, it was shown that plasma polymer coated MWCNTs could be dispersed in water and their surface chemistry could be used to enhance interaction with molecules such as CO₂, methylene blue and methyl orange.

It was first shown that MWCNTs could be coated with a nitrogen-rich coating (PPE:N), with 17.4 N at%, and an oxygen-rich coating (PPE:O), with 20.0 O at%. The coating had a thickness between 4 and 14 nm for PPE:N, and between 3 and 60 nm for PPE:O. Different deposition times had to be used for each type of coating as their deposition rates were different. PPE:O deposits more slowly than PPE:N because of the ‘poisoning effect’ of certain oxygen-containing compounds which can etch away the PP and scavenge a portion of the radicals formed in the plasma. Sonication of the plasma-treated MWCNTs in water caused dissolution of a portion of the PPE:X (where X is N or O). However, according to results from PPE:X deposited on Si wafers, chemical composition was not altered by exposure to water. MWCNT-PPE:X when dispersed in water were stable at all pH values except at pH 12 for MWCNT-PPE:N and pH 2 for MWCNT-PPE:O. At pH 12, functional groups such as amines -NH₂ cannot be protonated on PPE:N, and at pH 2, carboxylic acid groups -COOH cannot be deprotonated. These neutral groups are not efficient at keeping the MWCNTs separated. Nevertheless, the agglomerates formed at pH 12 with MWCNT-PPE:N and those at pH 2 with MWCNT-PPE:O can be separated and the nanoparticles redispersed to form stable nanofluids. It was possible to cycle from agglomerated to dispersed

MWCNTs by switching the pH from 2 to 12 and back to 2 repeatedly. When the salt content in the mixture exceeded 0.01 mol L^{-1} , the MWCNTs remained agglomerated regardless of the pH. The excess ions cause the electrostatic double layer around the nanoparticles to shrink. The nanoparticles can then approach each other at smaller interparticle distances where attractive forces can cause their agglomeration. However, washing and redispersing the MWCNTs in water was sufficient to obtain again a stable nanofluid.

To better understand the structure of PPE:O, its thermal stability was measured by thermal gravimetric analysis. The start of material loss at low temperatures suggested the presence of small oligomers. However, its chemical composition was not significantly altered by heating at 150°C .

The stability of the coating at low temperature meant that it was possible to test another treatment method to modify the surface chemistry of MWCNTs: vapor functionalization. MWCNT-PPE:O and MWCNTs were exposed to vapors of two molecules containing amine functional groups, APTS and TEPA. Both MWCNT-APTS and MWCNT-PPE:O-APTS were unstable in water. However, MWCNT-APTS nanoparticles were stable for at least a day in ethanol indicating that APTS adsorbed on the nanoparticle's surface. The amine functional group on APTS helped stabilize MWCNTs in ethanol. MWCNT-PPE:O is already stable in ethanol and the addition of APTS did not disrupt their stability. TEPA on both types of MWCNTs had a clear impact on their stability. These usually unstable nanoparticles at pH 2 were stable for at least two weeks. Analysis of their chemical composition also confirmed that large quantities of amine functional groups were present on both of these treated nanoparticles.

Knowing that the plasma-treated MWCNTs were stable in water and that their surface charge could be tuned by changing the pH of the mixture, the last step was to test

these nanofluids for capture applications. First, plasma-treated MWCNTs with different quantities of amine functional groups were tested for CO₂ capture. It was shown that with increasing quantities of nucleophilic groups (amines being a part of this category of functional groups), larger quantities of CO₂ could be absorbed, with a maximum of 1.67 mL of CO₂ g⁻¹ of MWCNT-10:10 nanofluid (which is the same as MWCNT-PPE:N used in Chapter 4). Nanofluids with MWCNT-10:10 also had the largest absorption rate of the four nanofluids tested. Furthermore, it was shown that these nanofluids could be regenerated and reused for at least 5 cycles, albeit with a decrease in efficiency after the first absorption cycle. The necessity of amine functional groups for CO₂ capture was confirmed by showing that oxygen-containing MWCNTs improved the absorption capacity with respect to pure water but were not as efficient as MWCNT-10:10. Although MWCNT-10:10 was stable in water (and therefore well separated) and had amine groups fixed on its surface, the absorption capacity obtained with these nanofluids was insufficient to compete with common amine-rich solutions for CO₂ absorption.

In order to test the interaction of MWCNT-PPE:X with dyes, an anionic dye, methyl orange, and a cationic dye, methylene blue, were chosen. This study started by evaluating the effect of pH and concentration on both dyes in order to choose the correct ranges in which to use them without running into reproducibility problems. It was shown that methyl orange could not be used at pH 2 due to formation of precipitates. Methylene blue could not be used at pH 12 due to reactions that altered its structure and thus its absorption spectrum. A single value for the absorption coefficient of methyl orange was found when the concentration was kept below saturation for the instrument used. However, an empirical equation relating absorption coefficient and absorbance intensity was developed to account for the fact that methylene blue solutions of different concentrations have different absorption spectra due to polymerization of the dye. Mixing the dyes with MWCNT-PPE:X at three

different pH values, 4, 5.5 and 10, showed that MWCNT-PPE:N at pH 4 (more positively charged) could adsorb 65 mg of methyl orange g^{-1} of adsorbent, and MWCNT-PPE:O at pH 10 (more negatively charged) could adsorb 60 mg of methylene blue g^{-1} of adsorbent. Lower adsorption capacities were observed for MWCNT-PPE:X at pH values that decrease the quantity of charged functional groups available, or when the dye and the nanoparticle are both positive or negative. These adsorbents can also be reused after using a pH switch to release the dye.

8.2 Statement of contributions

The following contributions were made to the fields of plasma polymers and nanofluids:

- Stable aqueous dispersions of plasma polymer coated MWCNTs (with nitrogen or oxygen-containing functional groups) were produced. The choice of heteroatom on the plasma polymer allows for tuning of the interaction of MWCNTs with its environment. MWCNTs coated with nitrogen-containing functional groups were stable at acidic pH values and completely unstable above pH 12. MWCNTs with oxygen-containing functional groups were stable at basic pH and unstable below pH 2.
- It was shown that the agglomerates formed by changing the pH or increasing the ionic strength of the mixture are reversible. Switching the pH to a value where the functional groups on the MWCNT surface are charged allows the agglomerates to separate, while redispersing the MWCNTs in an aqueous solution with low ionic strength also produces stable nanofluids.
- MWCNTs modified with two dry functionalization methods were presented. An oxygen-containing plasma polymer layer on the MWCNTs acted as a support for a high-amine

content molecule, tetraethylenepentamine. This layer of amine functional groups completely shielded the oxygen-containing functional groups of the plasma polymer. These treated MWCNTs were completely stable in water at pH 2 for more than two weeks.

- MWCNTs coated with nitrogen or oxygen-rich plasma polymers dispersed in water were tested for capture of CO₂, methyl orange and methylene blue. MWCNTs carrying amine functional groups were efficient at capturing CO₂. MWCNTs with plasma polymers negatively or positively charged were more efficient at capturing the dye of opposite charge. It was shown that the chemical affinity for the desired molecule is necessary to obtain the maximum absorption of CO₂ or adsorption of the dyes. These interactions were shown to be reversible allowing for the adsorbent material to be reused which is important for the sustainable development of novel materials.

8.3 Recommendations for future work

Numerous questions remain about these plasma polymer coated MWCNTs and their use for capture applications. Below are a few suggestions on potential future work.

- Study of the shape of MWCNTs and their proximity to each other in water: the applications described in this thesis rely on the available surface area of the MWCNTs for interaction with other molecules. Although it was shown that the plasma-treated MWCNTs are stable in water, nor their size nor their complete separation from other MWCNTs was evaluated. By obtaining information such as the length and diameter of MWCNTs in water, it would be possible to calculate their available surface area. Imaging of the agglomerate structures, if any, would also help in determining agglomeration mechanisms.
- Establishing the correlation between quantity of functional groups and adsorption capacities: to design the most efficient surface chemistry for the MWCNTs, it would

be necessary to study if there is an observable variation in stability of MWCNTs and their capacity to capture other molecules with changes in nitrogen or oxygen content on the plasma polymer, and more specifically with changes in the quantity of specific functional groups on the plasma polymers.

- Evaluating the impact of more complex mixtures on the stability of the nanoparticles and their adsorption capacities: the industrial waste streams where dyes and CO₂ are found are not simple mixtures with a single pollutant. They contain many other compounds and their interaction with the nanoparticles must be studied. In particular, these plasma treated MWCNTs may be useful to capture other pollutants as well.
- Scale-up of the production methods of the plasma polymer coated MWCNTs: as mentioned in Chapter 7, one of the main limitations of that study was the low quantity of MWCNTs available. With more material, it would be possible to use common titration techniques to quantify functional groups at the surface of plasma-treated MWCNTs, to use gas adsorption techniques to measure the surface area of the MWCNTs in the dry state, and to simply perform more experiments for better assessment of the reproducibility of results.
- Comparing the usefulness of MWCNTs with other carbonaceous materials: MWCNTs in this thesis are useful given their ease of synthesis and their separation which allows for plasma functionalization. However, industrial methods of producing amorphous carbon, carbon nanotubes and graphene can now produce large quantities of these materials, albeit often in more agglomerated forms. Given that MWCNTs are used here only as scaffolds for the plasma polymer coating, it would be necessary to compare this material with other similar industrial materials and assess their cost of production as well as their efficiency for the chosen applications. Another carbon-based material may prove to be more convenient for these applications.

REFERENCES

- [1] J. KLUYTMANS, B. VAN WACHEM, B. KUSTER, and J. SCHOUTEN, *Chemical Engineering Science* **58**, 4719 (2003).
- [2] D. BRILMAN, W. VAN SWAAIJ, and G. VERSTEEG, *Chemical Engineering and Processing: Process Intensification* **37**, 471 (1998).
- [3] J. N. COLEMAN, U. KHAN, W. J. BLAU, and Y. K. GUN'KO, *Carbon* **44**, 1624 (2006).
- [4] N. M. RODRIGUEZ, A. CHAMBERS, and R. T. K. BAKER, *Langmuir* **11**, 3862 (1995).
- [5] D. TASIS, N. TAGMATARCHIS, A. BIANCO, and M. PRATO, *Chemical Reviews* **106**, 1105 (2006).
- [6] N. HORDY, *Plasma Functionalized Carbon Nanotubes Suspensions for High Temperature Direct Absorption Solar Thermal Energy Harvesting*, PhD thesis, McGill University, 2014.
- [7] S. L. PIRARD, S. DOUVEN, and J.-P. PIRARD, *Frontiers of Chemical Science and Engineering* **11**, 280 (2017).
- [8] S. SINNOTT, R. ANDREWS, D. QIAN, A. RAO, Z. MAO, E. DICKEY, and F. DERBYSHIRE, *Chemical Physics Letters* **315**, 25 (1999).
- [9] C. E. BADDOUR, F. FADLALLAH, D. NASUHOGLU, R. MITRA, L. VANDSBURGER, and J.-L. MEUNIER, *Carbon* **47**, 313 (2009).
- [10] N. HORDY, S. COULOMBE, and J.-L. MEUNIER, *Plasma Processes and Polymers* **10**, 110 (2013).
- [11] N. HORDY, Direct growth of carbon nanotubes from stainless steel grids and plasma functionalization for poly(vinyl alcohol) composite production, Master's thesis, McGill University, 2011.
- [12] N. HORDY, N.-Y. MENDOZA-GONZALEZ, S. COULOMBE, and J.-L. MEUNIER, *Carbon* **63**, 348 (2013).

- [13] P. FABBRI and M. MESSORI, 5 - Surface Modification of Polymers: Chemical, Physical, and Biological Routes, in *Modification of Polymer Properties*, edited by C. F. JASSO-GASTINEL and J. M. KENNY, pp. 109 – 130, William Andrew Publishing, 2017.
- [14] S. SAMUKAWA, M. HORI, S. RAUF, K. TACHIBANA, P. BRUGGEMAN, G. KROESEN, J. C. WHITEHEAD, A. B. MURPHY, A. F. GUTSOL, S. STARIKOVSKAIA, U. KORTSHAGEN, J.-P. BOEUF, T. J. SOMMERER, M. J. KUSHNER, U. CZARNETZKI, and N. MASON, *Journal of Physics D: Applied Physics* **45**, 253001 (2012).
- [15] H. YASUDA, *Luminous chemical vapor deposition and interface engineering*, New York : Marcel Dekker, 2005.
- [16] B. N. KHARE, P. WILHITE, R. C. QUINN, B. CHEN, R. H. SCHINGLER, B. TRAN, H. IMANAKA, C. R. SO, C. W. BAUSCHLICHER, and M. MEYYAPPAN, *The Journal of Physical Chemistry B* **108**, 8166 (2004).
- [17] B. RUELLE, S. PEETERBROECK, T. GODFROID, C. BITTENCOURT, M. HECQ, R. SNYDERS, and P. DUBOIS, *Polymers* **4**, 296 (2012).
- [18] F. GORDILLO-VÁZQUEZ, V. HERRERO, and I. TANARRO, *Chemical Vapor Deposition* **13**, 267 (2007).
- [19] H. YASUDA, *Plasma Polymerization*, Academic Press, Orlando, 1985.
- [20] B. RUELLE, S. PEETERBROECK, R. GOUTTEBARON, T. GODFROID, F. MONTEVERDE, J.-P. DAUCHOT, M. ALEXANDRE, M. HECQ, and P. DUBOIS, *J. Mater. Chem.* **17**, 157 (2007).
- [21] A. FELTEN, C. BITTENCOURT, J. J. PIREAUX, G. V. LIER, and J. C. CHARLIER, *Journal of Applied Physics* **98**, 074308 (2005).
- [22] J. Y. YOON, J. JUN, and S. KWAK, *Applied Surface Science* **256**, 6941 (2010).
- [23] H. BUBERT, S. HAIBER, W. BRANDL, G. MARGINEAN, M. HEINTZE, and V. BRÜSER, *Diamond and Related Materials* **12**, 811 (2003).
- [24] Y. H. YAN, J. CUI, M. B. CHAN-PARK, X. WANG, and Q. Y. WU, *Nanotechnology* **18**, 115712 (2007).
- [25] J. FRIEDRICH, *Plasma Processes and Polymers* **8**, 783 (2011).
- [26] H. YASUDA, M. O. BUMGARNER, and J. J. HILLMAN, *Journal of Applied Polymer Science* **19**, 531 (1975).
- [27] F. AREFI-KHONSARI, J. KURDI, M. TATOULIAN, and J. AMOUROUX, *Surface and Coatings Technology* **142-144**, 437 (2001).

- [28] W.-D. YANG, P.-N. WANG, Z.-P. LIU, L. MI, S.-C. CHEN, and F.-M. LI, *Journal of Physics D: Applied Physics* **33**, 3223 (2000).
- [29] M. BUDDHADASA and P.-L. GIRARD-LAURIAULT, *Thin Solid Films* **591**, 76 (2015).
- [30] S. LEROUGE, J. BARRETTE, J.-C. RUIZ, M. SBAI, H. SAVOJI, B. SAOUDI, M. GAUTHIER, and M. R. WERTHEIMER, *Plasma Processes and Polymers* **12**, 882 (2015).
- [31] J. DORST, M. VANDENBOSSCHE, M. AMBERG, L. BERNARD, P. RUPPER, K.-D. WELTMANN, K. FRICKE, and D. HEGEMANN, *Langmuir* **33**, 10736 (2017).
- [32] R. PIETRZAK, *Fuel* **88**, 1871 (2009).
- [33] A. ALAM, C. WAN, and T. McNALLY, *European Polymer Journal* **87**, 422 (2017).
- [34] C. VANDENABEELE, M. BUDDHADASA, P.-L. GIRARD-LAURIAULT, and R. SNYDERS, *Thin Solid Films* **630**, 100 (2017).
- [35] D. J. BABU, S. YADAV, T. HEINLEIN, G. CHERKASHININ, and J. J. SCHNEIDER, *The Journal of Physical Chemistry C* **118**, 12028 (2014).
- [36] W. MENG-JIY, C. YOU-IM, and P.-E. F., *Surface and Interface Analysis* **37**, 348 (2005).
- [37] L. JORGE, P.-L. GIRARD-LAURIAULT, and S. COULOMBE, *Plasma Processes and Polymers* **14**, 1700026 (2017).
- [38] S. BABAEI and P.-L. GIRARD-LAURIAULT, *Plasma Chemistry and Plasma Processing* **36**, 651 (2016).
- [39] J.-C. RUIZ, P.-L. GIRARD-LAURIAULT, and M. R. WERTHEIMER, *Plasma Processes and Polymers* **12**, 225 (2015).
- [40] A. MANAKHOV, P. KIRYUKHANTSEV-KORNEEV, M. MICHLÍČEK, E. PERMYAKOVA, E. DVOŘÁKOVÁ, J. POLČÁK, Z. POPOV, M. VISOTIN, and D. V. SHTANSKY, *Applied Surface Science* **435**, 1220 (2018).
- [41] D. HEGEMANN, E. KÖRNER, K. ALBRECHT, U. SCHÜTZ, and S. GUIMOND, *Plasma Processes and Polymers* **7**, 889 (2010).
- [42] C. SAKA, *Critical Reviews in Analytical Chemistry* **48**, 1 (2018), PMID: 28722465.
- [43] C. J. V. OSS, *The properties of water and their role in colloidal and biological systems*, volume 16 of *Interface Science and Technology*, Elsevier, 2008.
- [44] I. W. HAMLEY, *Introduction to Soft Matter*, John Wiley & Sons, Ltd., 2007.
- [45] S. SIBONI and C. D. VOLPE, *Reviews of Adhesion and Adhesives* **3**, 253 (2015).

- [46] C. PONCET-LEGRAND, D. CARTALADE, J.-L. PUTAUX, V. CHEYNIER, and A. VERNHET, *Langmuir* **19**, 10563 (2003).
- [47] N. HORDY, D. RABILLOUD, J.-L. MEUNIER, and S. COULOMBE, *Solar Energy* **105**, 82 (2014).
- [48] E. HERNÁNDEZ-HERNÁNDEZ, M. G. NEIRA-VELÁZQUEZ, H. GUERRERO-ALVARADO, J. F. HERNÁNDEZ-GÁMEZ, P. GONZÁLEZ-MORONES, C. A. ÁVILA-ORTA, Y. A. PERERA-MERCADO, J. J. BORJAS-RAMOS, M. PÉREZ-ÁLVAREZ, A. D. ILINÁ, and P. BARTOLO-PÉREZ, *Plasma Chemistry and Plasma Processing* **35**, 757 (2015).
- [49] Y. J. KIM, H. MA, and Q. YU, *Nanotechnology* **21**, 295703 (2010).
- [50] C. ÁVILA-ORTA, V. CRUZ-DELGADO, M. NEIRA-VELÁZQUEZ, E. HERNÁNDEZ-HERNÁNDEZ, M. MÉNDEZ-PADILLA, and F. MEDELLÍN-RODRÍGUEZ, *Carbon* **47**, 1916 (2009).
- [51] L. G. NAIR, A. S. MAHAPATRA, N. GOMATHI, K. JOSEPH, S. NEOGI, and C. R. NAIR, *Applied Surface Science* **340**, 64 (2015).
- [52] B. SMITH, K. WEPASNICK, K. E. SCHROTE, H.-H. CHO, W. P. BALL, and D. H. FAIRBROTHER, *Langmuir* **25**, 9767 (2009).
- [53] X. YU, L. ZHANG, M. LIANG, and W. SUN, *Chemical Engineering Journal* **279**, 363 (2015).
- [54] A. KARTHIKEYAN, *Improvement of Boiling Heat Transfer using Nanofluid and Laser Textured Surface*, PhD thesis, McGill University, 2018.
- [55] D. HEGEMANN, B. HANSELMANN, N. BLANCHARD, and M. AMBERG, *Contributions to Plasma Physics* **54**, 162 (2014).
- [56] W. M. O. U. N. E. P. INTERGOVERNMENTAL PANEL ON CLIMATE CHANGE, Carbon dioxide capture and storage, <http://www.ipcc-wg3.de/special-reports/special-report-on-carbon-dioxide-capture-and-storage>, 2005, [Online; accessed August-2013].
- [57] J. K. LEE, J. KOO, H. HONG, and Y. T. KANG, *International Journal of Refrigeration* **33**, 269 (2010).
- [58] S. KOMATI and A. K. SURESH, *Journal of Chemical Technology & Biotechnology* **83**, 1094 (2008).
- [59] Q. WANG, J. LUO, Z. ZHONG, and A. BORGNA, *Energy & Environmental Science* **4**, 42 (2011).

- [60] W.-G. KIM, H. U. KANG, K.-M. JUNG, and S. H. KIM, *Separation Science and Technology* **43**, 3036 (2008).
- [61] S. MA, H. SONG, M. WANG, J. YANG, and B. ZANG, *Chemical Engineering Research and Design* **91**, 1327 (2013).
- [62] R. TAYLOR, S. COULOMBE, T. OTANICAR, P. PHELAN, A. GUNAWAN, W. LV, G. ROSENGARTEN, R. PRASHER, and H. TYAGI, *Journal of Applied Physics* **113**, 011301 (2013).
- [63] Z. ZHANG, J. CAI, F. CHEN, H. LI, W. ZHANG, and W. QI, *Renewable Energy* **118**, 527 (2018).
- [64] J.-Y. JUNG, J. LEE, and Y. KANG, *Journal of Mechanical Science and Technology* **26**, 2285 (2012).
- [65] J. W. LEE, J.-Y. JUNG, S.-G. LEE, and Y. T. KANG, *International Journal of Refrigeration* **34**, 1727 (2011).
- [66] A. GOLKHAR, P. KESHAVARZ, and D. MOWLA, *Journal of Membrane Science* **433**, 17 (2013).
- [67] J. W. LEE and Y. T. KANG, *Energy* **53**, 206 (2013).
- [68] S. HSU, C. LU, F. SU, W. ZENG, and W. CHEN, *Chemical Engineering Science* **65**, 1354 (2010).
- [69] Y.-C. CHIANG, W.-L. HSU, S.-Y. LIN, and R.-S. JUANG, *Materials* **10**, 511 (2017).
- [70] H. HU, T. ZHANG, S. YUAN, and S. TANG, *Adsorption* **23**, 73 (2017).
- [71] Q. LIU, J. SHI, Q. WANG, M. TAO, Y. HE, and Y. SHI, *Industrial & Engineering Chemistry Research* **53**, 17468 (2014).
- [72] N. P. WICKRAMARATNE, J. XU, M. WANG, L. ZHU, L. DAI, and M. JARONIEC, *Chemistry of Materials* **26**, 2820 (2014).
- [73] Y. OH, V.-D. LE, U. N. MAITI, J. O. HWANG, W. J. PARK, J. LIM, K. E. LEE, Y.-S. BAE, Y.-H. KIM, and S. O. KIM, *ACS Nano* **9**, 9148 (2015).
- [74] D. J. BABU, M. BRUNS, R. SCHNEIDER, D. GERTHSEN, and J. J. SCHNEIDER, *The Journal of Physical Chemistry C* **121**, 616 (2017).
- [75] L. SAEEDNIA, H. HASHEMIPOUR, and D. AFZALI, *Transp Phenom Nano Micro Scales* **3**, 46 (2015).
- [76] T. ROBINSON, G. McMULLAN, R. MARCHANT, and P. NIGAM, *Bioresource Technology* **77**, 247 (2001).

- [77] G. CRINI, *Dyes and Pigments* **77**, 415 (2008).
- [78] R. GONG, J. YE, W. DAI, X. YAN, J. HU, X. HU, S. LI, and H. HUANG, *Industrial & Engineering Chemistry Research* **52**, 14297 (2013).
- [79] M. SHIRMARDI, A. H. MAHVI, B. HASHEMZADEH, A. NAEIMABADI, G. HASSANI, and M. V. NIRI, *Korean Journal of Chemical Engineering* **30**, 1603 (2013).
- [80] S. WANG, C. W. NG, W. WANG, Q. LI, and L. LI, *Journal of Chemical & Engineering Data* **57**, 1563 (2012).
- [81] H. SADEGH, R. SHAHRYARI-GHOSHEKANDI, S. AGARWAL, I. TYAGI, M. ASIF, and V. K. GUPTA, *Journal of Molecular Liquids* **206**, 151 (2015).
- [82] L. AI and J. JIANG, *Chemical Engineering Journal* **192**, 156 (2012).
- [83] L. D. PROLA, F. M. MACHADO, C. P. BERGMANN, F. E. DE SOUZA, C. R. GALLY, E. C. LIMA, M. A. ADEBAYO, S. L. DIAS, and T. CALVETE, *Journal of Environmental Management* **130**, 166 (2013).
- [84] W. LIU, X. JIANG, and X. CHEN, *Journal of Solid State Chemistry* **229**, 342 (2015).
- [85] L. SELLAOUI, G. L. DOTTO, E. C. PERES, Y. BENGUERBA, É. C. LIMA, A. B. LAMINE, and A. ERTO, *Journal of Molecular Liquids* **248**, 890 (2017).
- [86] J. ABDI, M. VOSSOUGH, N. M. MAHMOODI, and I. ALEMZADEH, *Chemical Engineering Journal* **326**, 1145 (2017).
- [87] A. AHMAD, M. H. RAZALI, M. MAMAT, F. S. B. MEHAMOD, and K. A. M. AMIN, *Chemosphere* **168**, 474 (2017).
- [88] P. WANG, M. CAO, C. WANG, Y. AO, J. HOU, and J. QIAN, *Applied Surface Science* **290**, 116 (2014).
- [89] A. ELSAGH, O. MORADI, A. FAKHRI, F. NAJAFI, R. ALIZADEH, and V. HADDADI, *Arabian Journal of Chemistry* **10**, S2862 (2017).
- [90] H. M. MOKBUL, H. A. S., and H. DIRK, *Plasma Processes and Polymers* **4**, 135 (2007).
- [91] K. L. JARVIS and P. MAJEWSKI, *Water, Air, & Soil Pollution* **225**, 2227 (2014).
- [92] E. KASPAREK, J. R. TAVARES, M. R. WERTHEIMER, and P.-L. GIRARD-LAURIAULT, *Plasma Processes and Polymers* **13**, 888 (2016).
- [93] E. KASPAREK and C. KAFIE, Targeted Ageing Studies of N-rich Plasma Polymers, Technical report, McGill University, 2017.

- [94] H. MIN, P. L. GIRARD-LAURIAULT, T. GROSS, A. LIPPITZ, P. DIETRICH, and W. E. S. UNGER, *Analytical and Bioanalytical Chemistry* **403**, 613 (2012).
- [95] T. F. TADROS, *Characterization of Suspensions and Assessment of Their Stability*, chapter 11, pp. 193–217, Wiley-Blackwell, 2012.
- [96] J. R. BABU, K. K. KUMAR, and S. S. RAO, *Renewable and Sustainable Energy Reviews* **77**, 551 (2017).
- [97] C.-P. KLAGES, Z. KHOSRAVI, and A. HINZE, *Plasma Processes and Polymers* **10**, 307 (2013).
- [98] P.-L. GIRARD-LAURIAULT, R. ILLGEN, J.-C. RUIZ, M. R. WERTHEIMER, and W. E. S. UNGER, *Applied Surface Science* **258**, 8448 (2012).
- [99] A. SHAIKH and M. AL-DAHMAN, *International Journal of Chemical Reactor Engineering* **5** (2007).
- [100] X. SU, M. F. CUNNINGHAM, and P. G. JESSOP, *Chem. Commun.* **49**, 2655 (2013).
- [101] E. B. DE BORBA, C. L. C. AMARAL, M. J. POLITI, R. VILLALOBOS, and M. S. BAPTISTA, *Langmuir* **16**, 5900 (2000).
- [102] C. SUN, Q. YUE, B. GAO, R. MU, J. LIU, Y. ZHAO, Z. YANG, and W. XU, *Desalination* **281**, 243 (2011).
- [103] J. LIANG, J. LIU, X. YUAN, H. DONG, G. ZENG, H. WU, H. WANG, J. LIU, S. HUA, S. ZHANG, Z. YU, X. HE, and Y. HE, *Chemical Engineering Journal* **273**, 101 (2015).
- [104] H.-K. LEE, J. W. CHOI, W. OH, and S.-J. CHOI, *Journal of Radioanalytical and Nuclear Chemistry* **309**, 477 (2016).
- [105] H. XIE, H. LEE, W. YOUN, and M. CHOI, *Journal of Applied Physics* **94**, 4967 (2003).
- [106] J. WENSEL, B. WRIGHT, D. THOMAS, W. DOUGLAS, B. MANNHALTER, W. CROSS, H. HONG, J. KELLAR, P. SMITH, and W. ROY, *Applied Physics Letters* **92**, 023110 (2008).
- [107] Z. CHEN, X. J. DAI, K. MAGNIEZ, P. R. LAMB, B. L. FOX, and X. WANG, *Composites Part A: Applied Science and Manufacturing* **56**, 172 (2014).
- [108] S. BAI, K. K. HO, G. KNOX, and A. BISMARCK, *Composite Interfaces* **20**, 761 (2013).
- [109] L. JORGE, S. COULOMBE, and P.-L. GIRARD-LAURIAULT, *Plasma Processes and Polymers* **12**, 1311 (2015).
- [110] X. HAN, Y. LI, S. WU, and Z. DENG, *Small* **4**, 326 (2008).

- [111] D. WANG and L. CHEN, *Temperature and pH-Responsive "Smart" Carbon Nanotube Dispersions*, pp. 27–38, Humana Press, Totowa, NJ, 2010.
- [112] P.-L. GIRARD-LAURIAULT, P. M. DIETRICH, T. GROSS, T. WIRTH, and W. E. S. UNGER, *Plasma Processes and Polymers* **10**, 388 (2013).
- [113] N. E. BLANCHARD, B. HANSELMANN, J. DROSTEN, M. HEUBERGER, and D. HEGEMANN, *Plasma Processes and Polymers* **12**, 32 (2015).
- [114] D. L. SMITH, A. S. ALIMONDA, and F. J. VON PREISSIG, *Journal of Vacuum Science & Technology B: Microelectronics Processing and Phenomena* **8**, 551 (1990).
- [115] F. TRUCA-MARASESCU, P.-L. GIRARD-LAURIAULT, A. LIPPITZ, W. E. S. UNGER, and M. R. WERTHEIMER, *Thin Solid Films* **516**, 7406 (2008).
- [116] J.-C. RUIZ, A. ST-GEORGES-ROBILLARD, C. THERESY, S. LEROUGE, and M. R. WERTHEIMER, *Plasma Processes and Polymers* **7**, 737 (2010).
- [117] D. HEGEMANN, B. HANSELMANN, S. GUIMOND, G. FORTUNATO, M.-N. GIRAUD, and A. G. GUEX, *Surface and Coatings Technology* **255**, 90 (2014).
- [118] K. VASILEV, A. MICHELMORE, P. MARTINEK, J. CHAN, V. SAH, H. J. GRIESSER, and R. D. SHORT, *Plasma Processes and Polymers* **7**, 824 (2010).
- [119] R. T. CHEN, B. W. MUIR, L. THOMSEN, A. TADICH, B. C. C. COWIE, G. K. SUCH, A. POSTMA, K. M. MCLEAN, and F. CARUSO, *The Journal of Physical Chemistry B* **115**, 6495 (2011), PMID: 21542588.
- [120] A. MICHELMORE, P. MARTINEK, V. SAH, R. D. SHORT, and K. VASILEV, *Plasma Processes and Polymers* **8**, 367 (2011).
- [121] V. DATSYUK, M. KALYVA, K. PAPAGELIS, J. PARTHENIOS, D. TASIS, A. SIOKOU, I. KALLITSIS, and C. GALIOTIS, *Carbon* **46**, 833 (2008).
- [122] C. MATTEVI, G. EDA, S. AGNOLI, S. MILLER, K. A. MKHOYAN, O. CELIK, D. MASTROGIOVANNI, G. GRANOZZI, E. GARFUNKEL, and M. CHHOWALLA, *Advanced Functional Materials* **19**, 2577 (2009).
- [123] C. HONTORIA-LUCAS, A. LÓPEZ-PEINADO, J. D. LÓPEZ-GONZÁLEZ, M. ROJAS-CERVANTES, and R. MARTÍN-ARANDA, *Carbon* **33**, 1585 (1995).
- [124] J. E. KIMURA and A. SZENT-GYÖRGYI, *Proceedings of the National Academy of Sciences of the United States of America* **62**, 286 (1969).
- [125] T. G. VAN DE VEN, *Colloids and Surfaces A: Physicochemical and Engineering Aspects* **138**, 207 (1998).

- [126] J. M. TAN, P. ARULSELVAN, S. FAKURAZI, H. ITHNIN, and M. Z. HUSSEIN, *Journal of Nanomaterials* **2014**, 917024 (2014).
- [127] R. ABJAMEH, O. MORADI, and J. AMANI, *International Nano Letters* **4**, 97 (2014).
- [128] J. LI, M. J. VERGNE, E. D. MOWLES, W.-H. ZHONG, D. M. HERCULES, and C. M. LUKEHART, *Carbon* **43**, 2883 (2005).
- [129] M. GRZELCZAK, M. CORREA-DUARTE, V. SALGUEIRIÑO-MACEIRA, B. RODRÍGUEZ-GONZÁLEZ, J. RIVAS, and L. LIZ-MARZÁN, *Angewandte Chemie International Edition* **46**, 7026 (2007).
- [130] P. RUPPER, M. VANDENBOSSCHE, L. BERNARD, D. HEGEMANN, and M. HEUBERGER, *Langmuir* **33**, 2340 (2017).
- [131] W. R. ASHURST, C. CARRARO, and R. MABOUDIAN, *IEEE Transactions on Device and Materials Reliability* **3**, 173 (2003).
- [132] H.-L. LI, Y. ZHU, D. XU, Y. WAN, L. XIA, and X. SONG ZHAO, *Journal of Applied Physics* **105**, 114307 (2009).
- [133] Y. X. ZHUANG, O. HANSEN, T. KNIELING, C. WANG, P. ROMBACH, W. LANG, W. BENECKE, M. KEHLENBECK, and J. KOBLITZ, *Journal of Micromechanics and Microengineering* **16**, 2259 (2006).
- [134] J. D. MENCZEL and R. B. PRIME, *Thermal analysis of polymers*, John Wiley, Hoboken, N.J., 2009.
- [135] C. BEYLER and M. HIRSCHLER, *Thermal Decomposition of Polymers. SFPE Handbook of Fire Protection Engineering*, chapter 7, pp. 111–131., Springer, 2002.
- [136] C. DESCHENAUX, A. AFFOLTER, D. MAGNI, C. HOLLENSTEIN, and P. FAYET, *Journal of Physics D: Applied Physics* **32**, 1876 (1999).
- [137] K. G. DONOHOE and T. WYDEVEN, *Journal of Applied Polymer Science* **23**, 2591 (1979).
- [138] G. F. LEVCHIK, K. SI, S. V. LEVCHIK, G. CAMINO, and C. A. WILKIE, *Polymer Degradation and Stability* **65**, 395 (1999).
- [139] S. MICHAEL, B. E. M., and S. MITCHEL, *Journal of Polymer Science: Polymer Chemistry Edition* **13**, 1541 (1975).
- [140] Y. ROH, N. YAMASAKI, T. KAWAI, H. ARAKI, K. YOSHINO, S. HOJYO, M. TAKASE, and T. SUZUKI, *Synthetic Metals* **71**, 1771 (1995).

- [141] A. T. BELL, *The Mechanism and kinetics of plasma polymerization*, pp. 43–68, Springer Berlin Heidelberg, Berlin, Heidelberg, 1980.
- [142] J. D. PETERSON, S. VYAZOVKIN, and C. A. WIGHT, *Macromolecular Chemistry and Physics* **202**, 775 (2001).
- [143] S. FIORILLI, P. RIVOLO, E. DESCROVI, C. RICCIARDI, L. PASQUARDINI, L. LUNELLI, L. VANZETTI, C. PEDERZOLLI, B. ONIDA, and E. GARRONE, *Journal of Colloid and Interface Science* **321**, 235 (2008).
- [144] C. VELASCO-SANTOS, A. L. MARTÍNEZ-HERNÁNDEZ, M. LOZADA-CASSOU, A. ALVAREZ-CASTILLO, and V. M. CASTAÑO, *Nanotechnology* **13**, 495 (2002).
- [145] X. WANG, W. XING, P. ZHANG, L. SONG, H. YANG, and Y. HU, *Composites Science and Technology* **72**, 737 (2012).
- [146] S.-M. HONG, S. H. KIM, and K. B. LEE, *Energy & Fuels* **27**, 3358 (2013).
- [147] SIDS Initial Assessment Report For SIAM 17 - 3-AMINOPROPYLTRIETHOXYSILANE, Technical report, OECD, 2003.
- [148] J. PANG, G. XU, S. YUAN, Y. TAN, and F. HE, *Colloids and Surfaces A: Physico-chemical and Engineering Aspects* **350**, 101 (2009).
- [149] M. MIKHAYLOVA, D. K. KIM, C. C. BERRY, A. ZAGORODNI, M. TOPRAK, A. S. G. CURTIS, and M. MUHAMMED, *Chemistry of Materials* **16**, 2344 (2004).
- [150] S. MOHAPATRA, N. PRAMANIK, S. MUKHERJEE, S. K. GHOSH, and P. PRAMANIK, *Journal of Materials Science* **42**, 7566 (2007).
- [151] O. ZABIHI, M. AHMADI, S. SHAFEI, S. M. SERAJI, A. OROUMEI, and M. NAEBE, *Composites Part A: Applied Science and Manufacturing* **88**, 243 (2016).
- [152] NAEEMULLAH, M. TUZEN, T. G. KAZI, and D. CITAK, *Anal. Methods* **8**, 2756 (2016).
- [153] L. CAO, C. FANG, R. ZENG, X. ZHAO, F. ZHAO, Y. JIANG, and Z. CHEN, *Sensors and Actuators B: Chemical* **252**, 44 (2017).
- [154] J. SHEN, W. HUANG, L. WU, Y. HU, and M. YE, *Materials Science and Engineering: A* **464**, 151 (2007).
- [155] H. ESTRADÉ-SZWARCKOPF, *Carbon* **42**, 1713 (2004).
- [156] P.-A. PASCONE, J. DE CAMPOS, J.-L. MEUNIER, and D. BERK, *Applied Catalysis B: Environmental* **193**, 9 (2016).
- [157] J. PELS, F. KAPTEIJN, J. MOULIJN, Q. ZHU, and K. THOMAS, *Carbon* **33**, 1641 (1995).

- [158] R. SETNESCU, S. JIPA, T. SETNESCU, W. KAPPEL, S. KOBAYASHI, and Z. OSAWA, *Carbon* **37**, 1 (1999).
- [159] M. IRANI, A. T. JACOBSON, K. A. GASEM, and M. FAN, *Fuel* **206**, 10 (2017).
- [160] H. TAKAGI, K. MARUYAMA, N. YOSHIKAWA, Y. YAMADA, and Y. SATO, *Fuel* **83**, 2427 (2004).
- [161] B. MANOJ and A. KUNJOMANA, *Int. J. Electrochem. Sci.* **7**, 3127 (2012).
- [162] F. PORCHERON, M. JACQUIN, N. EL HADRI, D. A. SALDANA, A. GOULON, and A. FARAJ, *Oil Gas Sci. Technol. & Rev. IFP Energies nouvelles* **68**, 469 (2013).
- [163] J. JIANG, B. ZHAO, M. CAO, S. WANG, and Y. ZHUO, *Energy Procedia* **37**, 518 (2013).
- [164] Z. SAMADI, M. HAGHSHENASFARD, and A. MOHEB, *Chemical Engineering & Technology* **37**, 462 (2014).
- [165] I. T. PINEDA, C. K. CHOI, and Y. T. KANG, *International Journal of Greenhouse Gas Control* **23**, 105 (2014).
- [166] C.-H. YU, C.-H. HUANG, and C.-S. TAN, *Aerosol and Air Quality Research* **12**, 745 (2012).
- [167] N. DAI and W. A. MITCH, *Environmental Science & Technology* **47**, 13175 (2013).
- [168] F. A. CHOWDHURY, H. YAMADA, T. HIGASHII, K. GOTO, and M. ONODA, *Industrial & Engineering Chemistry Research* **52**, 8323 (2013).
- [169] J. MANE, F. LE NORMAND, R. MEDJO, C. COJOCARU, O. ERSEREN, A. SENGER, C. LAFFON, B. SENDJA, C. BIOUELE, G. BEN-BOLIE, P. ATEBA, and P. PARENT, *Materials Sciences and Applications* **5**, 966 (2014).
- [170] A. CHOUKOUROV, H. BIEDERMAN, I. KHOLODKOV, D. SLAVINSKA, M. TRCHOVA, and A. HOLLANDER, *Journal of Applied Polymer Science* **92**, 979 (2004).
- [171] P. FAVIA, M. STENDARDO, and R. D'AGOSTINO, *Plasmas and Polymers* **1**, 91 (1996).
- [172] C. CHEN, B. LIANG, D. LU, A. OGINO, X. WANG, and M. NAGATSU, *Carbon* **48**, 939 (2010).
- [173] F. TRUCA-MARASESCU and M. R. WERTHEIMER, *Plasma Processes and Polymers* **5**, 44 (2008).
- [174] Y. TANG, T. SHAM, Y. HU, C. LEE, and S. LEE, *Chemical Physics Letters* **366**, 636 (2002).

- [175] S. POINT, T. MINEA, B. BOUCHET-FABRE, A. GRANIER, and G. TURBAN, *Diamond and Related Materials* **14**, 891 (2005).
- [176] G. ABBAS, P. PAPAKONSTANTINOY, G. IYER, I. KIRKMAN, and L. CHEN, *Phys. Rev. B* **75**, 195429 (2007).
- [177] A. G. SHARD, J. D. WHITTLE, A. J. BECK, P. N. BROOKES, N. A. BULLETT, R. A. TALIB, A. MISTRY, D. BARTON, and S. L. MCARTHUR, *The Journal of Physical Chemistry B* **108**, 12472 (2004).
- [178] D. HEGEMANN, *Thin Solid Films* **581**, 2 (2015).
- [179] Y. LIU, J. SHI, J. CHEN, Q. YE, H. PAN, Z. SHAO, and Y. SHI, *Microporous and Mesoporous Materials* **134**, 16 (2010).
- [180] J. ZHANG, R. MISCH, Y. TAN, and D. W. AGAR, *Chemical Engineering & Technology* **34**, 1481 (2011).
- [181] B. OLLE, S. BUCAK, T. C. HOLMES, L. BROMBERG, T. A. HATTON, and D. I. C. WANG, *Industrial & Engineering Chemistry Research* **45**, 4355 (2006).
- [182] A. BIANCO, K. KOSTARELOS, and M. PRATO, *Chem. Commun.* **47**, 10182 (2011).
- [183] C. U. DEPT. OF TEXTILES, State Of The Art Of Textile Waste Treatment, Environmental Protection Agency, 1971.
- [184] Textile industry and water treatment.
- [185] Y. YAO, H. BING, X. FEIFEI, and C. XIAOFENG, *Chemical Engineering Journal* **170**, 82 (2011).
- [186] D. R. LEMIN and T. VICKERSTAFF, *Trans. Faraday Soc.* **43**, 491 (1947).
- [187] A. K. MISHRA, T. AROCKIADOSS, and S. RAMAPRABHU, *Chemical Engineering Journal* **162**, 1026 (2010).
- [188] B. PAN and B. XING, *Environmental Science & Technology* **42**, 9005 (2008).
- [189] M. RAJABI, K. MAHANPOOR, and O. MORADI, *RSC Adv.* **7**, 47083 (2017).
- [190] C. PITTMAN, G.-R. HE, B. WU, and S. GARDNER, *Carbon* **35**, 317 (1997).
- [191] M. J. SWEETMAN, S. MAY, N. MEBBERSON, P. PENDLETON, K. VASILEV, S. E. PLUSH, and J. D. HAYBALL, *C* **3**, 18 (2017).
- [192] N. M. MAHMOODI, S. KHORRAMFAR, and F. NAJAFI, *Desalination* **279**, 61 (2011).

- [193] U. PAL, A. SANDOVAL, S. I. U. MADRID, G. CORRO, V. SHARMA, and P. MOHANTY, *Chemosphere* **163**, 142 (2016).
- [194] J. S. NOH and J. A. SCHWARZ, *Carbon* **28**, 675 (1990).
- [195] H. BOEHM, *Carbon* **32**, 759 (1994).
- [196] A. B. GONZÁLEZ-GUERRERO, E. MENDOZA, E. PELLICER, F. ALSINA, C. FERNÁNDEZ-SÁNCHEZ, and L. M. LECHUGA, *Chemical Physics Letters* **462**, 256 (2008).
- [197] M. G. TRULLI, E. SARDELLA, F. PALUMBO, G. PALAZZO, L. C. GIANNOSSA, A. MANGONE, R. COMPARELLI, S. MUSSO, and P. FAVIA, *Journal of Colloid and Interface Science* **491**, 255 (2017).
- [198] J. TRIESCHMANN and D. HEGEMANN, *Journal of Physics D: Applied Physics* **44**, 475201 (2011).
- [199] G. YONG, H. PENG, L. JIE, S. M. J., Z. JIANG, W. WEI, W. XIAQIN, Z. JING, Z. XINGPING, and S. DONGLU, *Journal of Applied Polymer Science* **103**, 3792.
- [200] J. IVALL, G. LANGLOIS-RAHME, S. COULOMBE, and P. SERVIO, *Nanotechnology* **28**, 055702 (2017).
- [201] D. LOSIC, M. A. COLE, B. DOLLMANN, K. VASILEV, and H. J. GRIESSER, *Nanotechnology* **19**, 245704 (2008).
- [202] M. ZELZER, D. SCURR, B. ABDULLAH, A. J. URQUHART, N. GADEGAARD, J. W. BRADLEY, and M. R. ALEXANDER, *The Journal of Physical Chemistry B* **113**, 8487 (2009).
- [203] J. XU and K. K. GLEASON, *Chemistry of Materials* **22**, 1732 (2010).
- [204] Y.-R. ZHANG, K. V. LAER, E. C. NEYTS, and A. BOGAERTS, *Applied Catalysis B: Environmental* **185**, 56 (2016).

APPENDIX A

Spatial homogeneity of PPE:X deposition on MWCNTs

Differences in deposition rate and PP composition on samples with complex geometry have been reported [21, 198]. For the particular case of plasma treatment of MWCNTs, most researchers opt for powders and employ some method to stir the powders during treatment to expose as much material as possible to the plasma [107, 197, 199]. In this thesis, MWCNTs were plasma treated while still on the SS mesh where they were synthesized. As shown in Figure 6.2, MWCNTs form an open forest which is amenable to plasma treatment. However, given that the mesh was laid flat on the electrode, a portion of the MWCNTs were hidden under the mesh and could be expected to be less exposed to the plasma. Furthermore, the density of MWCNTs increases as we approach the mesh. These potential barriers to the PP deposition compelled us to verify the uniformity of the PP on the MWCNTs given our current PECVD setup.

When coating a flat surface, the coating's thickness can be chosen based on a known deposition rate. For a porous material like the MWCNTs on the mesh however, not all sections of the material may be coated uniformly. Given that the end goal for this project was to have coated MWCNTs which could be dispersed in water, variations in the coating's thickness among MWCNTs wouldn't necessarily be an issue as long as they were all coated. Therefore, two sets of plasma treatments on MWCNTs, with changing deposition times (PPE:N: 0.5, 1, 4 and 10 min; PPE:O: 0.5, 4, 10, 20 min), were conducted to try to find the optimal treatment time. For each experiment, a MWCNT-covered mesh and a piece of Si wafer were placed on the electrode. XPS measurements were conducted on each mesh

approximately at the points shown on Figure A.1. The chemical composition of the deposit on the Si wafer was also recorded.

Figure A.2 shows the nitrogen content of Si-PPE:N and MWCNT-PPE:N with different PP deposition time¹. The composition of Si-PPE:N does not change with deposition time. However, on the front side of the MWCNT samples (exposed directly to the plasma), the nitrogen content increases from 1 to 4 min and then stays constant. On the back of the samples, an increase is also observed but does not reach the same value as in the front even after 10 min of deposition. The changes in composition observed for MWCNTs are simply due to changes in the PP thickness. With shorter deposition times, the signal detected by the XPS is a mixture of MWCNT and PP, and as the PP coating becomes thicker, only it is being detected by the XPS. This evolution is more easily observed with the change in shape of the C 1s peak (Figure A.3). The C 1s peak for MWCNTs coated with PPE:N for 30 s looks like a combination of the pure MWCNT C 1s peak and some added functional groups at higher binding energies. As the MWCNTs are treated for longer periods of time, the C 1s peak shape transitions from that of MWCNT to pure PPE:N after 4 min. On the back of the MWCNT mesh, the C 1s peak takes even longer (10 min) to correspond to that of PPE:N. In contrast, the shape of the peak does not change over time for Si:PPE:N (not shown here), again reinforcing the notion that it is not the coating which is changing in composition but how much of the MWCNT forest is actually covered. As for the N 1s peak on MWCNT-PPE:N (not shown here), it does not change in shape with different deposition time. It only grows in intensity as more PP gets deposited on the MWCNTs.

¹ Note that the oxygen content of these samples is not shown here as it was always under 2 at%, except for the 30 s sample. On this sample, which would have a very thin PPE:N coating, the oxygen measured probably comes from the MWCNT and not the PP coating. Oxygen content of as-synthesized MWCNTs can be as high as 3.8 at% [200].

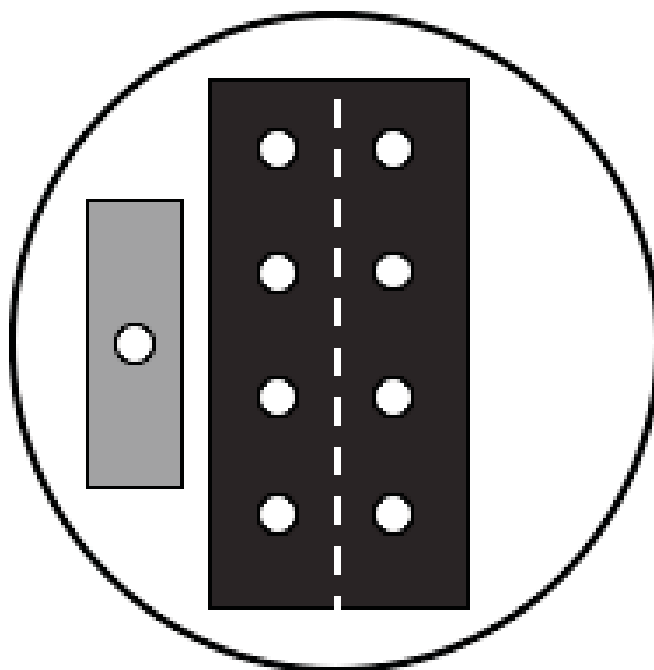


Figure A.1: Sample position on electrode, MWCNT mesh in the middle (dark grey) and Si wafer on the side (light grey). For XPS measurements, the MWCNT mesh was cut along the dashed line and one half of the sample was flipped in order to analyze its backside. The circles show the approximate measurement positions (spot sizes are not to scale).

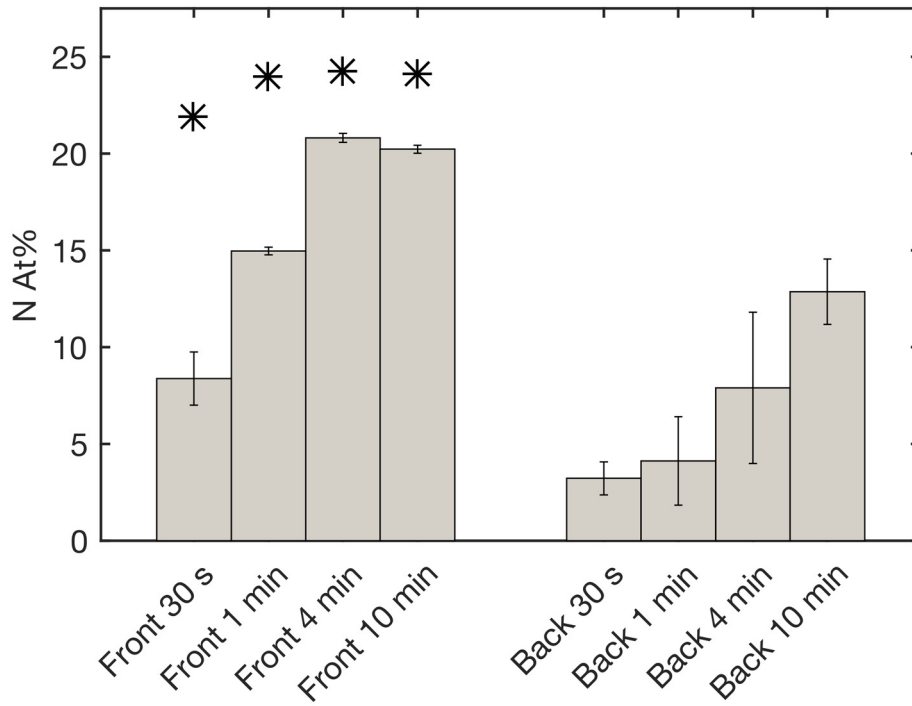


Figure A.2: Nitrogen content of MWCNT-PPE:N with respect to deposition time. Asterisks show N At% for Si-PPE:N.

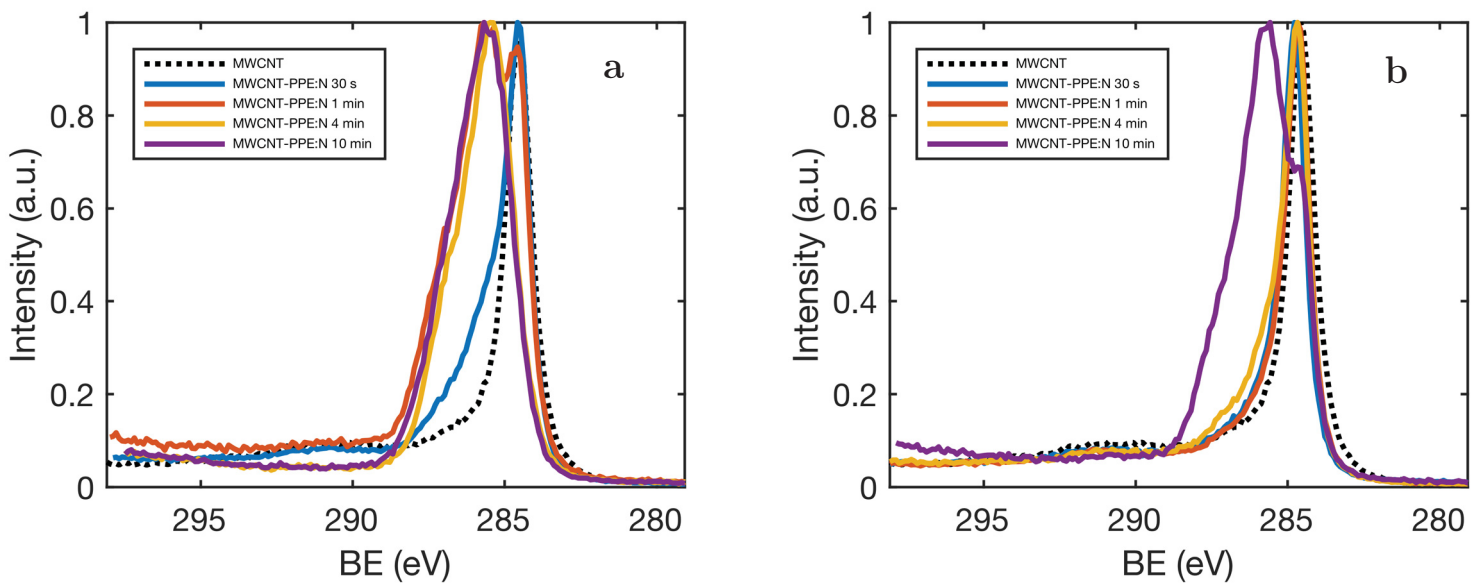


Figure A.3: Evolution of C 1s peak for MWCNT-PPE:N a) front, b) back.

Another interesting observation is the variation in composition at different positions on the samples (see error bars in Figure A.2). For the front, the variation between positions on the sample are very small (except for 30 s) suggesting a uniform thickness of the PP coating throughout. However, more variability is observed for the back of the samples. A plausible explanation is that, since the meshes are not flat, but rather undulated due to the heating process and carbon absorption into the mesh during MWCNT synthesis, some sections of the mesh (especially the edges) are sometimes curled up and may be more exposed to the plasma. A thicker coating can then be found on those sections of the sample.

Figure A.4 shows the oxygen content of MWCNT-PPE:O (nitrogen content was less than 1 at% on all samples). Note that the O content for Si-PPE:O at 30 s is not provided because the coating was too thin and the XPS survey spectrum showed the PP as well as the substrate underneath. Nevertheless, similar observations as with PPE:N can be made for PPE:O, notably that the composition of the PP does not change with time as can be seen with the results for Si:PPE:O. Again, the increase in PP thickness deposited on the MWCNTs can be observed through the shape changes of the C 1s peak (Figure A.5). The back of the meshes with MWCNT-PPE:O seem to be coated very thinly as the C 1s peak shape barely changes from that of pure MWCNT. However, the O 1s peak from the back side of the MWCNT samples shows that there is a change occurring even as early as 30 s after plasma initiation (Figure A.6).

When working with a 3D structure, not only is it important to verify how the PP deposits on all the different exposed faces, but also if PP deposition happens in porous structures. In the case of the samples in this study, the MWCNTs are well separated far from the mesh but towards the mesh, their density increases. For the purposes of making a stable nanofluid, it is not necessary to coat the entire MWCNT, as about 1 μm remains rooted to the mesh after sonication [6]. However, it would still be useful to better evaluate how much of the tube is

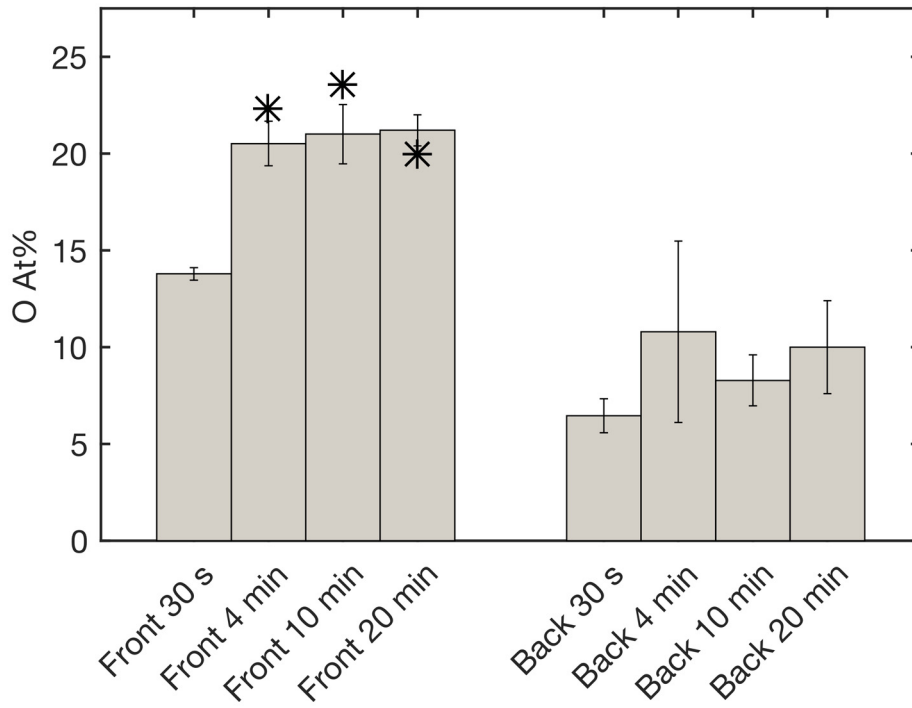


Figure A.4: Oxygen content of MWCNT-PPE:O with respect to deposition time. Asterisks show O At% for Si-PPE:O.

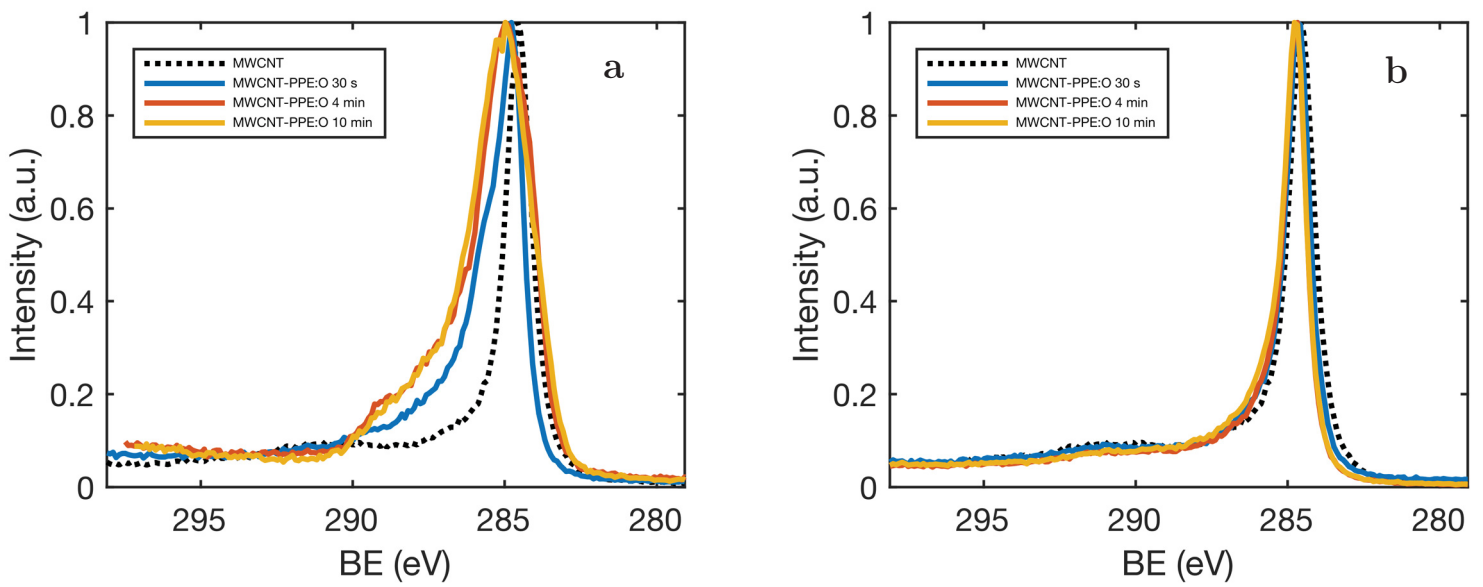


Figure A.5: Evolution of C 1s peak for MWCNT-PPE:O a) front, b) back.

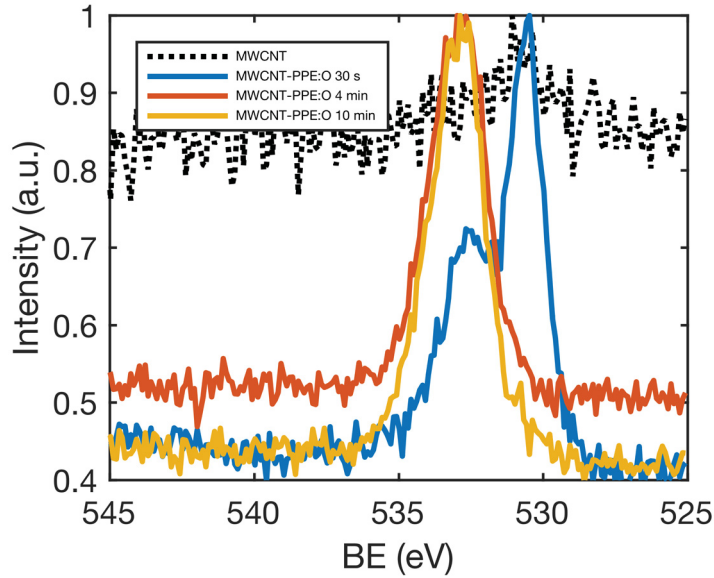


Figure A.6: Evolution of O 1s peak for MWCNT-PPE:O (back side).

coated. Other researchers have investigated how PP coatings deposit in high aspect ratio features (trenches for example) [201, 202, 203]. They observed that for pores below a few μm , no deposition occurs. This is due to the fact that a plasma cannot be sustained inside such small pores [204]. Furthermore, although neutral gaseous molecules may diffuse inside the pore, the charged species generated in the plasma bulk that participate in the plasma polymerization may not diffuse inside the pore due to the plasma sheath [202]. Even in cases where the plasma sheath does not stop diffusion of the charged species, if these species have high sticking coefficients, they may not coat the inside of pores. These species with high sticking coefficient will immediately react and deposit as they reach the pore opening if they touch the walls [114]. For deposition at the end of the pore, a molecule would need to enter the pore in a straight line and suffer no collisions which is more unlikely. Unfortunately, no experiments could be designed to properly investigate this issue with the MWCNTs on the mesh, and therefore this remains an open question to be investigated.

The results above do not justify the choice of deposition time used for the studies presented in this thesis. For MWCNT-PPE:N, samples were treated for 4 min, which is sufficient for the front side of the samples but insufficient for the back side. For MWCNT-PPE:O, samples were treated for 20 min, but according to the XPS results presented in this appendix, 4 min would have been sufficient for the front side. These choices were mostly based on trial and error and on the performance of the MWCNT-PPE:X when dispersed in water.

Clearly many questions remain regarding the composition and structure of MWCNT-PPE:X. In conjunction with the development of new methods to characterize this material, design of a more suitable PECVD chamber for the samples used would be necessary to avoid heterogeneous deposition (for example, a PECVD chamber where the mesh can be held upright and both sides are exposed to the plasma).